NEW MEXICO BUREAU OF GEOLOGY AND MINERAL RESOURCES
Bulletin 166 2024

2024 Hydrothermal Geochemistry and Critical Minerals Meeting: Abstracts

Editors: Alexander P. Gysi, Nicole C. Hurtig, and Laura E. Waters

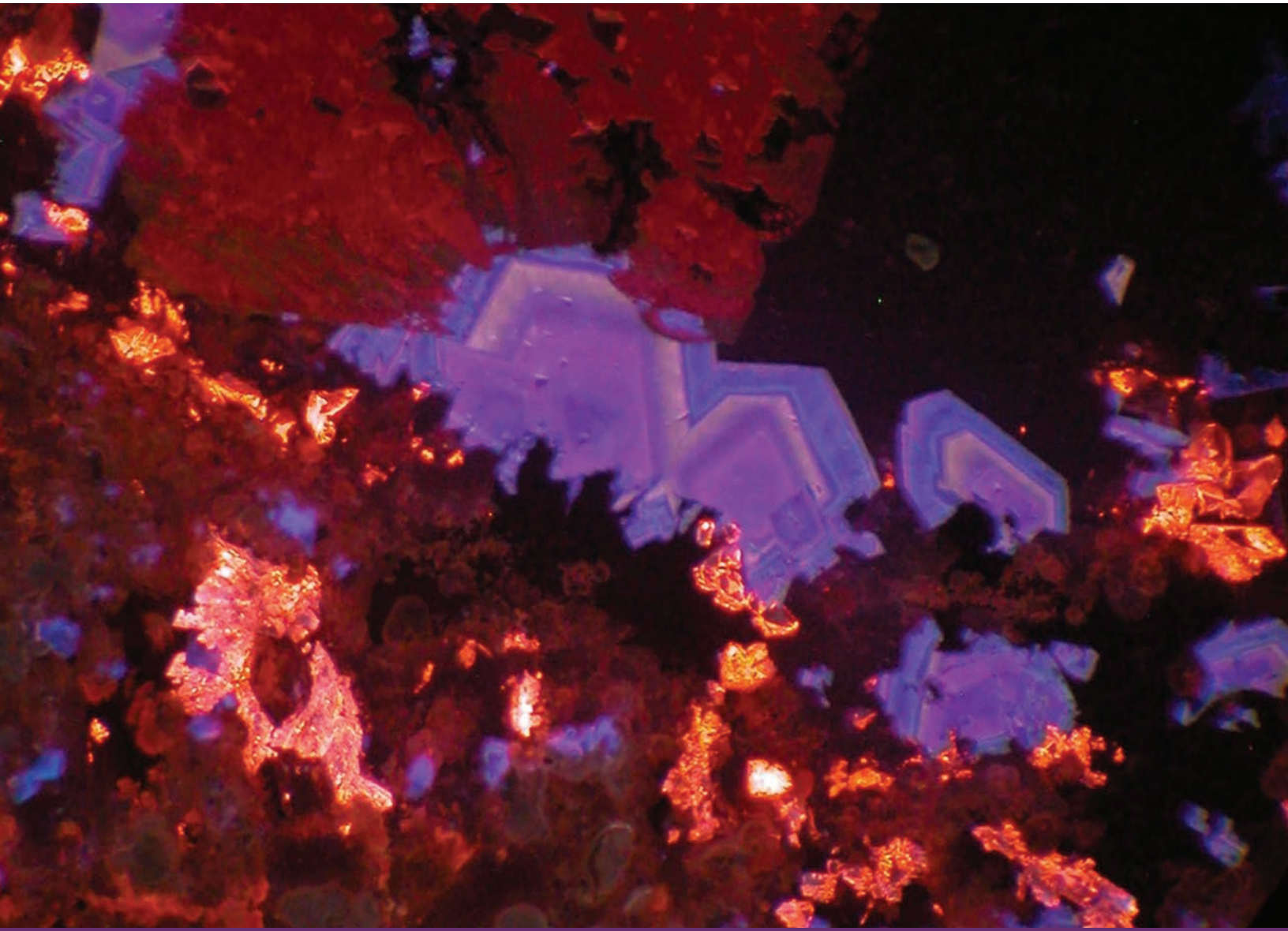

ENERGY AND MINERAL RESOURCES

2024 Hydrothermal Geochemistry and Critical Minerals Meeting: Abstracts

Editors: Alexander P. Gysi, Nicole C. Hurtig, and Laura E. Waters

Bulletin 166
June 2024

New Mexico Bureau of Geology and Mineral Resources
A research and service division of New Mexico Institute of Mining and Technology

Bulletin 166—2024 Hydrothermal Geochemistry and Critical Minerals Meeting: Abstracts

Editors: Alexander P. Gysi, Nicole C. Hurtig, and Laura E. Waters

New Mexico Bureau of Geology and Mineral Resources
A research and service division of New Mexico Institute of Mining and Technology

Dr. Mahyar Amouzegar, *President, New Mexico Tech*

Dr. J. Michael Timmons, *Director and State Geologist, New Mexico Bureau of Geology*

Copyediting: Frank Sholedice

Layout: Lauri Logan

Publications Program Manager: Barbara J. Horowitz

Cover Photograph: Fluorite and gittinsite from the Strange Lake REE-Zr-Nb deposit, Quebec, Canada.
Photo by A. Gysi

Project Funding: Office of Science, U.S. Department of Energy, Basic Energy Science, Grant DE-SC0022269 to Dr. Alexander Gysi, Dr. Nicole Hurtig, Dr. Laura Waters

NSF CAREER EAR-2039674 to Dr. Alexander Gysi

NSF-EAR 2039271 to Dr. Gordon Moore and NSF-EAR 2022465 to Dr. Laura Waters

Suggested Citation: Gysi, A.P., Hurtig, N.C., and Waters, L.E., eds., 2024, 2024 Hydrothermal Geochemistry and Critical Minerals Meeting—Abstracts: New Mexico Bureau of Geology and Mineral Resources Bulletin 166, 90 p. **https://doi.org/10.58799/B-166.**

June 3–7, 2024

Hosted by New Mexico Bureau of Geology and Mineral Resources and New Mexico Institute of Mining and Technology

Sponsored by U.S. Department of Energy and National Science Foundation under the following grants:

Office of Science, U.S. Department of Energy, Basic Energy Science, Grant DE-SC0022269 to Dr. Alexander Gysi, Dr. Nicole Hurtig, and Dr. Laura Waters

NSF CAREER EAR-2039674 to Dr. Alexander Gysi

NSF-EAR 2039271 to Dr. Gordon Moore and NSF-EAR 2022465 to Dr. Laura Waters

U.S. DEPARTMENT OF ENERGY | Office of Science

NSF

NEW MEXICO TECH
SCIENCE · ENGINEERING · RESEARCH · UNIVERSITY

New Mexico Bureau of Geology and Mineral Resources
New Mexico Tech
Earth Science for the 21st Century

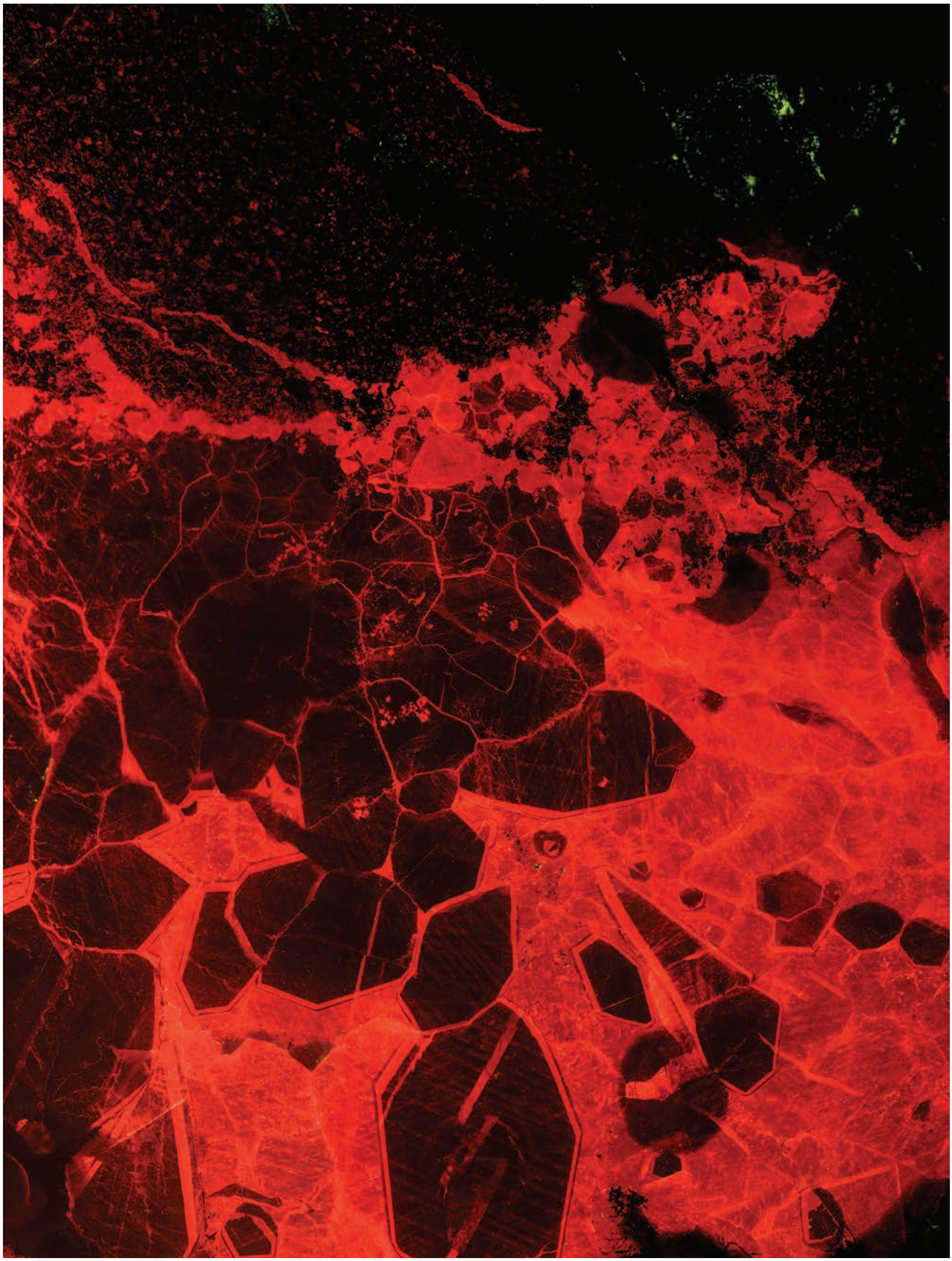

Cathodoluminescence image of Lemitar Mountains calcite. *Photo by Eric Ruggles and Evan Owen*

CONTENTS

Welcome to our ThermoCon meeting! The aim of this meeting is to bring together fans of thermodynamics—hence the name "ThermoCon"—and form a community across disciplines to advance cutting-edge science on critical minerals and hydrothermal geochemistry. The field of thermodynamics touches many aspects of geosciences, chemistry, material sciences, and much more, and is currently seeing a renewed interest because of critical minerals. Critical minerals are defined as any non-fuel mineral, element, substance, or material essential to the United States' economic and national security and that is provided by a supply chain vulnerable to global and national disruption (Energy Act of 2020). A list of 50 mineral commodities was published in 2022 by the U.S. Geological Survey (Federal Register, 87 FR 10381; USGS, 2024), some of which are found in New Mexico (McLemore and Gysi, 2023). Similar definitions and lists of minerals/elements are found in other countries. This renewed interest is echoed by governmental agencies, the public, and scientists because of the importance of critical minerals for high-tech and green technologies. However, surprisingly little is known about the thermodynamic properties of critical elements, in particular at the high temperature and pressure conditions of ore-forming processes that are important for their enrichment in the crust.

Many critical mineral deposits form in magmatic-hydrothermal systems, and hence there is an important link between fundamental science and understanding the geologic processes that transport, fractionate, and enrich critical elements in the Earth's crust. Knowledge of the properties of hydrothermal fluids and critical minerals therefore has many applications, including mineral exploration and extraction, development of technologies, geothermal energy, and many more. Studying these hydrothermal geologic systems and conducting the fundamental research associated with them is challenging because it necessitates an understanding of processes in a wide pressure, temperature, and compositional range and at scales that span from molecular-level interactions to kilometer-scale fluid flow and fluid-rock interaction. We are therefore excited to present this bulletin, which compiles abstracts submitted to this meeting.

A major goal of this conference is to tackle the challenges described above and build a new network of scientists and professionals with different expertise, including but not limited to experimental geochemistry/chemistry, thermodynamic/geochemical modeling and databases, reactive mass transport modeling, molecular dynamic simulations, element extraction/separation technologies, theoretical thermodynamics and equations of state, and mineralogy, ore deposits, and processes in natural systems. Another important aspect is the participation of students and training the next generation of leaders in the field of critical minerals and thermodynamics. Participants at this meeting include scientists from academia and national laboratories, graduate and undergraduate students, as well as liaisons from industry, governmental agencies, and geological surveys.

This five-day meeting includes daily talks, keynotes, small workshops, discussion sessions, and two evenings of poster sessions for students. One day includes an excursion to the nearby Lemitar Mountains carbonatite rare earth elements deposit to discover the geology of New Mexico and allow participants to link geosciences with other areas of basic energy sciences. We will also organize a geochemical modeling workshop using our "in-house" MINES thermodynamic database (Gysi et al., 2023) to show an application of thermodynamics to modeling critical mineral deposits.

REFERENCES

Gysi A. P., Hurtig N. C., Pan R., Miron G. D., and Kulik D. A. (2023) MINES thermodynamic database, version 23: New Mexico Bureau of Geology and Mineral Resources. https://doi.org/10.58799/mines-tdb

McLemore V. T. and Gysi A. P. (2023) Critical minerals in New Mexico. New Mexico Earth Matters, *23*(1), 1–4.

U.S. Geological Survey (2024) Mineral commodity summaries 2024: U.S. Geological Survey, 212 p. https://doi.org/10.3133/mcs2024

MEETING SCHEDULE

SUNDAY, JUNE 2, 2024

Participants arrive, shuttle from Albuquerque International Sunport to Socorro

MONDAY, JUNE 3, 2024 (first day of conference)

Location: Bureau of Geology room 253 (unless otherwise noted)

Morning

8:30–9:15 am	Conference logistics and introduction/goals of meeting (Alexander Gysi)
9:15–10:00 am	Hermann Lebit, Alma Energy, USA Talk: Direct lithium extraction from geothermal brines: The new oil
10:00–10:30 am	*Coffee break*
10:30–11:15 am	John Kaszuba, University of Wyoming, USA Talk: Lithium mobility in interbedded sandstone and mudstone, Powder River Basin, Wyoming
11:15 am–12:00 pm	Hongkyu Yoon, Sandia National Laboratories, USA Talk: Pore-scale modeling and experimental applications for reactive transport and flow behavior along mineral-fluid interfaces
12:00–1:30 pm	*Lunch break*

Afternoon

1:30–2:15 pm	Lars Rüpke, GEOMAR, Germany Talk: Understanding what's below: Using the open-source toolbox HydrothermalFoam to simulate submarine hydrothermal systems
2:15–3:00 pm	James Kubicki, University of Texas at El Paso, USA Talk: Computational chemistry: Potential applications in economic geology
3:00–3:30 pm	*Coffee break*
3:30–4:30 pm	Student speed talks
5:00–7:00 pm	*Dinner/free time*
7:00–9:00 pm	Poster session, Deju House, NM Tech campus

TUESDAY, JUNE 4, 2024

Morning

8:30–9:15 am	Daniel Harlov, Deutsches GeoForschungsZentrum GFZ, Germany Talk: Fluid-aided REE and actinide mobility in phosphate minerals: Nature and experiment
9:15–10:00 am	Laura Waters, New Mexico Tech, USA Talk: Isotope dilution methods in small experimental charges at high temperatures in cold-seal pressure vessels and applications
10:00–10:30 am	*Coffee break*
10:30–11:15 am	Xiaofeng Guo, Washington State University, USA Talk: Experimental thermodynamic studies on mixing models of REE mineral phases
11:15 am–12:00 pm	Jeffrey Catalano, Washington University, USA Talk: Surface-specific selectivity patterns during rare earth element adsorption: Implications for fractionation patterns in regolith-hosted deposits
12:00–1:30 pm	*Lunch break*

Afternoon

1:30–2:15 pm	Tanya Prozorov, Ames National Laboratory, USA Talk: Lanthanide adsorption in muscovite and phlogopite micas: Implications for rare earth elements separations
2:15–3:00 pm	Artas Migdisov, Los Alamos National Laboratory, USA Talk: Transport and deposition of Nd in carbonate-bearing hydrothermal systems
3:00–3:30 pm	*Coffee break*
3:30–4:00 pm	Bryan Maciag, New Mexico Tech, USA Focus Talk: *In situ* Raman spectroscopy of rare earth element speciation in acidic sulfate-bearing aqueous fluids from 25 to 500 °C
4:00–4:30 pm	Sarah Smith-Schmitz, New Mexico Tech, USA Focus Talk: Raman spectroscopic investigation of Dy complexation in Cl-bearing hydrothermal solutions
5:00–7:00 pm	*Dinner/free time*
7:00–9:00 pm	Poster session, Deju House, NM Tech campus

WEDNESDAY, JUNE 5, 2024

Morning

8:00–11:30 am	Lemitar Mountains excursion, Group A
8:30 am–12:00 pm	GEMS workshop, Group B
12:00–1:00 pm	*Lunch break (boxed lunch)*

Afternoon

1:00–4:30 pm	Lemitar Mountains excursion, Group B
1:00–4:30 pm	GEMS workshop, Group A
5:00–7:00 pm	*Dinner/free time*

Evening microbrewery tour

THURSDAY, JUNE 6, 2024

Morning

7:30–9:30 am	Bosque del Apache birdwatching tour
10:00–10:30 am	*Coffee break*
10:30–11:15 am	Qiushi Guan, CSIRO Mineral Resources, Australia Talk: Molecular simulations to understand how critical metals transport in hydrothermal fluids
11:15 am–12:00 pm	Sandro Jahn, University of Cologne, Germany Talk: Toward the development of new thermodynamic models for hydrothermal fluids using molecular dynamics simulations
12:00–1:30 pm	*Lunch break*

Afternoon

1:30–2:15 pm	Marion Louvel, Institut des Sciences de la Terre d'Orléans, France Talk: Characterization of the speciation, solubility, and partitioning of metals in magmatic-hydrothermal systems using *in situ* X-ray spectroscopy
2:15–3:00 pm	Nicole Hurtig, New Mexico Tech, USA Talk: Rare earth element coordination chemistry using *in situ* Raman spectroscopy
3:00–3:30 pm	*Coffee break*
3:30–4:15 pm	Hannah Han, New Mexico Tech, USA Talk: UV-Vis spectrophotometric determination of the hydrolysis of erbium in near neutral to alkaline aqueous solutions from 25 to 75 °C
4:15–5:00 pm	Discussion panel
6:30–9:00 pm	Dinner, Deju House, NM Tech campus

FRIDAY, JUNE 7, 2024

Morning

8:30–9:15 am	Dmitrii Kulik, Paul Scherrer Institute, Switzerland Talk: GEMS as an asset of geochemical modeling: 24 years of development and use
9:15–10:00 am	Dan Miron, Paul Scherrer Institute, Switzerland Talk: Beyond GEMS: Integration of thermodynamic datasets, activity models, and parameter optimization
10:00–10:30 am	*Coffee break*
10:30–11:15 am	Alexander Gysi, New Mexico Tech, USA Talk: Hydrothermal mobilization, fractionation, and mineralization of REE in critical mineral deposits: A holistic approach combining field observations, experiments, and modeling
11:15 am–12:00 pm	Shaul Hurwitz, U.S. Geological Survey, USA Talk: Suggested future research on the geochemistry of continental hydrothermal systems for improved understanding of hazards, energy and mineral resources, and the limits of life on Earth and elsewhere in the solar system
12:00–1:00 pm	*Lunch break*

Participants depart, shuttle from Socorro to Albuquerque International Sunport

POSTER SESSIONS, MONDAY AND TUESDAY, 7:00–9:00 PM
SPEED TALKS, MONDAY, 3:30–4:30 PM

Jonathan Adams, New Mexico Tech, USA
Tellurium solubility in water vapor with implications for ore-forming processes: An experimental and numerical simulation study

Olivia Bahhage, Washington State University, USA
Scandium dissolution in alkaline carbonate media

Debarati Banerjee, New Mexico Tech, USA
The effects of salinity and pH on the hydrothermal solubility of $DyPO_4$ at 500 °C and 1.5 kbar

James Chapman, University of Texas at El Paso, USA

Jan Dreschmann, University of Cologne, Germany
Speciation in carbonatitic brine-melts and fluids from molecular simulations

Jasper Engelmann, GEOMAR, Germany
Investigating the influence of fluid-rock interaction in the formation of high-temperature hydrothermal vent sites: Insights from coupled numerical modeling

Yerko Figueroa Penarrieta, New Mexico Tech, USA
Revisiting the standard partial molal thermodynamic properties of Nd^{3+} and Nd aqueous species from 25 to 250 °C

Charles Kershaw, New Mexico Tech, USA
The experimental determination of Ce, Y, and Er solubility and thermodynamic predictions in hydrothermal fluids at 350 to 500 °C

Emma Carlsen Kindall, Washington State University, USA
Calorimetric and structural characterization of gamma irradiated rare earth rhabdophanes

Juejing Liu, Washington State University, USA
Large language model-based structured information retrieval and dataset construction: Examples on rare earth mineral thermodynamic properties

Fernanda Loza, Washington University, USA
Impact of ammonia on platinum(II) binding to goethite

Kevin Padilla, New Mexico Tech, USA
Hydrothermal solubility experiments and determination of the stability of La^{3+} aqua ion and La hydroxyl complexes in acidic to mildly acidic aqueous solutions to 250 °C

Perla Rodriguez Contreras, University of Texas at El Paso, USA

Eric Ruggles, New Mexico Tech, USA
Apatite rare earth elements chemistry and fluid evolution in the Lemitar Mountains carbonatite, New Mexico

Sophia Stuart, Los Alamos National Laboratory, USA
Machine learning to constrain geologic controls on critical mineral occurrence at Wyodak Mine, Powder River Basin, Wyoming

Aadish Velmani, New Mexico Tech, USA
Hydrothermal rare earth elements partitioning into fluorite: A fluid inclusion study from the Gallinas Mountains REE-bearing fluorite deposit in New Mexico

Emily Wright, Washington University, USA
Mineral-specific inhibition of palladium adsorption to iron (oxyhydr)oxides by chloride

Hongwu Xu, Los Alamos National Laboratory, USA

Natalie Yaw, Washington State University, USA
Preparation of divalent Eu materials for thermodynamic study under hydrothermal conditions

Xin Zhang, Pacific Northwest National Laboratory, USA

Xiaodong Zhao, Pacific Northwest National Laboratory, USA
The structure of Yb(III) sulfate complexes in aqueous solutions at elevated pressure and temperature

TELLURIUM SOLUBILITY IN WATER VAPOR WITH IMPLICATIONS FOR ORE-FORMING PROCESSES: AN EXPERIMENTAL AND NUMERICAL SIMULATION STUDY

Jonathan Adams[1], Nicole Hurtig[1], Alexander Gysi[1,2], Artaches Migdisov[3]

[1] Department of Earth and Environmental Science, New Mexico Institute of Mining and Technology, Socorro, NM 87801, USA
[2] New Mexico Bureau of Geology and Mineral Resources, New Mexico Institute of Mining and Technology, Socorro, NM 87801, USA
[3] Earth and Environmental Sciences Division, Los Alamos National Laboratory, Los Alamos, NM 87545, USA

Tellurium (Te) is a critical mineral of increasing importance in green energy technologies. Tellurium is enriched to economic grades in magmatic-hydrothermal systems such as Cu-porphyry, epithermal, and volcanicogenic massive sulfide (VMS) deposits. In these systems, it forms in late Au-Ag and base metal veins as tellurides and/or as trace impurities in Cu-Fe sulfides. Existing thermodynamic data predict the dominance of the $H_2Te_{(g)}$ species with concentrations up to 0.1 ppm in simulations applied to epithermal ore formation contrasting with 100s of ppm Te measured in fluid inclusions from epithermal ore deposits (Wallier et al., 2006; Grundler et al., 2013). Controls on Te mobility in magmatic-hydrothermal systems are not as extensively studied as precious and base metals such as Au, Ag, and Cu, where previous studies have shown that their solubility in water vapor is an important transport mechanism for ore formation (Hurtig et al., 2021).

The solubility of Te in water vapor is determined as a function of temperature, water vapor pressure, and redox. Experiments are conducted at 250–320 °C and a range of water vapor pressures (P_{H2O}) in batch-type Ti Parr reactors using different oxygen buffers (e.g., MoO_2-MoO_3, WO_2-WO_3, and Ni-NiO). Kinetic experiments at 250 °C and 20 bar for different redox conditions were conducted between 1–25 days. At oxidizing conditions, equilibrium conditions were reached after ~10 days and 1 ppm Te and in N_2-degassed experiments after ~22 days and 0.7 ppm indicating slower reaction kinetics and reduced solubility at more reducing conditions. Experiments at 250 °C and $\log f_{O2}$ = -24 (MoO_2-MoO_3 buffer), show increasing Te solubility with increasing P_{H2O} from 1–3 ppm at 15 bar to 12 ppm at 35 bar. In the MoO_2-MoO_3 buffered experiments at 300 °C and 320 °C, Te concentrations increase with increasing P_{H2O} reaching up to 12 ppm and 4 ppm at 300 °C and 80 bar and 320 °C and 105 bar, respectively. Previous experimental studies indicate that the dominant species is $TeO_2(H_2O)_y$ with hydration numbers of y = 1 and 2 (Glemser et al., 1964, 1966). In this study, we predict higher hydration numbers and extracted thermodynamic properties for up to 5 hydration steps.

The experimentally determined thermodynamic properties of the hydrated $TeO_2(H_2O)_y$ species were implemented into the MINES database (https://doi.org/10.58799/mines-tdb) to simulate ore-formation using the GEMS code package (https://gems.web.psi.ch/). Two simulations are presented using vapor-like and liquid-like fluid evolution paths applied to the Cripple Creek Au-Te epithermal ore deposit (Fig. 1). In the vapor model, the fluid was cooled from 350 °C to 100 °C at constant fluid density (0.1 g/cm^3) and is buffered by pyrite-hematite-anhydrite-rutile. Tellurium fugacity becomes higher than the Au fugacity at 250 °C and sharply decreases by several orders of magnitude below 160 °C, indicating precipitation of calaverite, which is the main Te mineral precipitating in these simulations. In the liquid model, the fluid has a salinity of 3 wt% NaCl and is buffered by phonolite rock at a fluid to rock ratio of 20 with pyrite-hematite-rutile-hessite stable. Gold solubility is 4 orders of magnitude greater than Te solubility, which gradually

decreases with decreasing temperature indicating the precipitation of hessite and calaverite minerals. For both models mineral paragenesis is comparable but metal transport in the vapor phase is orders of magnitude greater than that predicted for liquids using existing thermodynamic data for aqueous speciation and our new experimentally derived data for the vapor phase. The coupled experimental and numerical results show that hydrothermal vapors can play a significant role in the transport of Te and the formation of Au-Te deposits.

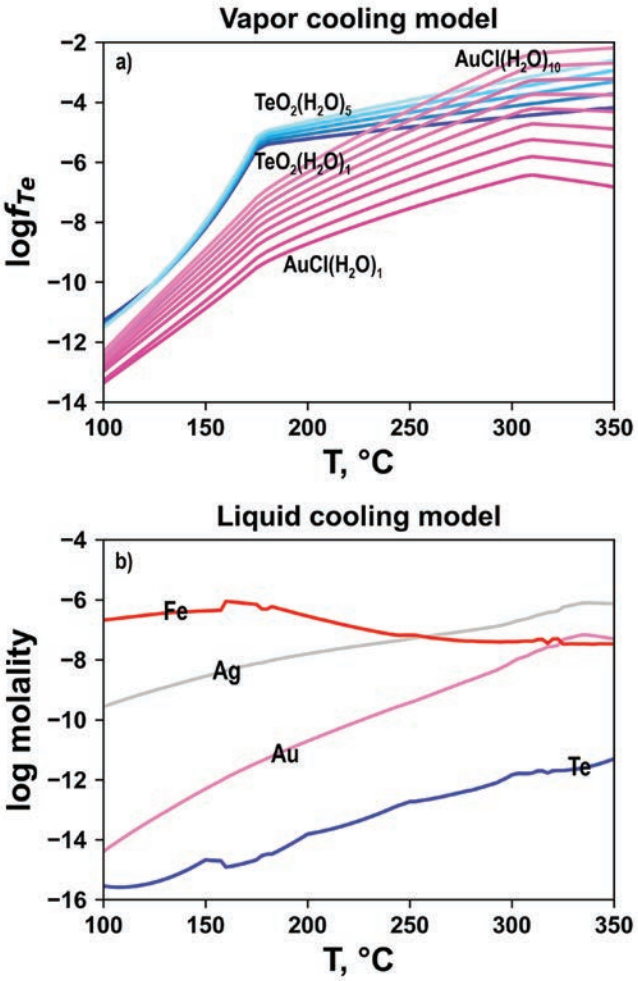

Figure 1. Cooling models simulating Te and Au solubility in (a) vapor- and (b) liquid-like fluids between 350 °C and 100 °C. a) Vapor cooling model at constant vapor density (100 g/cm^3) and relatively oxidizing conditions buffered by pyrite-hematite-rutile-anhydrite showing higher Te solubility compared to Au solubility. b) Liquid cooling model of a low salinity epithermal fluid (3 wt% NaCl) buffered by a representative phonolite host rock from Cripple Creek showing low solubility of Te and higher Au solubility in liquid-like fluids.

REFERENCES

Glemser O., Haeseler R. V., and Müller A. (1964) Gasförmige Hydroxide. VII. Über gasförmiges $TeO(OH)_2$. *Zeitschrift für anorganische und allgemeine Chemie* **329**, 51–55.

Glemser O., Müller A., and Schwarzkopf H. (1966) Über die Reaktion von TeO_2 mit Wasserdampf bei höheren Drucken und Temperaturen. In *Omagiu lui C.I. Parhon Editura Acedemiei Republici Socialiste* Romania, Bucarest. pp. 253–262.

Grundler P. V., Brugger J., Etschmann B. E., Helm L., Liu W., Spry P. G., Tian Y., Testemale D., and Pring A. (2013) Speciation of aqueous tellurium(IV) in hydrothermal solutions and vapors, and the role of oxidized tellurium species in Te transport and gold deposition. *Geochimica et Cosmochimica Acta* **120**, 298–325.

Hurtig N. C., Migdisov A. A., and Williams-Jones A. E. (2021) Are vapor-like fluids viable ore fluids for Cu-Au-Mo porphyry ore formation? *Economic Geology* **116**, 1599–1624.

Wallier S., Rey R., Kouzmanov K., Pettke T., Heinrich C. A., Leary S., O'Connor G., Tămaş C. G., Vennemann T., and Ullrich T. (2006) Magmatic fluids in the Breccia-hosted epithermal Au-Ag deposit of Roşia Montană, Romania. *Economic Geology* **101**, 923–954.

SCANDIUM DISSOLUTION IN ALKALINE CARBONATE MEDIA

Olivia Bahhage[1], Natalie S. Yaw[1], Sam Karcher[1], Xiaodong Zhao[2], Ping Chen[2], Xin Zhang[2], John McCloy[1], Xiaofeng Guo[1]

[1] Washington State University, Pullman, WA 99163, USA

[2] Pacific Northwest National Laboratory, Richland, WA 99354, USA

Scandium (Sc) is a rare earth element (REE) that has important applications in high-tech fields ranging from ceramics, electronics, and more. Different than other REE, Sc is sparsely distributed in the Earth's crust, without a major hosting mineral phase. The primary source of REE's is mainland China, with about 70% of the global supply. In order to ensure continued and plentiful access to this critical element, we need to diversify our access; however, in order to do so we must understand how Sc behaves in the geosphere. In this work, we have conducted solubility experiments to determine the reference phase of several common Sc compounds, which is needed before we can study and model their behavior in hydrothermal fluids. Previously, Sc has been discarded in red mud waste while mining other minerals, i.e., from aluminum extraction from bauxite, containing many REEs (including Sc), which has economically valuable concentration. Studying the behavior of Sc in geological conditions to model and predict depositions will enable more economically viable exploitation of the valuable element. To do this, we conducted six dissolution experiments of scandium carbonates, hydroxides, and oxyhydroxides at 100 °C using autoclaves. We then collected Raman data to find three potential reference phases α-ScOOH, γ-ScOOH, or $ScOH_3$. We then took these three phases and repeated the experiment at 150 °C and 200 °C. Sc solids were equilibrated in a 1 molar carbonate solution for two weeks to ensure that equilibrium was reached. The solids and liquids were then separated, and ICP and pH were both taken for the resulting liquid to compare the relative rate of dissolution of scandium. The resultant solids were studied with Raman, SEM with EDX to observe if there were phase alterations on the surface during hydrothermal treatment (Fig. 1). Our results demonstrate the instability of scandium carbonate phases in carbonate-bearing solutions based on extreme surface alteration and elevated solubility. Scandium hydroxides and oxyhydroxides were more recalcitrant, suggested by lower solubility and minimum surface phase alteration. Initial findings suggest these solubilities might be different in silica-rich fluids, which will be followed up on with future testing. Experimentation is ongoing to definitively determine the reference phase of Sc under these hydrothermal conditions; however, at this point it has been narrowed down to three possible phases: α-ScOOH, γ-ScOOH, or $ScOH_3$. Future hydrothermal spectroscopic and solubility studies on these Sc phases are developing. This information will be useful to understand the transport and precipitation behavior of Sc in hydrothermal fluids.

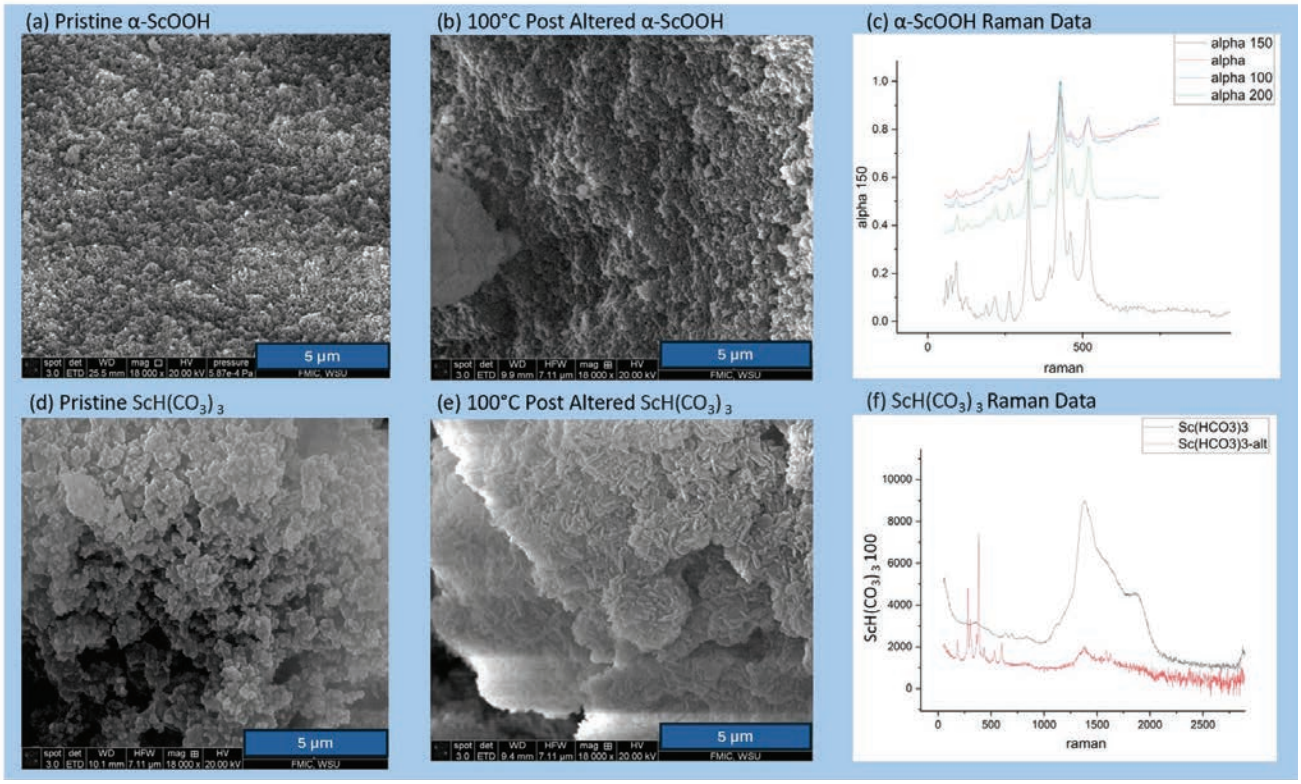

Figure 1. (a) and (b) show no alterations between the pristine and 100 °C post-alteration shots, whereas there are clear surface alterations shown from (d) and (e). Raman data (c) and (f) confirm there was indeed alteration in the carbonate phase, whereas the alpha phase remained unaltered. Thus, the alpha phase contends to be the Sc reference phase we are looking for.

THE EFFECTS OF SALINITY AND PH ON THE HYDROTHERMAL SOLUBILITY OF $DyPO_4$ AT 500 °C AND 1.5 KBAR

Debarati Banerjee[1], Laura E. Waters[1], Nicole C. Hurtig[1], Alexander P. Gysi[1,2], Daniel Harlov[3,4,5], Chen Zhu[6], Artaches Migdisov[7]

[1] Department of Earth and Environmental Science, New Mexico Institute of Mining and Technology, Socorro, NM 87801, USA
[2] New Mexico Bureau of Geology and Mineral Resources, New Mexico Institute of Mining and Technology, Socorro, NM 87801, USA
[3] Division of Chemistry and Physics of Earth Materials, Deutsches GeoForschungsZentrum GFZ, Telegrafenberg, 14473 Potsdam, Germany
[4] Faculty of Earth Resources, China University of Geosciences, Wuhan 430074, China
[5] Department of Geology, University of Johannesburg, South Africa
[6] Department of Earth and Atmospheric Sciences, Indiana University, Bloomington, IN 47408, USA
[7] Earth and Environmental Sciences Division, Los Alamos National Laboratory, Los Alamos, NM 87545, USA

Dysprosium (Dy) is part of the heavy rare earth elements (HREE) and has many important applications in the green technology industry to build components for laser materials, energy-efficient lights, and magnets (Chakhmouradian and Wall, 2012). The HREE are commonly hosted in REE phosphates such as xenotime, which form in magmatic-hydrothermal REE mineral deposits. Aqueous complexes play a key role for mobilizing and fractionating the REE in hydrothermal fluids. Their stability in supercritical fluids is controlled by an interplay of temperature, pressure, and fluid composition (i.e., pH and ligand activity). Although chloride is among the most abundant mobilizing ligands for REE in hydrothermal fluids, there are only very few experimental studies investigating the stability of the aqueous REE chloride complexes ($REECl_n^{+(3-n)}$) at temperatures above 300 °C. The solubility of $DyPO_4$ with the xenotime structure has been experimentally determined up to 250 °C at saturated water vapor pressure in the $HClO_4$-H_2O system, which does not promote the formation of Dy chloride species (Gysi et al., 2015). Dy chloride complexation has been experimentally determined up to 300 °C in HCl-bearing acidic solutions using REE fluorides (Migdisov et al., 2009). The goal of this study is to investigate the stability of $DyCl_n^{+(3-n)}$ species and the solubility of $DyPO_4$ at higher temperatures to evaluate the role of chloride complexes in mobilizing Dy in supercritical hydrothermal fluids.

In this study, solubility experiments were conducted using synthetic $DyPO_4$ crystals equilibrated with saline (0.5 mNaCl) and non-saline HCl-bearing solutions at 500 °C and 1.5 kbar. Experimental fluids were spiked with 100 ppm ^{162}Dy, which enabled us to determine the total $DyPO_4$ dissolved at experimental conditions using isotope dilution, despite precipitation of $DyPO_4$ during quenching. At 500 °C, total dissolved $DyPO_4$ is 48 ppm (log $mDyPO_4$ = -3.9) in non-saline solutions and 182 ppm (log $mDyPO_4$ = -3.3) in saline solutions with a staring pH of 2 (Fig. 1). The solubility increases with increasing salinity indicating the formation of Dy chloride complexes.

The GEMS code package (Kulik et al., 2013; https://gems.web.psi.ch/) and the MINES thermodynamic database (Gysi et al., 2023; https://geoinfo.nmt.edu/mines-tdb/) are used to calculate the pH of the experimental solutions and predict the speciation and solubility of Dy. Comparison of these models with our experimental datas indicate that the solubility of $DyPO_4$ is underpredicted by 3–4 orders of magnitude at 500 °C and 1.5 kbar (Fig. 1). The observed difference between predicted and measured $DyPO_4$ solubility suggests that the low temperature solubility data (Migdisov et al., 2009; Gysi et al., 2015) cannot be extrapolated to supercritical conditions, and that Dy solubility strongly depends on temperature and pressure. Speciation

calculations at the experimental conditions suggest that the observed increase in $DyPO_4$ solubility is due to the increased stabilization of Dy chloride complexes, which coincides with acidic to mildly acidic pH for these two experimental series.

This work is supported by the U.S. Department of Energy, Office of Science, Basic Energy Sciences, Geosciences program under Award DE-SC0022269.

REFERENCES

Chakhmouradian A. R. and Wall F. (2012) Rare earth elements: Minerals, mines, magnets (and more). *Elements* **8**(5), 333–340.

Gysi A. P., Williams-Jones A. E., and Harlov D. (2015) The solubility of xenotime-(Y) and other HREE phosphates ($DyPO_4$, $ErPO_4$ and $YbPO_4$) in aqueous solutions from 100 to 250 °C and p sat. *Chemical Geology* **401**, 83–95.

Gysi A. P., Hurtig N. C., Pan R., Miron G. D. and Kulik D. A. (2023) https://doi.org/10.58799/mines-tdb

Kulik D. A., Wagner T., Dmytrieva S. V., Kosakowski G., Hingerl F. F., Chudnenko K. V., and Berner U. R. (2013) GEM-Selektor geochemical modeling package: Revised algorithm and GEMS3K numerical kernel for coupled simulation codes. *Computational Geosciences* **17**(1), 1–24.

Migdisov A. A., Williams-Jones A. E., and Wagner T. (2009) An experimental study of the solubility and speciation of the rare earth elements (III) in fluoride- and chloride-bearing aqueous solutions at temperatures up to 300 °C. *Geochimica et Cosmochimica Acta* **73**(23), 7087–7109.

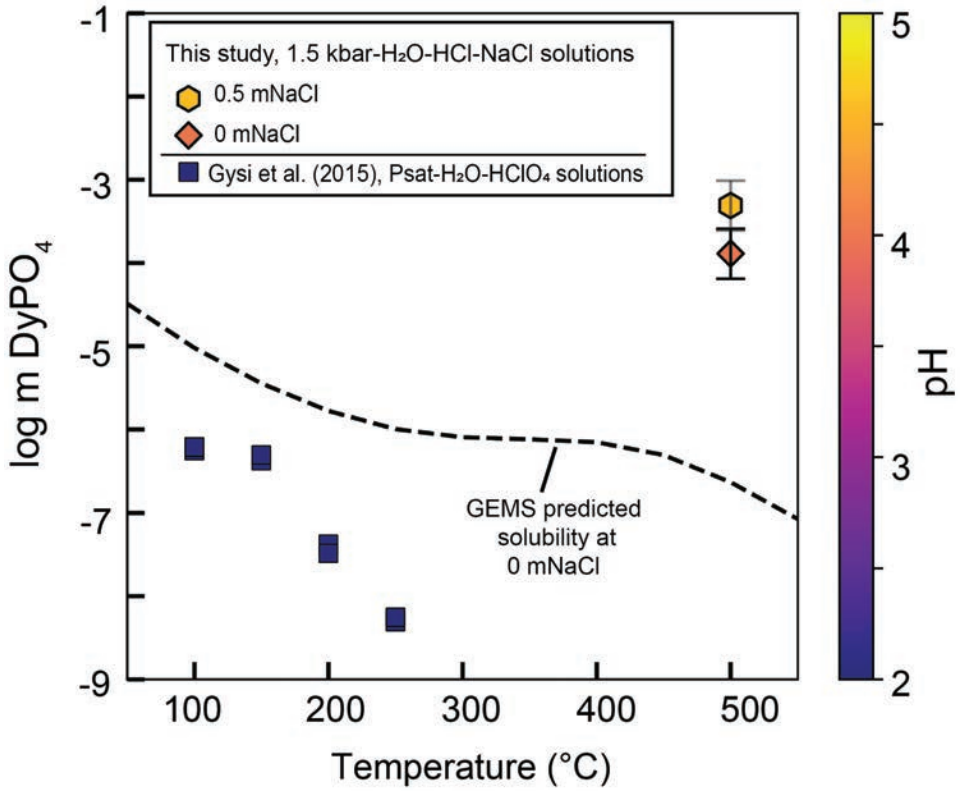

Figure 1. Logarithmic molality of total dissolved $DyPO_4$ as a function of temperature showing the measured solubility in Cl-bearing solutions from this study at 500 °C and 1.5 kbar and $DyPO_4$ solubility data from Gysi et al. (2015) in $HClO_4$-solutions. The modeled $DyPO_4$ solubility was simulated using the GEMS code package and the MINES thermodynamic database for a solution with 0.01 m NaCl and a pH of 2 at room temperature. The predicted $DyPO_4$ solubility underpredicts data from this study by ~3–4 orders of magnitude.

SURFACE-SPECIFIC SELECTIVITY PATTERNS DURING RARE EARTH ELEMENT ADSORPTION: IMPLICATIONS FOR FRACTIONATION PATTERNS IN REGOLITH-HOSTED DEPOSITS

Jeffrey G. Catalano[1], Yihang Fang[1], Greg J. Ledingham[1], Olwen Stagg[1], Joanne E. Stubbs[2], Peter J. Eng[2]

[1] Department of Earth, Environmental, and Planetary Sciences, Washington University, St. Louis, MO 63130, USA

[2] Center for Advanced Radiation Sources, University of Chicago, Chicago, IL 60439, USA

Regolith-hosted deposits serve as major rare earth element (REE) resources (Estrade et al., 2019; Li and Zhou, 2020). These deposits form via chemical weathering of granites and often display relative enrichment in the heavy REEs (Sanematsu and Watanabe, 2016; Li et al., 2020). Retention of REEs occurs primarily via adsorption to clay minerals (Li and Zhou, 2020), such as kaolinite, halloysite, and gibbsite, with recovery possible using mild chemical extractions (Moldoveanu and Papangelakis, 2016). The underlying interfacial chemistry that controls REE retention, fractionation, and extractability in these deposits remains unresolved. Strong retention suggests a ligand-exchange binding mechanism, yet the ease of extractability implies weak binding. Molecular-scale information on interfacial reaction mechanisms of REEs is challenging to access via traditional approaches, such as X-ray absorption spectroscopy, because of the disordered nature of the first coordination shells of these elements and the weak spectral contributions of structural cations in clays.

We have applied element-specific, surface X-ray scattering techniques to probe the comparative binding of a light (Nd), middle (Dy), and heavy (Yb) REE to two crystallographic surfaces of alumina. The first surface, (001), is isostructural with basal plans of kaolinite and gibbsite, while the second, (012), serves as a reactivity proxy for the edges of these abundant clay minerals. When reacting individually with the (001) surface at pH 6.5 in a dilute NaCl fluid, light, middle, and heavy REEs show similar total binding. However, Nd adsorbs primarily via a direct, ligand-exchange reaction but outer-sphere adsorption, in which the REE retains its hydration shell, becomes increasingly important moving to middle and heavy REEs. This trend correlates with the increase in hydration energy across the REE series.

When all three elements co-adsorb to alumina (001), competitive effects create strong selectivity for Nd over Dy and Yb as well as the complete disappearance of all hydrated outer-sphere species (Fig. 1). In contrast, adsorption of Nd, Dy, and Yb to the alumina (012) surface shows minimal selective adsorption behavior and the formation of similar proportions of inner- and outer-sphere complexes for all three REEs (Fig. 1). We have also explored competitive adsorption of Nd, Dy, and Yb on the basal plane-like (001) surface of alumina under different chemical conditions. Lower REE concentration, lower pH (5.5), and a change to a $CaCl_2$ fluid all preserve the overall selectivity for light REEs via adsorption. The presence of citrate, and small organic acid common in weathering zones, enhances overall REE adsorption at pH 6.5 but still favors Nd over heavier REEs. This study reveals that specific mineral surfaces display distinct selective adsorption behavior, implying that chemical fractionation of REEs in weathering environments is affected by clay particle morphology, with secondary modulation by fluid composition.

REFERENCES

Estrade G., Marquis E., Smith M., Goodenough K., and Nason P. (2019) REE concentration processes in ion adsorption deposits: Evidence from the Ambohimirahavavy alkaline complex in Madagascar. *Ore Geology Reviews* **112**, 103027.

Li M.Y.H. and Zhou M.-F. (2020) The role of clay minerals in formation of the regolith-hosted heavy rare earth element deposits. *American Mineralogist* **105**, 92–108.

Li M.Y.H., Zhou M.-F., and Williams-Jones A.E. (2020) Controls on the dynamics of rare earth elements during subtropical hillslope processes and formation of regolith-hosted deposits. *Economic Geology* **115**, 1097–1118.

Moldoveanu G.A. and Papangelakis V.G. (2016) An overview of rare-earth recovery by ion-exchange leaching from ion-adsorption clays of various origins. *Mineralogical Magazine* **80**, 63–76.

Sanematsu K. and Watanabe Y. (2016) Characteristics and genesis of ion adsorption-type rare earth element deposits, In: Verplanck P.L. and Hitzman M.W. (Eds.), *Rare Earth and Critical Elements in Ore Deposits*. Society of Economic Geologists, pp. 55–79.

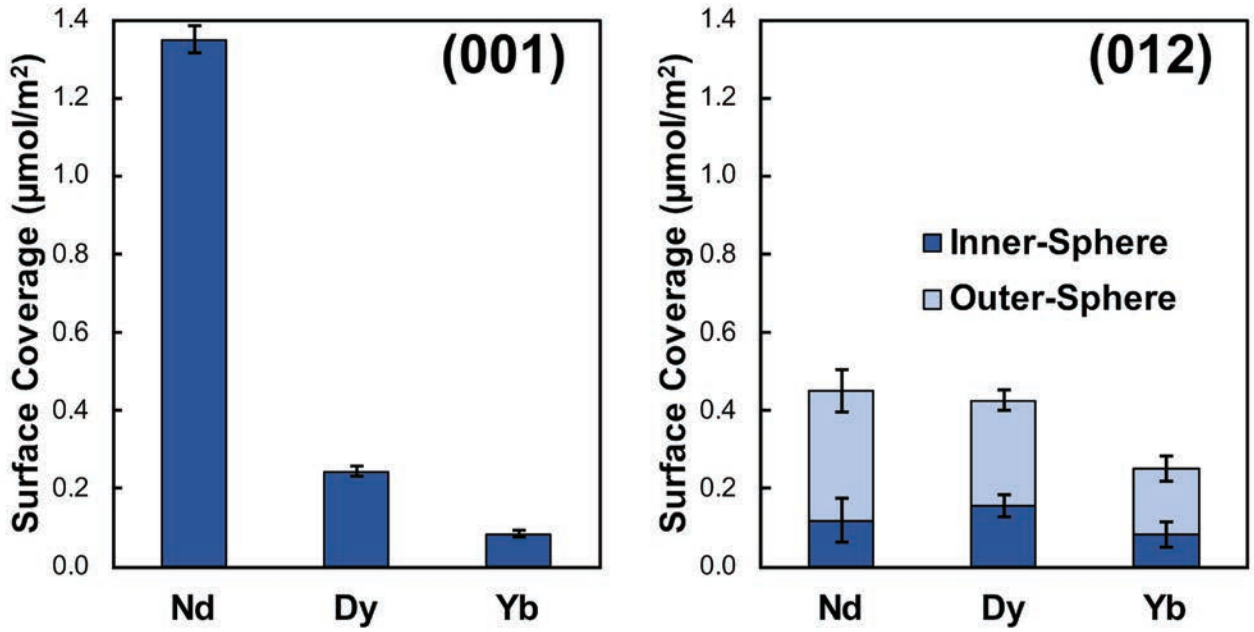

Figure 1. Surface coverage and distribution among inner-sphere (ligand-exchanged) and outer-sphere (fully hydrated) REE species on the basal-like (001) and edge-like (012) alumina surfaces at pH 6.5 in 10 mmol L^{-1} NaCl.

SPECIATION IN CARBONATITIC BRINE-MELTS AND FLUIDS FROM MOLECULAR SIMULATIONS

Jan Dreschmann[1], Sandro Jahn[1]

[1] Institute of Geology and Mineralogy, University of Cologne, Köln, Germany

In ore-forming environments such as the carbonatite system, fluids and melts play a crucial role in transporting metals such as rare earth elements (REE). Their chemical compositions vary throughout the system depending on several factors and can be accessed through experimental analysis of melt and fluid inclusions (Yaxley et al., 2022). However, to understand the transport dynamics, it is essential to gain insight into the molecular structure or speciation of melts and fluids, which are not directly accessible through fluid and melt inclusion studies. Here, molecular-scale simulations can provide important complementary information on the structure and thermodynamic properties of melts and fluids under ore-forming conditions. These conditions vary approximately from 700 to 1000 K and are present in the late-stage magmatic-hydrothermal carbonatite system represented by the model system H_2O-CO_2-Na_2CO_3-NaCl. Our simulations of this system are considering two main types of fluids: a higher density brine melt and a lower density hydrothermal fluid (Anenburg et al., 2021). The use of *ab initio* density functional theory (DFT; Marx and Hutter, 2009) calculations as well as the further development and use of existing reactive force fields (ReaxFF; van Duin et al., 2001), both in combination with the molecular dynamics approach, are required to accurately computationally describe the considered fluids. Here, we will present an outline of the recently started PhD project and preliminary results on structural and speciation data of the model system or of smaller subsystems contained within.

REFERENCES

Anenburg M., Broom-Fendley S., and Chen W. (2021) Formation of rare earth deposits in carbonatites. *Elements* **17**(5), 327–332.

van Duin, A. C. T., Dasgupta S., Lorant F., and Goddard W. A. (2001) ReaxFF: A reactive force field for hydrocarbons. *The Journal of Physical Chemistry A* **105**(41), 9396–9409.

Marx D. and Hutter J. (2009) *Ab Initio Molecular Dynamics: Basic Theory and Advanced Methods*. Cambridge, Cambridge University Press.

Yaxley G. M., Anenburg M., Tappe S., Decree S., and Guzmics T. (2022) Carbonatites: Classification, sources, evolution, and emplacement. *Annual Review of Earth and Planetary Sciences* **50**, 261–293.

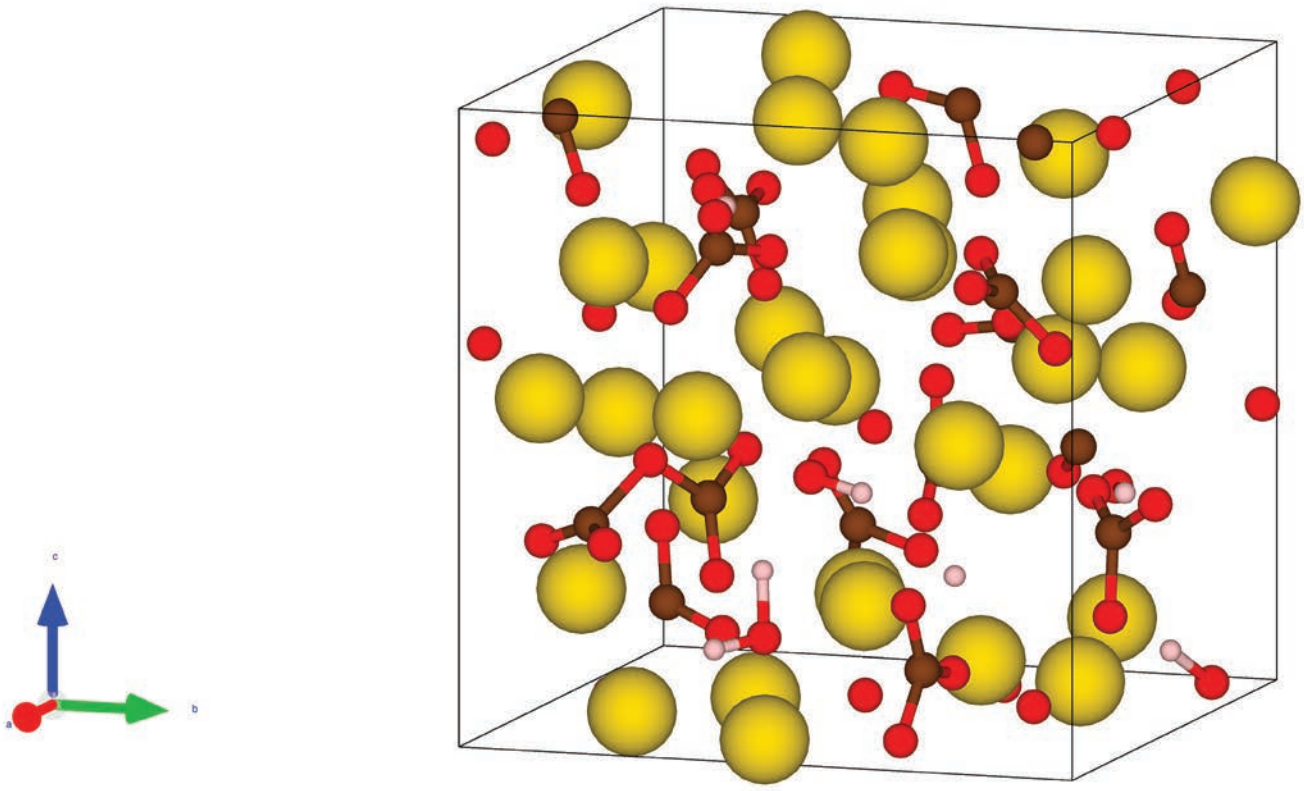

Figure 1. Snapshot from an *ab initio* molecular dynamics simulation of a hydrous Na_2CO_3 melt (Na – large yellow balls, O – red, C – brown, H – white).

INVESTIGATING THE INFLUENCE OF FLUID-ROCK INTERACTION IN THE FORMATION OF HIGH-TEMPERATURE HYDROTHERMAL VENT SITES: INSIGHTS FROM COUPLED NUMERICAL MODELING

Jasper Engelmann[1], Lars Rüpke[1], Zhikui Guo[1,2]

[1] GEOMAR Helmholtz Centre for Ocean Research Kiel, Germany

[2] Key Laboratory of Submarine Geosciences, MNR, Second Institute of Oceanography, China

Along mid-ocean ridges, seawater infiltrates and penetrates deep into the newly formed crust, generating hot, metal-bearing hydrothermal fluids. These fluids then rise up toward the ocean floor, continuously interacting with the surrounding rocks and facilitating the transport of both energy and chemistry. Most discharge is diffusive, where the hydrothermal fluids arrive at the surface already cooled by mixing with seawater in the surrounding rock. There are, however, many examples of highly localized discharge of hot hydrothermal fluids at small vent sites, such as the TAG hydrothermal field on the Mid-Atlantic Ridge, commonly forming black smoker chimneys on top of massive sulfide deposits. Despite much research being done on the topic, it remains unclear what mechanisms enable these hot fluids to reach the seafloor with little cooling by mixing with seawater.

Because *in situ* observation of these subsurface processes is not available, numerical fluid flow models offer a way to investigate the mechanisms behind these phenomena. Many previous studies have failed, however, to explain the occurrence of hot vents, predicting the mixing of fluids in the shallow oceanic crust and thus only low-temperature fluids reaching the surface.

A possible solution to this issue is presented here with the inclusion of fluid-rock interaction and reactive transport into existing models. In essence, the question is how the precipitation and dissolution of minerals in hydrothermal systems influences the permeability structure of the rock, thus potentially enhancing, channeling, or, in some cases, blocking flow within the system. On the base of the well-established open-source computational fluid dynamics platform OpenFOAM, we employ a special set of solvers for hydrothermal conditions and porous flow according to Darcy's law (Guo et al., 2020a).

Combining this with the equally open-source C++ library GEMS3K (Kulik et al., 2013), which uses Gibbs-energy minimization to predict the equilibrium composition of fluid and rock at every timestep, we can investigate the effects of chemical reactions on the flow beneath hydrothermal vents. In a simplified chemical system, we investigate the effects of the precipitation of anhydrite, which commonly occurs in almost monomineralic zones beneath seafloor massive sulfide deposits and has been shown to enable higher vent temperatures in previous numerical studies (Lowell et al., 2003; Guo et al., 2020b).

REFERENCES

Guo Z., Rüpke L., and Tao C. (2020a) HydrothermalFoam v1. 0: a 3-D hydrothermal transport model for natural submarine hydrothermal systems. *Geoscientific Model Development* **13**(12), 6547–6565.

Guo Z., Rüpke L. H., Fuchs S., Iyer K., Hannington M. D., Chen C., Tao C., and Hasenclever J. (2020b) Anhydrite-assisted hydrothermal metal transport to the ocean floor—Insights from thermo-hydro-chemical modeling. *Journal of Geophysical Research: Solid Earth* **125**(7), e2019JB019035.

Kulik D.A., Wagner T., Dmytrieva S. V., Kosakowski G., Hingerl F. F., Chudnenko K. V., and Berner U. R. (2013) GEM-Selektor geochemical modeling package: Revised algorithm and GEMS3K numerical kernel for coupled simulation codes. *Computational Geosciences* **17**, 1–24.

Lowell R. P., Yao Y., and Germanovich L. N. (2003) Anhydrite precipitation and the relationship between focused and diffuse flow in seafloor hydrothermal systems. *Journal of Geophysical Research: Solid Earth* **108.** B9.

REVISITING THE STANDARD PARTIAL MOLAL THERMODYNAMIC PROPERTIES OF ND^{3+} AND ND AQUEOUS SPECIES FROM 25 TO 250 °C

Yerko Figueroa Penarrieta[1,2], Alexander P. Gysi[1,2]

[1] New Mexico Bureau of Geology and Mineral Resources, New Mexico Institute of Mining and Technology, Socorro, NM 87801, USA
[2] Department of Earth and Environmental Science, New Mexico Institute of Mining and Technology, Socorro, NM 87801, USA

Rare earth elements (REE) play an important role in society due to their numerous industrial and environmental applications. Mineral deposits that contain REE commonly form through magmatic and hydrothermal processes (Gysi et al., 2016). Thermodynamic modeling provides important insights into the factors controlling the solubility, speciation, and mobility of REE in natural hydrothermal aqueous fluids (Migdisov et al., 2016; Pan et al., 2024). However, the accuracy of the predictions strongly depends on the underlying standard partial molal thermodynamic properties of the REE species. Previous experimental work on REE speciation has focused on the stability of REE chloride, sulfate, and fluoride complexes in acidic fluids. In contrast, the thermodynamic properties for the REE^{3+} aqua ion and REE hydroxyl complexes have not been revisited for over 25 years (Migdisov et al., 2016). In this study, we present new experimental data using hydrothermal solution calorimetry for determining the thermodynamic properties of the Nd^{3+} aqua ion and the Nd chloride complexes.

The enthalpy of solution ($\Delta_{sol}H°$) was measured using solution calorimetry (Fig. 1a) for the dissolution of solid Nd hydroxide in perchloric acid and solid Nd chloride in hydrochloric acid based aqueous solutions. The experiments were conducted from 25 to 150 °C using a starting pH of 2 and varying ionic strength (0.01 to 0.09 mol/kg $NaClO_4$; 0.05 to 0.35 mol/kg NaCl). The measured $\Delta_{sol}H°$ of Nd hydroxide solid (Fig. 1b) allowed us to determine the partial molal enthalpy of formation ($\Delta_fH°$), Gibbs energy of formation ($\Delta_fG°$), and heat capacity (C_p) of the Nd^{3+} aqua ion as a function of temperature. Comparison of the experiment heat capacity with calculated values using Helgeson-Kirkham-Flowers (HKF) equation of state (Shock et al., 1997) reveals accurate predictions for C_p. However, the $\Delta_fG°$ at reference conditions yields a $\Delta_fG°_{298}$ value of -679.7 ± 0.7 kJ/mol, which is ~8 kJ/mol more negative than listed by Shock et al. (1997). The same methodology was applied to Nd chloride calorimetric experiments, which results in measured $\Delta_{sol}H°$ ranging from -7.68 ± 2.1 to -20.48 ± 2.02 kJ/mol at 25 and 150 °C, respectively. These values differ by up to 25 kJ/mol in comparison to the predicted $\Delta_{sol}H°$ values calculated from available HKF parameters for the aqueous Nd chloride ($NdCl^{2+}$ or $NdCl_2^+$) species listed in Migdisov et al. (2016) combined with available literature data for the $NdCl_3$(s) solid. Hence, calorimetric experiments are needed to revise the enthalpy values for the REE chloride species and to allow better extrapolations to high temperatures.

The experimentally derived $\Delta_fG°$ of Nd^{3+} obtained in this study can be used to calculate the solubility of monazite (Fig. 1c). The resulting solubility increases by one order of magnitude in comparison to the predictions based on the $\Delta_fG°$ of Nd^{3+} from Shock et al. (1997). The updated thermodynamic properties for the Nd^{3+} results in an excellent agreement with the monazite solubility experimental data by Van Hoozen et al. (2020) measured up to 250 °C. Our results are also in good agreement with the thermodynamic dataset presented by Pan et al. (2024), which indicates that a correction is necessary for $\Delta_fG°_{298}$ values for all of the light REE in order to accurately reproduce the measured experimental monazite solubility.

REFERENCES

Gysi A. P., Williams-Jones A. E., and Collins P. (2016) Lithogeochemical vectors for hydrothermal processes in the Strange Lake peralkaline granitic REE-Zr-Nb deposit. *Economic Geology* **111**, 1241–1276.

Migdisov A., Williams-Jones A. E., Brugger J., and Caporuscio F. A. (2016) Hydrothermal transport, deposition, and fractionation of the REE: Experimental data and thermodynamic calculations. *Chemical Geology* **439**, 13–42.

Pan R., Gysi A. P., Miron G. D., and Zhu C. (2024) Optimized thermodynamic properties of REE aqueous species (REE^{3+} and $REEOH^{2+}$) and experimental database for modeling the solubility of REE phosphate minerals (monazite, xenotime, and rhabdophane) from 25 to 300 °C. *Chemical Geology* **643**, 121817.

Shock E. L., Sassani D. C., Willis M., and Sverjensky D. A. (1997) Inorganic species in geologic fluids: Correlations among standard molal thermodynamic properties of aqueous ions and hydroxide complexes. *Geochimica et Cosmochimica Acta* **61**, 907–950.

Van Hoozen C. J., Gysi A. P., and Harlov D. E. (2020) The solubility of monazite ($LaPO_4$, $PrPO_4$, $NdPO_4$, and $EuPO_4$) endmembers in aqueous solutions from 100 to 250 °C. *Geochimica Cosmochimica et Acta* **280**, 302–316.

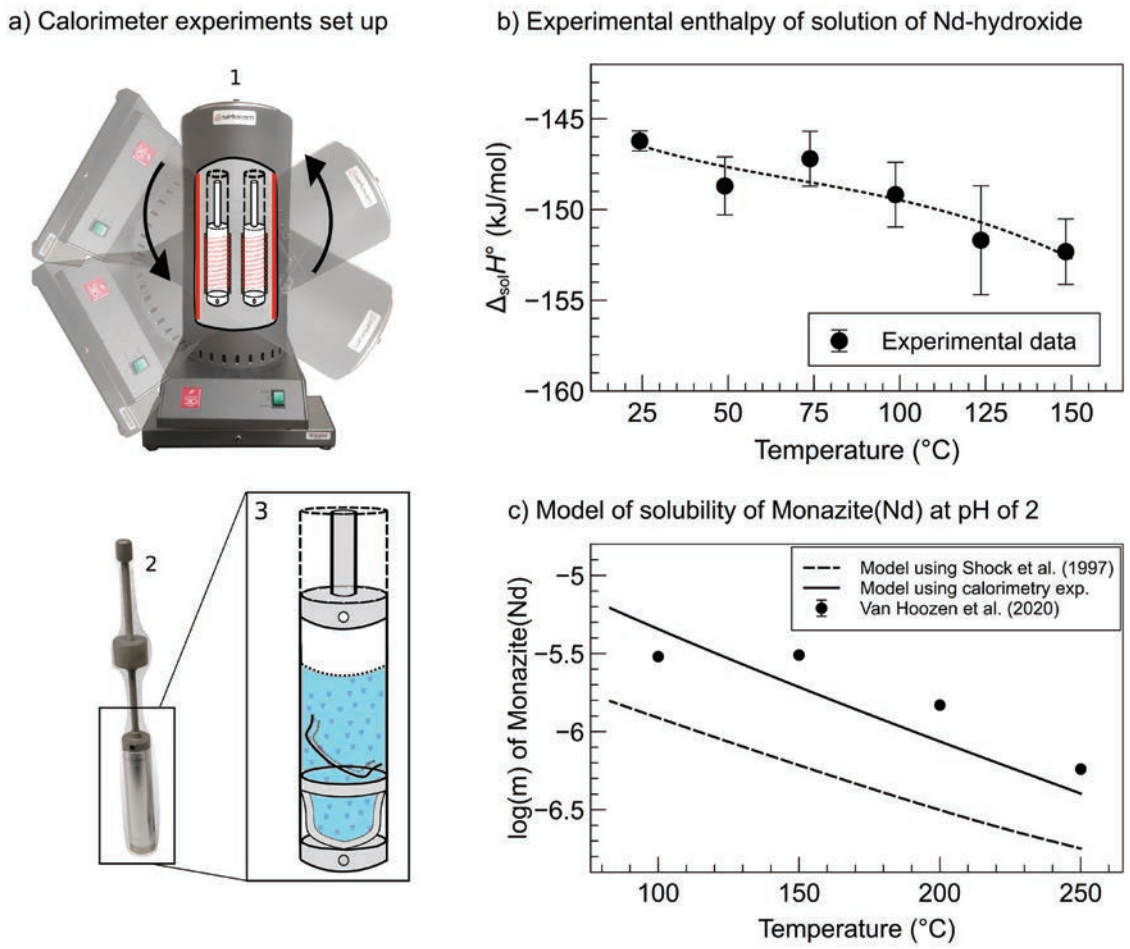

Figure 1. a) Calorimeter assembly and Hastelloy reaction cells: 1) Setaram C-80 solution calorimeter with rocking mechanism, 2) mixing reactor cell, 3) reacted experimental solution after rocking the calorimeter. b) Experimental enthalpy of solution of Nd hydroxide as a function of temperature. c) Thermodynamic model of the logarithm of the total Nd dissolved from monazite-(Nd) as a function of temperature.

MOLECULAR SIMULATIONS TO UNDERSTAND HOW CRITICAL METALS TRANSPORT IN HYDROTHERMAL FLUIDS

Qiushi Guan[1], Yuan Mei[1], Joël Brugger[2], Fang Huang[1], Weihua Liu[1]

[1] CSIRO Mineral Resources, Kensington, Australia
[2] Monash University, Clayton, Australia

Metals are transported within the deep earth at high pressure and temperature by fluids possessing a complex chemical composition. Reliable knowledge of metal behaviour in ore-forming fluids is essential for understanding the enrichment, transport, and precipitation of metals and the formation of ore deposits—we can predict how fluids of different compositions, pressures, and temperatures transport metals only if reliable thermodynamic properties are available. However, the understanding of the cycling of critical metals, elements with unsubstituted industrial application but uncertain supply, in geofluids is limited by a poor understanding of their behaviour compared with other major elements, which further limits our understanding of the formation of the related ore deposits.

The development of quantum chemistry approaches, especially the pseudopotentials within density functional theory (DFT) together with new generation force fields, have made molecular dynamics (MD) simulations a solid tool in studying the nature and thermodynamic properties of metal complexes in geofluids. In geochemistry, MD also helps with interpreting the experiments in the aspect of providing the knowledge of the basic features of metal complexation, i.e., the bond distances and coordination numbers. In the last 10 years, the combination of *in situ* X-ray absorption spectroscopy (XAS) and MD has been proven as a solid method to study the metal speciation in geochemical systems. The calculated geometries (metal-ion distance, coordination) from MD can be compared with the results of XAS, and the comparisons can help to identify speciation in solution (Brugger et al., 2016). In general, the results are in good agreement with the experiments.

In the past decade, *ab initio* MD (AIMD) simulations have dramatically improved our understanding of the chemical processes of metal transport in geofluids and offer the opportunity to achieve conditions that cannot be reached via the experimental approach. From our recent study of critical metal hydrothermal transport, we have obtained the thermodynamic properties of Y(III)-Cl^- (Guan et al., 2020), Y(III)-SO_4^{2-} (Guan et al., 2022a), La(III)-Cl^- (Guan et al., 2022b), and Mo(VI)-Cl^- (Guan et al., 2023) at temperature up to 500–700 °C. The data produced by MD allow accurate modelling of metal transport in ore-forming processes, which promotes the understanding of ore-forming processes.

Although AIMD provides molecular-level understanding about metal behaviour at extreme conditions, the performance of AIMD is constrained by computational capacity. Recently, we employed a new automatic workflow accelerated by machine learning potentials to calculate thermodynamic properties (Wang and Cheng, 2022). Within this workflow, the calculation was accelerated by machine learning potentials from a concurrent learning scheme, within the accuracy of AIMD level, which enables a much longer time scale at lower CPU costs. A case study of the calculation of the acidic constants (pKa) of hydrofluoric acid and the thermodynamic properties of metal complex using enhanced sampling method will be presented. This will enable the geochemical simulations to a much larger size and longer time scales.

REFERENCES

Brugger J., Liu W., Etschmann B., Mei Y., Sherman D. M., and Testemale D. (2016). A review of the coordination chemistry of hydrothermal systems, or do coordination changes make ore deposits?. *Chemical Geology* **447**, 219–253.

Guan Q., Mei Y., Etschmann B., Testemale D., Louvel M., and Brugger J. (2020). Yttrium complexation and hydration in chloride-rich hydrothermal fluids: A combined ab initio molecular dynamics and in situ X-ray absorption spectroscopy study. *Geochimica et Cosmochimica Acta* **281**, 168–189.

Guan Q., Mei Y., Etschmann B., Testemale D., Louvel M., and Brugger J. (2022a) Yttrium speciation in sulfate-rich hydrothermal fluids. *Geochimica et Cosmochimica Acta* **325**, 278–295.

Guan Q., Mei Y., Etschmann B., Testemale D., Louvel M., and Brugger J. (2022b) Speciation and thermodynamic properties of La(III)-Cl complexes in hydrothermal fluids: A combined molecular dynamics and in situ X-ray absorption spectroscopy study. *Geochimica et Cosmochimica Acta* **330**, 27–46.

Guan Q., Mei Y., Liu W., and Brugger J. (2023). Different metal coordination in sub-and super-critical fluids: Do molybdenum (IV) chloride complexes contribute to mass transfer in magmatic systems?. *Geochimica et Cosmochimica Acta* **354**, 240–251.

Wang F. and Cheng J. (2022). Automated workflow for computation of redox potentials, acidity constants, and solvation free energies accelerated by machine learning. *The Journal of Chemical Physics* **157**(2).

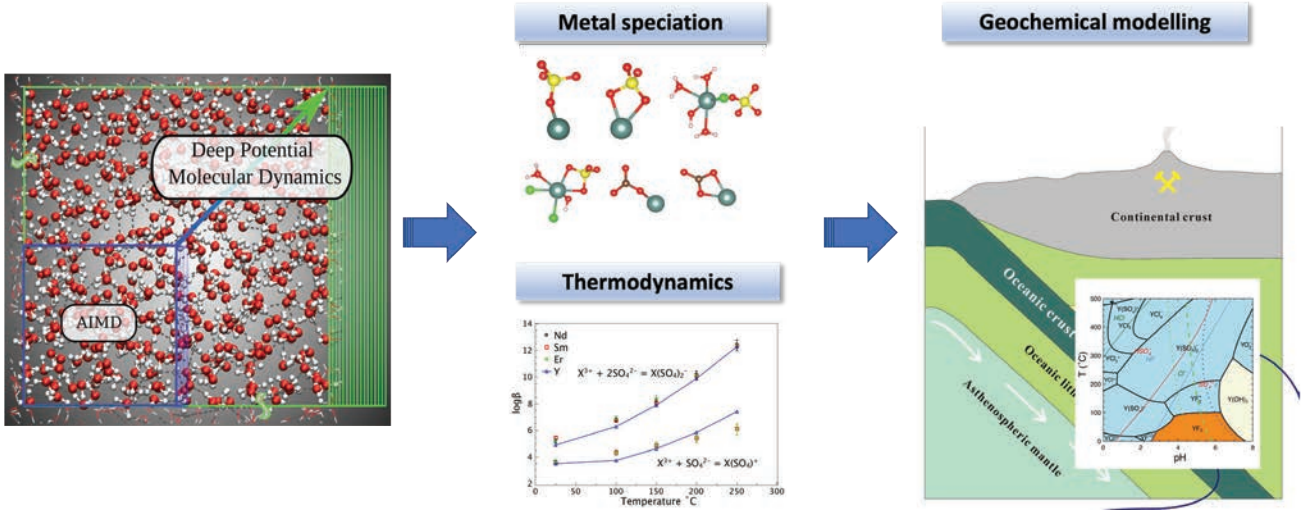

Figure 1. Molecular modelling to understand critical metals in hydrothermal fluids.

EXPERIMENTAL THERMODYNAMIC STUDIES ON MIXING MODELS OF REE MINERAL PHASES

Xiaofeng Guo[1]

[1] Department of Chemistry, Washington State University, Pullman, WA 99163, USA

Rare earth element (REE) ores are commonly associated with enrichment in U and Th and form solid solutions. Accurately predicting their formation, transport, and alteration requires descriptions of their mixing. It is also important to be able to predict conditions under which An-depleted ores are formed. However, our understanding of the mixing thermodynamics of various REE with or without U/Th in mineral phases is still incomplete. Conventionally, the mixing of various REE is assumed to be ideal and described by the random distribution or regular solution models. Although being a convenient model used for geochemical modeling, its application in REE hydrothermal systems may yield incorrect or inaccurate geochemical predictions. In this talk, we will present three case studies of non-ideal mixing and its impacts on REE mineralization and fractionation in solid phases. In the first case, we examined the thermodynamics of LREE binary hydroxylbastnäsite solid solutions (Goncharov et al., 2022); in the second case, we measured the enthalpies of mixing of HREE binary xenotime solid solutions, which have positive enthalpies of mixing and lead to miscibility gaps at low temperatures (Strzelecki et al., 2022). Preliminary results of multiple REE phosphate will also be shown. In the last case, we showed that the mixing of U and Th in uranothorite (isostructural to REE xenotime phosphates) has a negative enthalpic effect and can only be described by a subregular solid solution model (Marcial et al., 2021; Strzelecki et al., 2024). The consequence of the non-ideal mixing is an extended phase boundary in terms of temperature and oxygen fugacity, where pure U endmember (coffinite) is unstable. These cases highlight the importance of correctly accounting for the non-ideal mixing effects in the accurate prediction of phase boundary and mineral behavior under hydrothermal systems, which will enable further development of new exploration techniques permitting the identification and localization of REE-fractioned or Th- and U-depleted REE ore deposits.

REFERENCES

Goncharov V. G., Nisbet H., Strzelecki A., Benmore C. J., Migdisov A. A., Xu H., and Guo X. (2022) Energetics of hydroxylbastnäsite solid solutions, $La_{1-x}Nd_xCO_3OH$. *Geochimica et Cosmochimica Acta* **330**, 47–66. https://doi.org/10.1016/j.gca.2022.04.002

Marcial J., Zhang Y., Zhao X., Xu H., Mesbah A., Nienhuis E. T., Szenknect S., Neuefeind J. C., Lin J., Qi L., Migdisov A. A., Ewing R. C., Dacheux N., McCloy J. S., and Guo X. (2021) Thermodynamic non-ideality and disorder heterogeneity in actinide silicate solid solutions. *Npj Materials Degradation* **5**(1), 34. https://doi.org/10.1038/s41529-021-00179-0

Strzelecki A. C., Reece M., Zhao X., Yu W., Benmore C., Ren Y., Alcorn C., Migdisov A., Xu H., and Guo X. (2022) Crystal chemistry and thermodynamics of HREE (Er, Yb) mixing in a xenotime solid solution. *ACS Earth and Space Chemistry* **6**(5), 1375–1389. https://doi.org/10.1021/acsearthspacechem.2c00052

Strzelecki A. C., Zhao X., Estevenon P., Xu H., Dacheux N., Ewing R. C., and Guo X. (2024) Crystal chemistry and thermodynamic properties of zircon structure-type materials. *American Mineralogist* **109**(2), 225–242. https://doi.org/10.2138/am-2022-8632

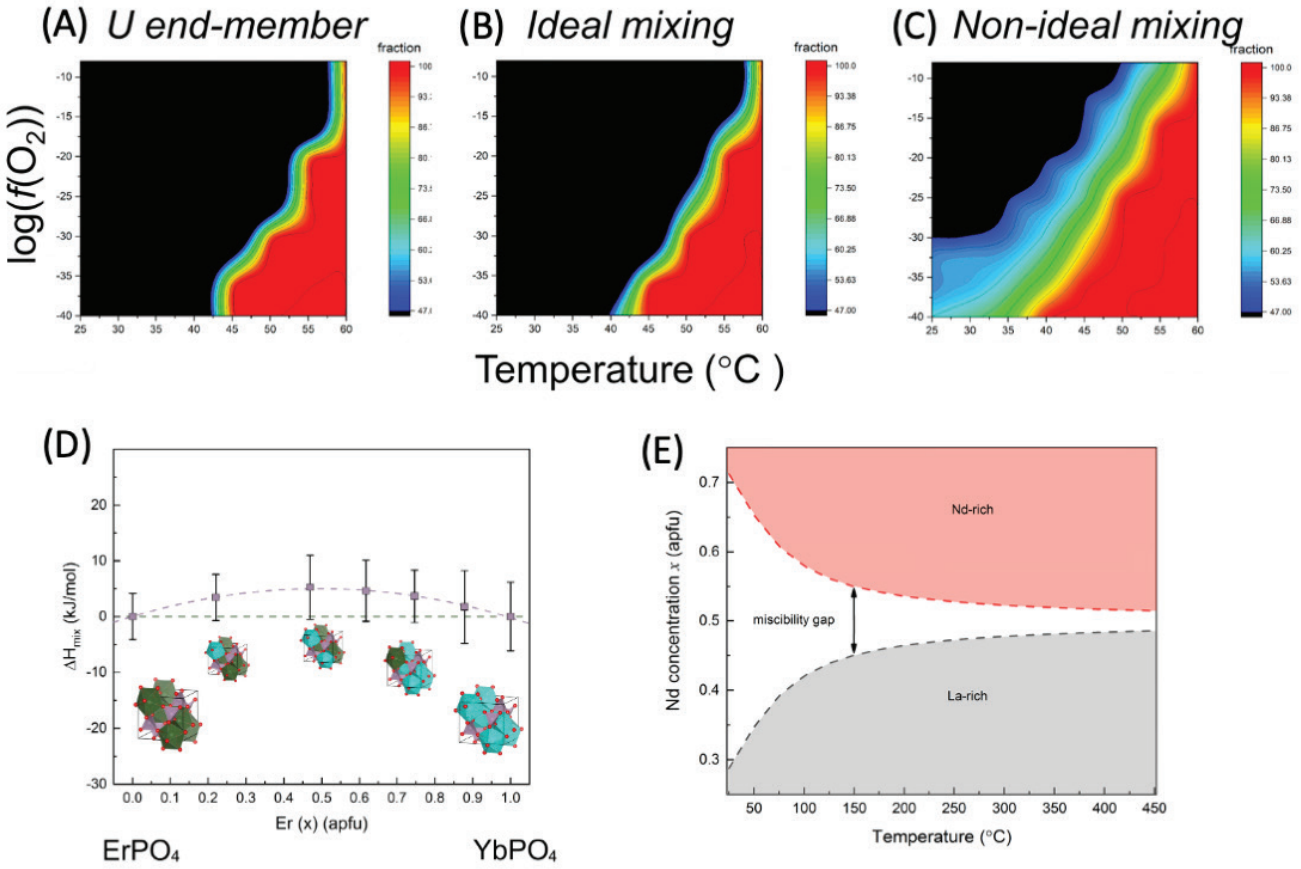

Figure 1. (A–C) The comparison of various mixing models of U-Th in zircon phase. (D) The measured enthalpy of mixing of Er-Yb in xenotime phase. (E) The miscibility gap in the La-Nd hydroxylbastnäsite revealed by the experimental calorimetry.

HYDROTHERMAL MOBILIZATION, FRACTIONATION, AND MINERALIZATION OF REE IN CRITICAL MINERAL DEPOSITS: A HOLISTIC APPROACH COMBINING FIELD OBSERVATIONS, EXPERIMENTS, AND MODELING

Alexander P. Gysi[1,2], Nicole C. Hurtig[2], Hannah J. Han[1], Bryan J. Maciag[1], Sarah E. Smith-Schmitz[1]

[1] New Mexico Bureau of Geology and Mineral Resources, New Mexico Institute of Mining and Technology, Socorro, NM 87801, USA
[2] Department of Earth and Environmental Science, New Mexico Institute of Mining and Technology, Socorro, NM 87801, USA

The rare earth elements (REE) play an important role in society due to their applications in the green energy and high-tech industries. Magmatic-hydrothermal REE mineral deposits are commonly overprinted by hydrothermal fluids capable of mobilizing and fractionating the REE (Gysi et al., 2016). The formation of aqueous REE complexes controls these processes, which strongly depend on temperature, pressure, and fluid chemistry. Geochemical modeling allows simulation of the speciation and solubility of REE in those fluids (Migdisov et al., 2016). Ligands that complex with the REE include Cl^-, F^-, and SO_4^{2-} in acidic fluids, whereas OH^- and other ligands control the mobility of REE in more alkaline fluids.

Here we present a holistic approach to understanding the behavior of REE in critical mineral deposits based on field observations, laboratory experiments, and thermodynamic modeling (Fig. 1). The Ore Deposits and Critical Minerals laboratory was established at the New Mexico Bureau of Geology to determine the thermodynamic properties of aqueous complexes and minerals in hydrothermal fluids. Current work focuses on the properties of REE and includes solubility, potentiometric, calorimetric, and *in situ* spectroscopic (UV-Vis and Raman) experiments. A series of experiments are used to study the stability of REE^{3+} aqua ion and REE hydroxyl complexes from acidic to alkaline pH between 100 and 300 °C, including (i) REE hydroxide solubility and potentiometric measurements using a hydrothermal Zr/Zr-oxide pH electrode system, (ii) heat of solution calorimetry of REE hydroxide dissolution, and (iii) UV-Vis spectrophotometry for determination of *in situ* pH and REE hydroxyl coordination. This setup allows retrieving the equilibrium constants (i.e., log$K$) for mineral solubilities and REE complexes, and the standard thermodynamic properties for these species as a function of temperature (i.e., $\Delta_f G°$, $\Delta_f H°$, and $\Delta Cp°$). Another series of monazite and xenotime solubility experiments and *in situ* Raman spectroscopic measurements (HDAC and quartz capillary cells) of REE sulfate/chloride-bearing solutions are used to study the stability of REE chloride, sulfate, and hydroxyl complexes at high temperatures (350–500 °C) to supercritical conditions.

The experimental data indicate that the $\Delta_f G°$ and $\Delta_f H°$ values of the REE^{3+} aqua ions and hydroxyl complexes differ by up to 10–20 kJ/mol in comparison to the extrapolated values used in the literature. Furthermore, the predicted REE chloride speciation based on thermodynamic data derived by Migdisov et al. (2016) remains accurate in acidic fluids up to ~400–450 °C. However, the measured solubility of REE phosphates is ~3–5 orders of magnitude higher than the modeled predictions at higher temperature. The models and experimental data diverge with increased pH, indicating a need to revise the thermodynamic properties

of REE^{3+} and the REE hydroxyl complexes, which can account for the fractionation of light versus heavy REE.

Here, we integrate this wide array of experimental data into a new open access experimental dataset (Pan et al., 2024), and demonstrate thermodynamic optimization methods to more accurately simulate the stability of REE complexes at conditions relevant to ore-forming systems. The thermodynamic data generated are implemented in the MINES thermodynamic database (Gysi et al., 2023), which is available open access for modeling the mobility of critical elements in hydrothermal systems. We present here a natural analogue application from the Gallinas Mountains hydrothermal fluorite vein/breccia deposit in New Mexico. This example is used to simulate a reactive transport model using the GEMS code package (https://gems.web.psi.ch/) and demonstrate possible controlling factors for REE mobilization during the formation of fluorite-bastnäsite veins during hydrothermal fluid-rock interaction.

This work is supported by the U.S. Department of Energy, Office of Sciences, Basic Energy Science, Geosciences, under Awards DE-SC0021106 and DE-SC0022269.

REFERENCES

Gysi A. P., Williams-Jones A. E., and Collins P. (2016) Lithogeochemical vectors for hydrothermal processes in the Strange Lake peralkaline granitic REE-Zr-Nb deposit. *Economic Geology* **111**, 1241–1276.

Gysi A. P., Hurtig N. C., Pan R., Miron G. D., and Kulik D. A. (2023) https://doi.org/10.58799/mines-tdb

Migdisov A., Williams-Jones A. E., Brugger J., and Caporuscio F. A. (2016) Hydrothermal transport, deposition, and fractionation of the REE: Experimental data and thermodynamic calculations. *Chemical Geology* **439**, 13–42.

Pan R., Gysi A. P., Miron G. D., and Zhu C. (2024) Optimized thermodynamic properties of REE aqueous species (REE^{3+} and $REEOH^{2+}$) and experimental database for modeling the solubility of REE phosphate minerals (monazite, xenotime, and rhabdophane) from 25 to 300 °C. *Chemical Geology* **643**, 121817.

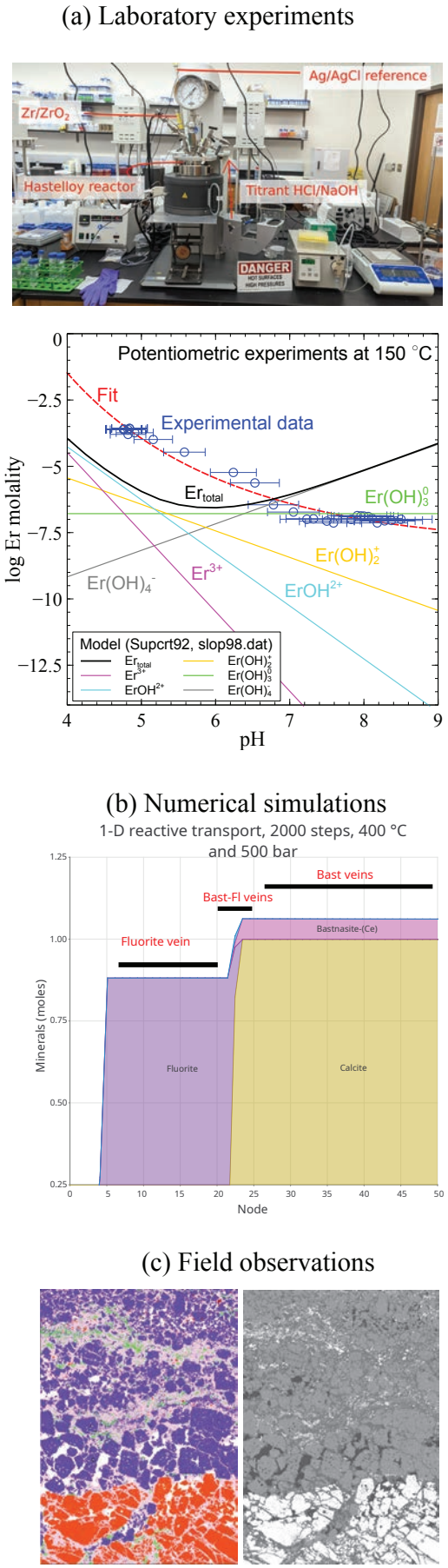

Figure 1. Integration of laboratory experiments, numerical simulations, and field observations to study the behavior of REE in hydrothermal fluids. (a) Potentiometric experiments conducted at 150 °C, showing discrepancies between previous modeling predictions and the measured Er solubility. (b) 1-D reactive transport model simulated using GEMS showing the formation of calcite-, fluorite-, and bastnäsite-bearing hydrothermal veins. (c) Automated mineralogy map and BSE image of a barite-fluorite and bastnäsite veins from the Gallinas Mountains, New Mexico.

UV-VIS SPECTROPHOTOMETRIC DETERMINATION OF THE HYDROLYSIS OF ERBIUM IN NEAR NEUTRAL TO ALKALINE AQUEOUS SOLUTIONS FROM 25 TO 75°C

Hannah Juan Han[1], Alexander P. Gysi[1,2]

[1] New Mexico Bureau of Geology and Mineral Resources, New Mexico Institute of Mining and Technology, Socorro, NM 87801, USA
[2] Department of Earth and Environmental Science, New Mexico Institute of Mining and Technology, Socorro, NM 87801, USA

Rare earth elements (REE) have gained an increased interest in society because of their magnetic, optical, electrical, and catalytic properties. The increased demand for REE has led to a need for a better understanding of their behavior in natural geologic systems and for the development of new separation technologies. Thermodynamic modeling provides important insights into the factors controlling the mobility and fractionation of REE in aqueous fluids. The latter largely depends on the stability of aqueous REE complexes. However, our knowledge on the stability of REE hydroxyl complexes in near-neutral to alkaline aqueous fluids is still entirely based on the extrapolations generated by Haas et al. (1995).

UV-Vis spectrophotometric experiments (Figs. 1a and 1b) were conducted to determine the Er^{3+} hydrolysis constants from 25 to 75 °C and pH from ~6.5 to 9.5. The color indicator *m*-cresol purple (mCP) is used to determine *in situ* pH and derive the Er hydrolysis constants based on the method developed at 25 °C by Stepanchikova et al. (2011). The optical properties and dissociation constant of mCP were determined from 25 to 75 °C in quartz cells using a Peltier temperature controller. All the experiments were conducted in NaOH-H_2O-mCP solutions. Addition of 0 to 0.253 mmol/kg Er to the solutions results in a proton release and decrease in pH because of the hydrolysis reaction for Er^{3+} according to: $Er^{3+} + nH_2O = Er(OH)_n^{3-n} + nH^+$. The mCP absorbance intensity of the basic form (I^{2-}) gradually decreases and the acidic form (HI^-) increases with the hydrolysis of Er (Fig. 1c). *In situ* pH determined using the UV-Vis/mCP methods permits calculating the average OH^- ligand number, which reflects the OH^- coordinated to Er^{3+} by averaging each contributing hydroxyl species. These values were used to derive the Er hydrolysis constants (β_n, n = 1 to 4) for all of the Er hydroxyl species.

The experimental results indicate an average OH^- ligand number that increases from ~1.0 to 2.5 at 25 °C (pH of 7.2–9.5) and from ~1.2 to 3.2 at 75 °C (pH of ~6.5–9.0). These results suggest that $Er(OH)^{2+}$, $Er(OH)_2^+$, and $Er(OH)_3^0$ are predominant at the experimental conditions, with an increase in stability of $Er(OH)_3^0$ over $Er(OH)_2^+$ from 25 to 75 °C. The $Er(OH)_4^-$ species appears to become stable at 75 °C, which is reflected by an increase in the average ligand number. The retrieved Er hydrolysis constants from 25 to 75 °C yield logβ values of -7.57 ± 0.04 for $Er(OH)^{2+}$, 14.59 ± 0.27 for $Er(OH)_2^+$, and increase from -23.24 ± 0.04 to 21.99 ± 0.02 for $Er(OH)_3^0$ and from -33.07 ± 0.15 to -30.78 ± 0.11 for $Er(OH)_4^-$.

Geochemical modeling of Er speciation was carried out as a function of pH at 25 °C using the GEMS code package (Kulik et al., 2013) and the MINE thermodynamic database (Gysi et al., 2023). A comparison between the speciation simulations based on the hydrolysis constants derived in this study and the predictions based on thermodynamic data derived by Haas et al. (1995) indicates a higher stability of the $Er(OH)_2^+$ and $Er(OH)_3^0$ over the $Er(OH)_4^-$ species in near-neutral to alkaline fluids. These speciation results have important implications for accurately simulating the REE adsorption behavior in groundwater of regolith-hosted ion adsorption deposits. Our results

suggest that the charged $REE(OH)_2^+$ species could play an important role for REE adsorption on clay mineral surfaces at near-neutral conditions.

This work is supported by the U.S. Department of Energy under Award DE-SC0021106.

REFERENCES

Gysi A. P., Hurtig N. C., Pan R., Miron G. D., and Kulik D. A. (2023) MINES Thermodynamic Database, https://doi.org/10.58799/mines-tdb.

Haas J. R., Shock E. L., and Sassani D. C. (1995) Rare earth elements in hydrothermal systems: Estimates of standard partial molal thermodynamic properties of aqueous complexes of the rare earth elements at high pressures and temperatures. *Geochimica et Cosmochimica Acta* **59**, 4329–4350.

Kulik D. A., Wagner T., Dmytrieva S. V., Kosakowski G., Hingerl F. F., Chudnenko K. V., and Berner U. R. (2013) GEM-Selektor geochemical modeling package: Revised algorithm and GEMS3K numerical kernel for coupled simulation codes. *Computational Geosciences* **17**, 1–24.

Stepanchikova S. A. and Biteikina R. P. (2011) Spectrophotometric study of rare-earth element complexation in alkaline and near-neutral solutions. *Russian Journal of Coordination Chemistry* **37**, 64–71.

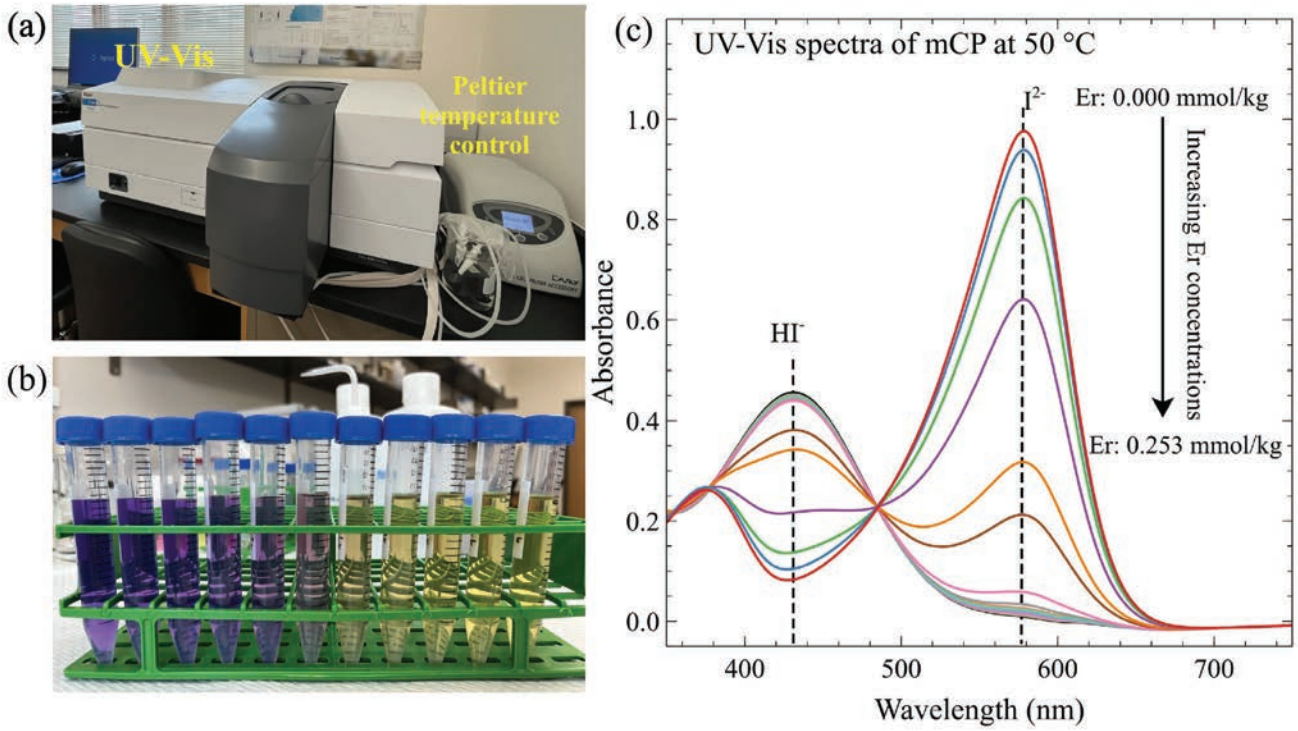

Figure 1. (a) Experimental setup for the determination of the hydrolysis constants of Er on the UV-Vis spectrophotometer at 25-75 °C. (b) The photograph of 0.030 mmol/kg meta-cresol purple (mCP) in the 0.445 mmol/kg NaOH with variable Er concentrations (left to right: low Er concentration to high Er concentration). (c) UV-Vis spectra of mCP (0.030 mmol/kg) in 0.445 mmol/kg NaOH with addition of varying Er concentrations ranging from 0.000 to 0.253 mmol/kg at 50 °C.

FLUID-AIDED REE AND ACTINIDE MOBILITY IN PHOSPHATE MINERALS: NATURE AND EXPERIMENT

Daniel Harlov[1]

[1] Deutsches GeoForschungsZentrum GFZ, Telegrafenberg, 14473 Potsdam, Germany

Rare earth element (REE)-bearing phosphate minerals, such as apatite [$Ca_{10}(PO_4)_6(OH,F,Cl)_2$], monazite [$(Ce,La,Nd,Th)(PO_4,SiO_4)$], and xenotime [$(Y,HREE,U)(PO_4,SiO_4)$], are primary hosts for REE, Th, and U in the Earth's crust and lithospheric mantle.

Apatite, as the most common phosphate mineral in the Earth's crust and lithospheric mantle, can act as a major reservoir for P, F, Cl, OH, CO_2, and REE as well as serve as a powerful thermochronometer (Chew and Spikings, 2015). Apatite can be chemically altered by aqueous brines (NaCl-KCl-$CaCl_2$-H_2O), pure H_2O, and aqueous fluids, which contain CO_2, HCl, H_2SO_4, and/or F (Harlov et al., 2003, 2005). It can also react with and be assimilated in peraluminous granitic magmas (Clarke et al., 2023). As such, apatite can be used for tracking the presence and chemistry of these fluids and melts during different metasomatic and igneous events over the histories of common metamorphic and igneous rocks, as well as apatite-bearing ore deposits. Metasomatically induced re-equilibration of apatite, and its relationship to other minerals in the rock, can provide important information regarding Cl, F, OH, CO_2, SO_2, and REE mass transfer; the chemistry of the fluids; the temperature during re-equilibration; as well as the time of the metasomatic event (Mair et al., 2017a). This is especially evident in metasomatic disturbances of the Sm-Nd and Sr isotopic systems in apatite as experimentally determined by Li et al. (2022a, 2022b). Hence, apatite can serve as a fingerprint for metasomatic and igneous processes in igneous rocks, metamorphic rocks, and ore deposits, which commonly manifests itself in the formation of monazite and xenotime inclusions in the apatite (Harlov, 2015).

Thorium, U, and Pb in these monazite and xenotime inclusions and rim grains allow for the metasomatic event to be dated. Monazite and xenotime form a very limited solid solution, which, when found together, allow for a geothermometer to be calibrated (Gratz and Heinrich, 1997). Monazite and xenotime are also principal hosts for Th and U, with monazite preferring to host Th over U and xenotime preferring to host U over Th, especially if the monazite and xenotime are co-existing in the same rock. Metasomatic incorporation of Th in monazite and xenotime utilizing alkali-bearing fluid has been experimentally demonstrated by Harlov et al. (2011) and Harlov and Wirth (2012), respectively (Fig. 1). In the case of monazite, Pb has experimentally been shown to be completely removed from the altered monazite metasomatically by alkali-bearing fluids, thereby resetting the monazite geochronometer (Williams et al., 2011). Uranium can also be metasomatically incorporated into xenotime using alkali-bearing fluids, as has been experimentally demonstrated by Harlov (2024). Lastly, dissolution experiments at 800 °C and 1000 MPa in a variety of NaCl-, KCl-, and NaF-bearing fluids involving monazite (Tropper et al., 2011; Mair et al., 2017b) and xenotime (Tropper et al., 2013; Mair et al., 2017b) have been made regarding the mobility of LREE and HREE in Cl- and F-bearing fluids. Here, the LREE are found to be more mobile in Cl-bearing fluids, whereas HREE are found to show greater mobility in the F-bearing fluids.

REFERENCES

Chew D. M. and Spikings R. A. (2015) *Elements* **11**, 189–194.

Clarke D. B., Harlov D. E., Brenan J. M., Jähkel A., Cichy S. B., Wilke F. D. H., and Yang X. *American Mineralogist* **108**, 1421–1435.

Gratz R. and Heinrich W. (1997) *American Mineralogist* **82**, 772–780.

Harlov D. E. (2015) *Elements* **11**, 171–176.

Harlov D. E. (2024) *Chemical Geology* (in press).

Harlov D. E. and Förster H. J. (2003) *American Mineralogist* **88**, 1209–1229.

Harlov D. E. and Wirth R. (2012) *American Mineralogist* **97**, 641–652.

Harlov D. E., Wirth R., and Förster H.-J. (2005) *Contributions to Mineralogy and Petrology* **150**, 268–286.

Harlov D. E., Wirth R., and Hetherington C. J. (2011) *Contributions to Mineralogy and Petrology* **162**, 329–348.

Li X.-C., Harlov D. E., Zhou M.-F., and Hu H. (2022a) *Geochimica et Cosmochimica Acta* **323**, 123–140.

Li X.-C., Harlov D. E., Zhou M.-F., and Hu H. (2022b) *Geochimica et Cosmochimica Acta* **330**, 191–208.

Mair P., Tropper P., Harlov D. E., and Manning C. E. (2017a) *Chemical Geology* **470**, 180–192.

Mair P., Tropper P., Harlov D. E., and Manning C. E. (2017b) *American Mineralogist* **102**, 2457–2466.

Tropper P., Manning C. E., and Harlov D. E. (2011) *Chemical Geology* **282**, 58–66.

Tropper P., Manning C. E., and Harlov D. E. (2013) *Geofluids* **13**, 372–380.

Williams M. L., Jerconovic M. J. Harlov D. E., Budzyn B., and Hetherington C. J. (2011) *Chemical Geology* **283**, 218–225.

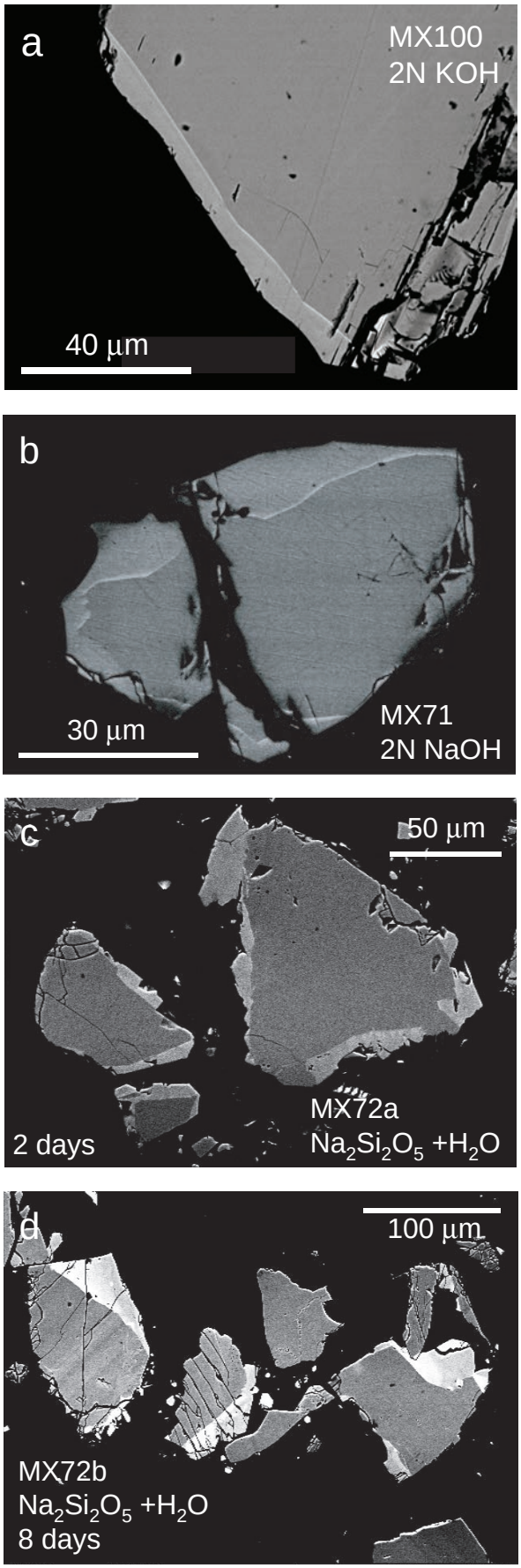

Figure 1. Examples of monazite grains experimentally metasomatized at 900°C and 1000 MPa using a CaF_2 assembly in the piston cylinder press from Harlov et al. (2011). Any cracks seen occurred during the mounting and polishing process of the monazite grain fragments. a. MX100: Monazite grain metasomatized in a 2N KOH solution for 8 days. b. MX71: Monazite grain metasomatized in a 2N NaOH solution for 25 days. c. MX72a: Monazite grain metasomatized in a $Na_2Si_2O_5$ + H_2O solution for 2 days. d. MX72b: Monazite grain metasomatized in a $Na_2Si_2O_5$ + H_2O solution for 8 days.

RARE EARTH ELEMENT COORDINATION CHEMISTRY USING IN SITU RAMAN SPECTROSCOPY

Nicole C. Hurtig[1], Alexander P. Gysi[1,2], Sarah E. Smith-Schmitz[2], Bryan J. Maciag[2]

[1] Department of Earth and Environmental Science, New Mexico Institute of Mining and Technology, Socorro, NM 87801, USA
[2] New Mexico Bureau of Geology and Mineral Resources, New Mexico Institute of Mining and Technology, Socorro, NM 87801, USA

Rare earth elements (REE) are critical elements important for society due to their use in the high-tech and green energy industries. They are economically enriched in magmatic-hydrothermal ore deposits, where they are hosted in phosphate, carbonate, fluoride, and zirconosilicate minerals. Hydrothermal fluids are important for high degrees of REE enrichment by increasing the mobility of REE in solution when complexing with ligands such as chloride, sulfate, and hydroxyl anions. Our capability to predict REE mobility in supercritical fluids is limited by the availability of thermodynamic and experimental data, which are often sparse and exist only for temperatures below 300 °C. Furthermore, REE complexation with chloride, sulfate, and hydroxyl ligands at high temperatures is not well understood, presenting a significant knowledge gap when it comes to understanding the formation conditions and stability of these REE aqueous species. Confocal Raman spectroscopy is a powerful tool to investigate REE complexation chemistry at the molecular level, and if combined with different experimental techniques, such as capillary Raman cells and hydrothermal diamond anvil cells (HDAC), applications can be expanded into the high T-P range of crustal fluids.

Here we use a Horiba LabRAM HR Evolution confocal Raman microscope equipped with a 532 nm Nd-YAG laser (100 mW) and a 266 nm DPSS UV (50 mW) laser to measure the spectra of high purity (>99.99%) synthetic REE solids and REE-bearing aqueous solutions with variable pH and salinity. Solutions are measured at room temperature and using a capillary cell up to 300 °C and a HDAC up to 500 °C. REE-O coordination chemistry was explored using REE sesquioxides with A-, B-, and C-type structures as well as REE hydroxides (Fig. 1). A-type sesquioxides have a hexagonal structure where REE-O polyhedra are coordinated 7-fold (Atkinson, 2013). B-type sesquioxides are monoclinic and show 6- and 7-fold coordinated REE-O polyhedral. C-type sesquioxides are cubic and show 6-fold coordinated REE-O polyhedra (Atkinson, 2013). In hydroxides, REE-O are coordinated 9-fold (Beall et al., 1977). The Raman band most prominently associated with the main REE-O vibrational energy ranges from 400–432 cm^{-1} in A-type oxides, 362–386 cm^{-1} and 411–430 cm^{-1} in B-type oxides, 339–420 cm^{-1} in C-type oxides, and 450–506 cm^{-1} in trihydroxides (Fig. 1a). These bands systematically shift to higher wavenumbers with decreasing ionic radii of the lanthanide series within their isostructural groups (Fig. 1b), indicating that this band is sensitive to small changes in bond chemistry and vibrational energies, which can be detected using Raman spectroscopy. In aqueous solutions, the REE-O band is generally found at ~370 cm^{-1} for Dy-O (Rudolf and Irmer, 2020) and at ~300 cm^{-1} for Nd-O, indicating that REE-O coordination chemistry can be described in aqueous solutions. Other REE species that were successfully identified using Raman spectroscopy include Dy- and Nd-chloride complexes at 200–240 cm^{-1}, Nd- and Yb-sulfate species at 980–996 cm^{-1} (Wan et al., 2021), and Yb-bisulfate complexes at 1046 cm^{-1}.

In conclusion, Raman spectroscopy is an excellent tool for investigating REE complexation chemistry in aqueous solutions, providing great detail on coordination chemistry at the molecular level.

This work is supported by the U.S. Department of Energy, Office of Science, Basic Energy Sciences, Geosciences program under Award DE-SC0022269.

REFERENCES

Atkinson S. C. (2013) Crystal structures and phase transition in rare earth oxides. Doctoral Dissertation, University of Stanford, 237 p.

Beall G. W., Milligan W. O., and Wolcott H. A. (1977) Structural trends in lanthanide trihydroxides. *Journal of Inorganic and Nuclear Chemistry* **39**, 65–70.

Rudolph W. W. and Irmer G. (2020). On the hydration of the rare earth ions in aqueous solution. *Journal of Solution Chemistry* **49**, 316–331.

Wan Y., Wang X., Chou I.-M., and Li X. (2021) Role of sulfate in the transport and enrichment of REE in hydrothermal systems. *Earth and Planetary Science Letters* **569**, 117068.

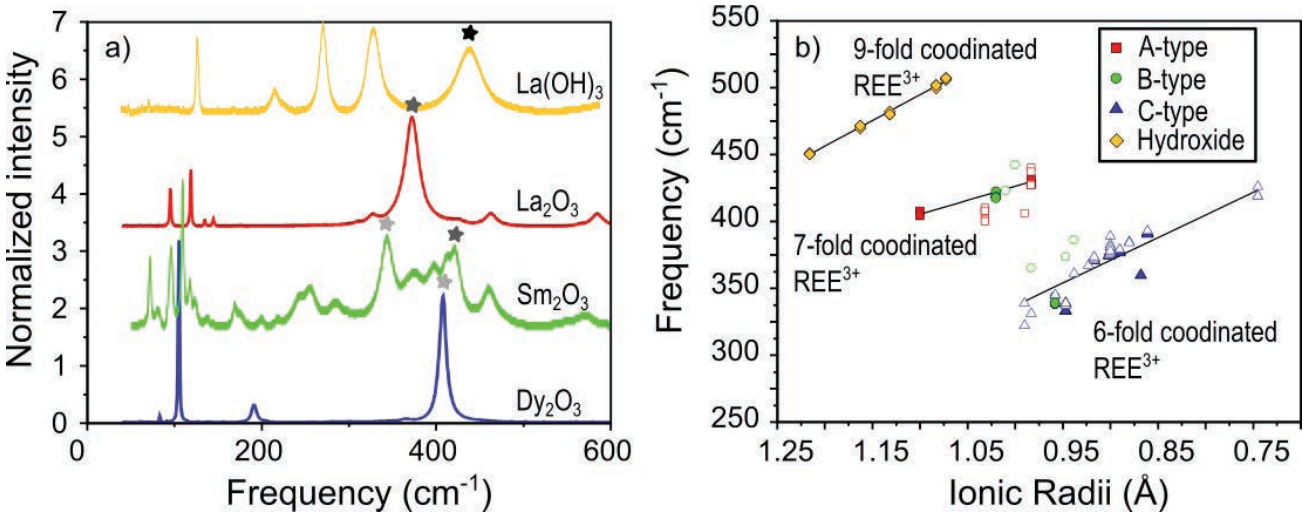

Figure 1. (a) Raman spectra of REE sesquioxides and hydroxides and (b) systematic trends for REE-O band shifts with decreasing ionic radii for different REE-O coordinated structures. The main REE-O band is marked with a black star for 9-fold, a dark gray star for 7-fold, and a light gray star for 6-fold coordinated REE-O polyhedra. Closed symbols are data from this study and open symbols are data compiled from literature.

SUGGESTED FUTURE RESEARCH ON THE GEOCHEMISTRY OF CONTINENTAL HYDROTHERMAL SYSTEMS FOR IMPROVED UNDERSTANDING OF HAZARDS, ENERGY AND MINERAL RESOURCES, AND THE LIMITS OF LIFE ON EARTH AND ELSEWHERE IN THE SOLAR SYSTEM

Shaul Hurwitz[1], Andri Stefánsson[2], Everett L. Shock[3], Barbara I. Kleine-Marshall[4]

[1] U.S. Geological Survey, Moffett Field, CA 94035, USA
[2] University of Iceland, Reykjavik, Iceland
[3] Arizona State University, Tempe, AZ 85281, USA
[4] Friedrich-Alexander-Universität, Erlangen-Nuremburg, Germany

Hydrothermal systems on the continents are of great significance because they are primary sources of economically important metals and geothermal energy, they are tourist attractions, they support bathing and health resorts, and they host extreme life forms. Research on hot springs and their deposits provides clues to early life on Earth and possibly on Mars and has led to major breakthroughs in biotechnology. Aqueous and gas-rich hydrothermal fluids also contribute to a range of volcanic hazards. A recent review chapter summarizes the state of knowledge on the chemistry of continental hydrothermal systems and *the myriad processes* that operate under a wide range of temperatures, pressures, chemical compositions, and oxidation states (Hurwitz et al., 2024). Some of the fundamental questions that remain to be addressed by the next generation of studies include: How is mass transmitted from magma to hydrothermal systems? What is the expected near-surface hydrogeochemical expression of magmatic unrest at depths of several kilometers? What are the time scales of ore deposit formation? How does hydrothermal circulation transport microbes, their food, and their respiration products within the subsurface biosphere? Addressing some of these questions will largely depend on the ability to better resolve spatial and temporal patterns of heat and mass transport into, within, and from hydrothermal systems, and better characterize and quantify the spatial and temporal correlations among hydrothermal processes and tectonic, magmatic, and climatic processes. Hopefully, addressing some of these issues will improve current estimates of the various hazards posed by hydrothermal activity, provide a framework for better understanding life in extreme environments on Earth and other planets, improve exploration methods for mineral and energy resources, and guide the protection and preservation of unique and diverse thermal features on Earth. Some more specific avenues for future research might include:

- Multidisciplinary studies that quantify the dynamic feedback between tectonic, magmatic, climatic, and hydrothermal processes at multiple temporal and spatial scales, and that establish cause-and-effect relationships. These studies require acquisition of accurate and precise time-series of the various processes. For example, what are the time scales for hydrothermal alteration of volcanic edifices, and how can the climate change susceptibility of hydrothermal environments be predicted?
- Laboratory experiments that quantify water-rock-gas-organic reactions at various pressure, temperature, and redox conditions relevant to continental hydrothermal systems.

Such experiments are crucial for improving quantitative models of multiphase and multicomponent reactions as well as heat and mass transport to account for thermodynamic and kinetic effects more accurately.

- Drilling could provide more *in situ* data on the hydrothermal shells surrounding magma. After drilling, the holes could be used as instrumented observatories (Lowenstern et al., 2017). The Krafla Magma Testbed project in Iceland (Eichelberger et al., 2018) could provide a crucial link between magma and the hydrothermal surroundings by drilling into magma and improving the knowledge on supercritical fluids.
- Characterize the chemical composition of aqueous-rich supercritical fluids from deep wells, conduct laboratory experiments to characterize the reactivity of these fluids with a range of rocks under relevant conditions, and enhance thermodynamic formulations relevant for these temperature and pressure conditions.
- Better characterize and quantify the role of high-temperature microbial activity in geochemical cycles across the periodic table.
- High-resolution imaging techniques, such as scanning electron microscopy (SEM), transmitted electron microscopy (TEM), and micro-proton-induced X-ray emission (micro-PIXE), could be applied to better understand and quantify how various metals and metalloids are partitioned and incorporated into hydrothermal deposits and altered rocks, and the role of microbial activity in high-temperature water-rock reactions.

REFERENCES

Eichelberger J., Ingolfsson H. P., Carrigan C., Lavallee Y., Tester J., and Markusson S. H. (2018) Krafla magma testbed: Understanding and using the magma-hydrothermal connection. *Transactions-Geothermal Resources Council* **42**, 2396–2405.

Hurwitz S., Stefánsson A., Shock E. L., and Kleine-Marshall B. I. (2024) The geochemistry of continental hydrothermal systems, in: *Treatise on Geochemistry 3rd ed.*, in press, Elsevier. https://doi.org/10.1016/B978-0-323-99762-1.00036-X

Lowenstern J. B., Sisson T. W., and Hurwitz S. (2017) Probing magma reservoirs to improve volcano forecasts, *Eos* **98**, https://doi.org/10.1029/2017EO085189

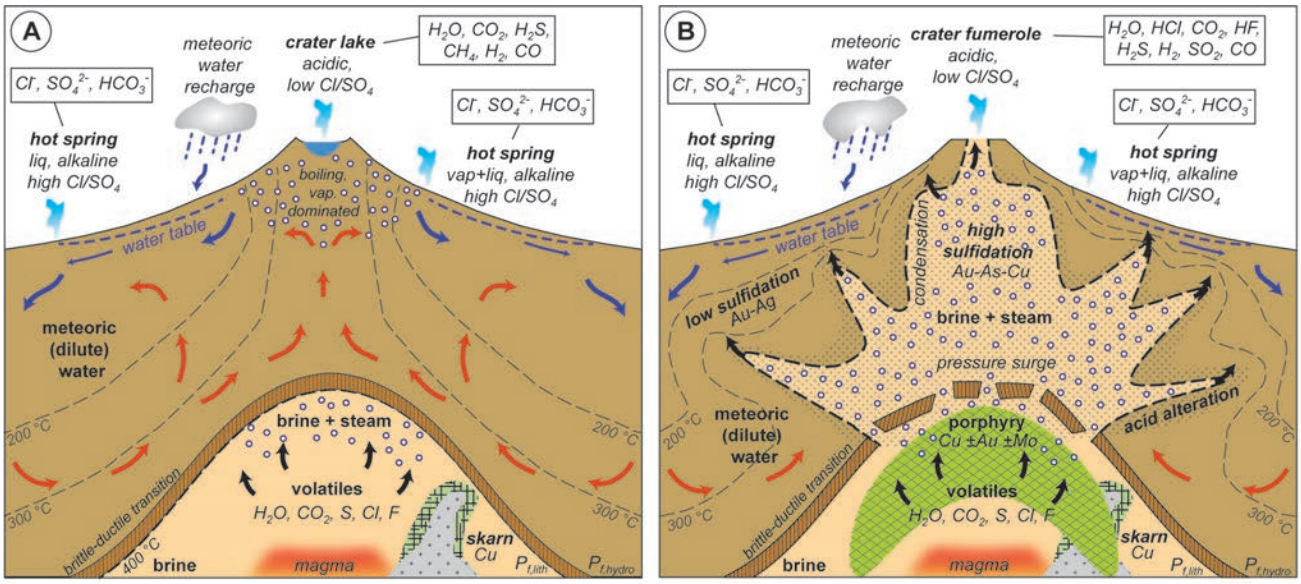

Figure 1. Schematic cross sections (not to scale) of an active magmatic-hydrothermal system that extends from the degassing magma to fumaroles and hot springs. A. The brittle to ductile (plastic) transition in silicic rocks is assumed to occur at temperatures of ~370–400 °C, but experimental studies have shown that under realistic strain rates, the temperature of the transition from brittle to ductile rheology can range from 260 °C to ~700 °C. Meteoric water circulates at near-hydrostatic pressures in brittle rock, while saline fluids accumulate at lithostatic pressure in ductile rocks surrounding the intrusion. B. Episodic and temporary breaching of the brittle-ductile transition causes magmatic volatiles and heat to be transported into the hydrothermal system. Also shown are the environments deduced for the formation of hydrothermal porphyry, skarn, and high- and low-sulfidation epithermal ore deposits. Low-sulfidation ore deposits form in hydrothermal systems characterized by neutral-pH waters that may discharge as hot springs and geysers. From Hurwitz et al. (2024). Modified after Fournier (1999) and Hedenquist and Lowenstern (1994).

LITHIUM MOBILITY IN INTERBEDDED SANDSTONE AND MUDSTONE, POWDER RIVER BASIN, WYOMING

John P. Kaszuba[1,2], Janet C. Dewey[1], Jordan C. Bratcher[1], Ryan T. Herz-Thyhsen[1]

[1] Department of Geology & Geophysics, University of Wyoming, Laramie, WY 82071, USA
[2] School of Energy Resources, University of Wyoming, Laramie, WY 82071, USA

A strategy for sustainable energy couples recovery of critical metals to development of petroleum systems. The Wall Creek Member of the Cretaceous Frontier Formation, Powder River Basin, Wyoming, USA, is an important unconventional reservoir composed of low-permeability sandstones interbedded with organic-rich mudstones. Six samples representing the full extent of hydraulic fracture propagation across the Wall Creek Member were collected from core recovered from depths of 12,467 to 12,573 ft (3,800–3,832 m; Herz-Thyhsen et al., 2020). Lithium was slightly above crustal abundance (20 ppm) in five subsamples from this core (range 29–57 ppm); one subsample contained lithium below crustal abundance.

A four-step sequential extraction procedure (Stewart et al., 2015) was used to target lithium release from readily accessible phases: (1) soluble salts, (2) surface exchangeable, (3) carbonate minerals, and (4) acid-soluble phases (partial silicate and oxides) plus high-charge interlayer cations. For each of the six samples, most of the lithium was liberated by the carbonate (2.6–6.6 ppm) and acid-soluble (3.2–9.3 ppm) extractions. The sum of all four extract aliquots ranged from 20 to 73% of total available lithium. The carbonate extraction removed 5–20 % (mean = 12%) and the acid-soluble extraction removed 11–50% (mean = 21%) of the lithium.

Hydrothermal experiments were conducted (Bratcher et al., 2021) at reservoir conditions (115 °C, 35 MPa) to evaluate potential lithium mobility due to more realistic geochemical interactions between reservoir and acidic fluid (pH ~2.3) spanning a range of ionic strengths (0.016 to 1.13 mol/kg). The six subsamples of the core were homogenized for use in the experiments. This rock mixture consisted of 33% quartz, 33% chert, 20% calcite, 6% illite, 5% albite, 1% kaolinite, 1% pyrite, 1% chlorite, and <1% TOC. The rock mixture was reacted for ~650 hours (27 days) with (1) acidic fluid (pH ~2.3) mixed from formation water spanning two orders-of-magnitude ionic strength (0.016, 0.16, and 1.13 mol/kg), and (2) fluid (ionic strength 0.11 mol/kg) of circumneutral pH (7.3). The fluid initially contained no aqueous Li. Trends of aqueous SiO_2, K, and Mg are consistent with dissolution of feldspar ± quartz and precipitation of clay; mineralogic evidence for dissolution was limited to calcite and feldspar, and no secondary clay was observed. Ionic strength was more important than acidity for feldspar-clay equilibrium. Progressively greater ionic strength of the fluid, from 0.016 to 0.16 to 1.13 mol/kg, increased aqueous lithium concentrations, from 132 to 201 to 250 ppb (Fig. 1), at the time the final sample was collected from the experiments (Bratcher, 2016). Fluid of circumneutral pH contained 167 ppb aqueous lithium at the time the final sample was collected. Aqueous lithium in the fluid in all four experiments is an order of magnitude lower than extractable lithium available from the rock. Lithium in the interbedded sandstone and mudstone examined in this study is relatively immobile under geochemical conditions expected for subsurface reservoirs in sedimentary basins.

REFERENCES

Bratcher J. (2016) Effect of ionic strength (salinity) and pH (acidity) on geochemical water-rock interactions during hydraulic fracturing in the Frontier Formation of the Powder River Basin, Wyoming. MS Thesis, Department of Geology and Geophysics, University of Wyoming, 70 p.

Bratcher J. C., Kaszuba J. P., Herz-Thyhsen R. T., and Dewey J. C. (2021) Ionic strength and pH controls on water-rock interaction of an unconventional siliceous reservoir: Using formation water in stimulation fluid. *Energy & Fuels* **35**, 18414–18429.

Herz-Thyhsen R. J., Kaszuba J. P., and Dewey J. C. (2020) Mineral dissolution and precipitation induced by hydraulic fracturing of a mudstone and a tight sandstone in the Powder River Basin, Wyoming, USA. *Applied Geochemistry* **119**, DOI: 10.1016/j.apgeochem.2020.104636.

Stewart B. W., Chapman E. C., Capo R. C., Johnson J. D., Graney J. R., Kirby C. S., and Schroeder K.T. (2015) Origin of brines, salts and carbonate from shales of the Marcellus Formation: Evidence from geochemical and Sr isotope study of sequentially extracted fluids. *Applied Geochemistry* **60**, 78–88.

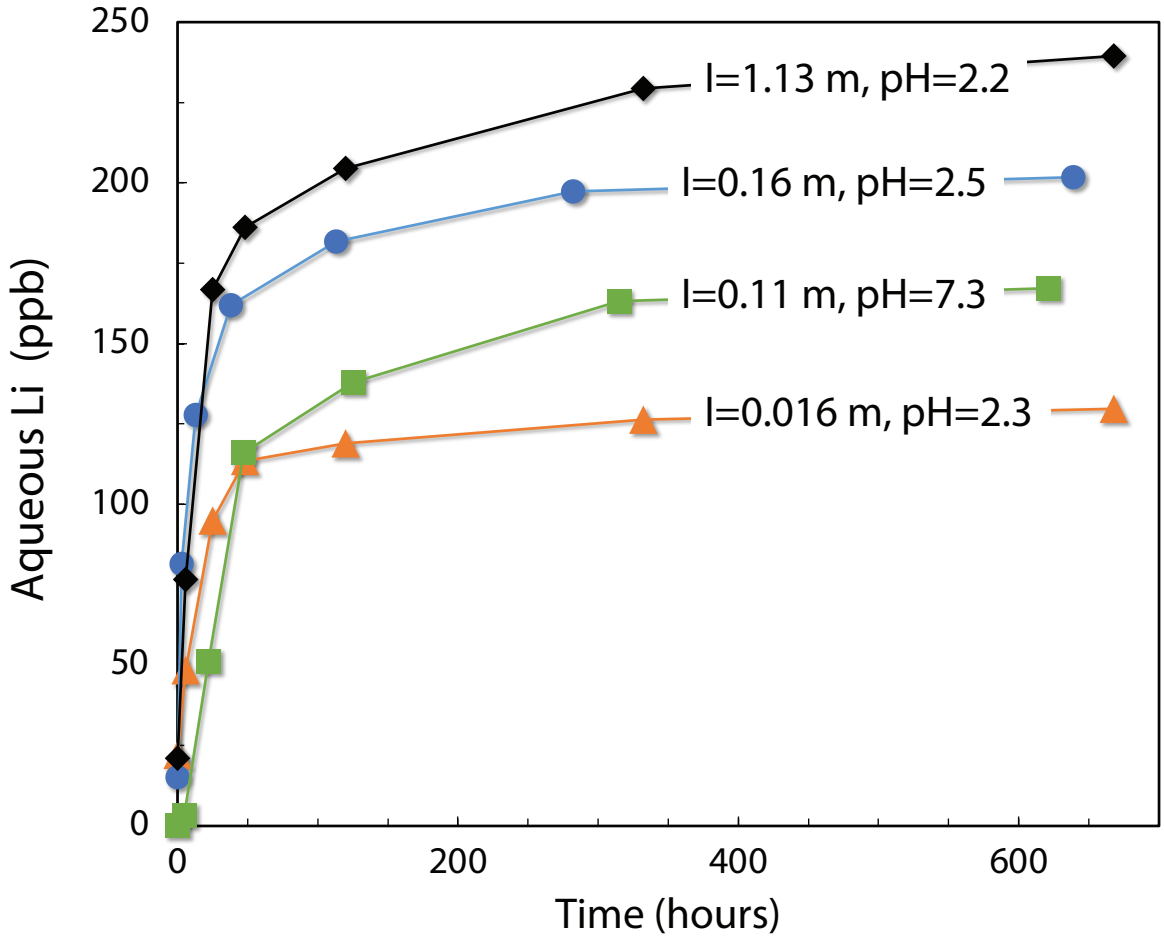

Figure 1. Evolution of aqueous Li concentrations in four hydrothermal experiments as a function of ionic strength and pH. Each symbol represents a sample collected from each experiment; uncertainties are smaller than the size of the symbol.

THE EXPERIMENTAL DETERMINATION OF CE, Y, AND ER SOLUBILITY AND THERMODYNAMIC PREDICTIONS IN HYDROTHERMAL FLUIDS AT 350 TO 500°C

Charles T. Kershaw[1], Nicole C. Hurtig[1], Alexander P. Gysi[1,2], Artas A. Migdisov[3], Laura Waters[1], Daniel Harlov[4]

[1] Department of Earth and Environmental Science, New Mexico Institute of Mining and Technology, Socorro, NM 87801, USA
[2] New Mexico Bureau of Geology and Mineral Resources, New Mexico Institute of Mining and Technology, Socorro, NM 87801, USA
[3] Earth and Environmental Sciences Division, Los Alamos National Laboratory, Los Alamos, NM 87545, USA
[4] Deutsches GeoForschungsZentrum GFZ, Telegrafenberg, 14473 Potsdam, Germany

Rare earth elements (REE) are a rapidly expanding commodity essential for many applications in modern technologies. In REE ore deposits, hydrothermal processes often play a critical role in REE enrichment. REE mobility in hydrothermal fluids is controlled by the stability of REE minerals and the availability of complexation ligands to promote REE aqueous species formation (Gysi et al., 2015, 2018; Migdisov et al. 2016). Predicted REE solubility based on existing thermodynamic models and data from low-temperature experiments (Haas et al., 1995; Gysi et al., 2015, 2018; Migdisov et al. 2016) often under- or overpredict REE solubility from high-temperature experiments, limiting our predictive capabilities. Here we use batch-type Inconel 625 Parr reactors to investigate synthetic $CePO_4$, YPO_4, and $ErPO_4$ solubility between 350 °C at P_{SAT} and 500 °C at 500 and 700 bar with variable starting pH (2, 3, 4, 7, and 10) and salinities (0.01, 0.1, and 0.5 molal NaCl).

At 350 °C and 0.01 m NaCl, the solubility of Ce was highest at all pH values, followed by Y, and lastly Er, which consistently shows the lowest solubility (Fig. 1a). As a function of pH, all three REE demonstrated the highest solubility in the most acidic solutions and a decrease in solubility at mildly acidic conditions. At alkaline conditions (starting pH 10), $CePO_4$ solubility increases, YPO_4 solubility remains constant, and $ErPO_4$ solubility slightly decreases, indicating diverging behavior between light REE (LREE) and heavy REE (HREE). At 450 °C and alkaline pH, Er solubility increases, showing a similar trend to that of Ce at 350 °C and indicating changes in the dominant Er speciation with increasing temperature. As salinity increases, Er solubility increases under acidic conditions and the solubility minimum shifts to higher pH. Speciation models of Er at experimental conditions were conducted using the GEM-Selektor code package (**https://gems.web.psi.ch/**) and the MINES database (**https://doi.org/10.58799/mines-tdb**). Simulations predict $ErCl^{2+}$, $ErCl_2^+$, and $ErCl_{3(aq)}$ dominance at acidic conditions for 350, 400, and 450 °C, respectively, and $Er(OH)_4^-$ at alkaline conditions. However, 350 and 400 °C experimental solubility trends do not follow predicted speciation under alkaline conditions; rather, they more closely correspond to the behavior of $ErOH_{3(aq)}$. The simulated solubility of Ce, Y, and Er at 350 °C indicates that modeled trends correlate with experimental results in acidic solutions. Near pH 4, Ce and Er switch, assuming trends opposite of those acquired experimentally (Fig. 1b). Erbium is overpredicted by 0.5 to 2 orders of magnitude except near pH 5 where experimental and modeled results are equivalent. Yttrium is overpredicted by 0.5 orders of magnitude under acidic conditions, underpredicted by 0.25 to 0.5 orders of magnitude at near neutral pH, and overpredicted by up to 0.5 orders of magnitude under alkaline conditions. Cerium is overpredicted by 0.5 orders of magnitude at low pH and underpredicted by 0.5 to 3 orders of magnitude at near neutral to alkaline pH.

These results highlight the fact that there are key behavioral differences between LREE and HREE and that there is a need for further high-temperature experimental data to improve our modeling capabilities of REE at supercritical conditions.

This work is supported by the U.S. Department of Energy, Office of Science, Basic Energy Sciences, Geosciences program under Award DE-SC0022269.

REFERENCES

Gysi A. P., Williams-Jones A. E., and Harlov D. (2015) The solubility of xenotime-(Y) and other HREE phosphates ($DyPO_4$, $ErPO_4$ and $YbPO_4$) in aqueous solutions from 100 to 250 °C and p_{sat}. *Chemical Geology* **401**, 83–95.

Gysi A. P., Harlov D., and Miron G. D. (2018) The solubility of monazite ($CePO_4$), $SmPO_4$, and $GdPO_4$ in aqueous solutions from 100 to 250 °C. *Geochemica et Cosmochemica Acta* **242**, 143–164.

Haas J. R., Shock E. L., and Sassani D. C. (1995) Rare earth elements in hydrothermal systems: Estimates of standard partial molal thermodynamic properties of aqueous complexes of the rare earth elements at high pressures and temperatures. *Geochemica et Cosmochemica Acta* **59**, 4329–4350.

Migdisov A., Williams-Jones A. E., Brugger J. and Caporuscio F. A. (2016) Hydrothermal transport, deposition, and fractionation of the REE: Experimental data and thermodynamic calculations. *Chemical Geology* **439**, 13–42.

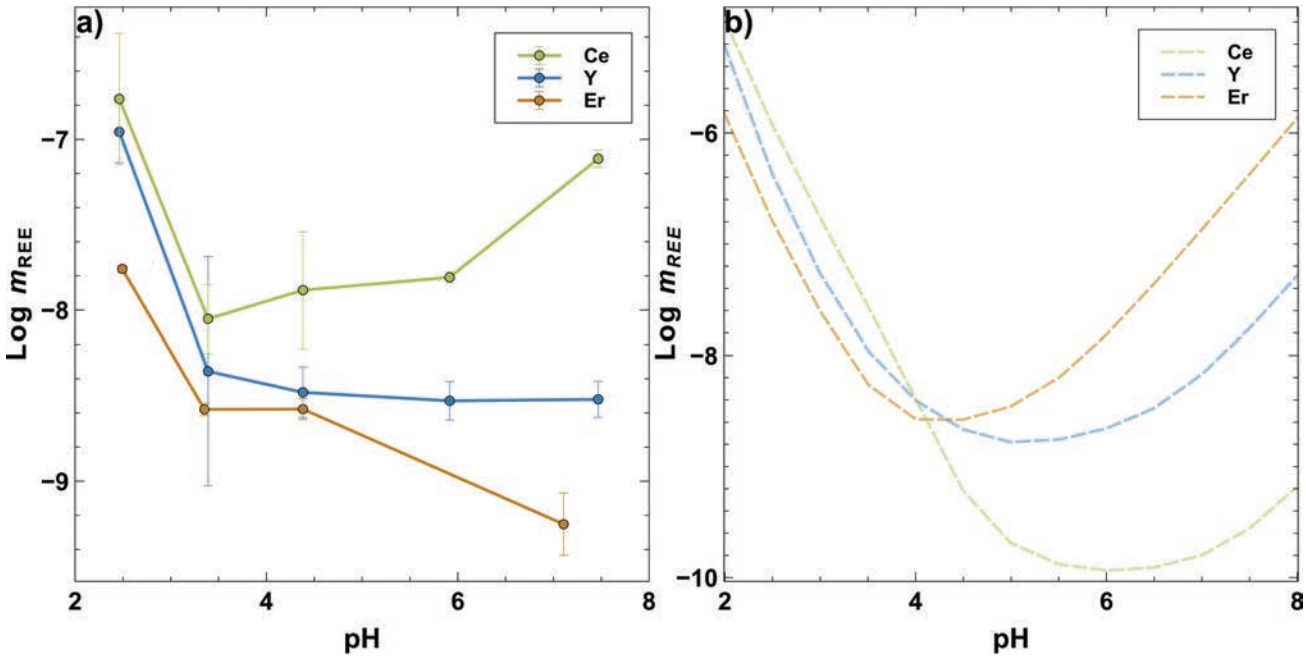

Figure 1. The experimental (a) and modeled (b) logarithm of molality of Ce, Y, and Er at 350 °C and 0.01 m NaCl as a function of pH. For experimental data, Ce (yellow) displays the highest solubility, followed by Y (blue) and Er (brown), respectively. Modeled results follow experimental solubility trends until ~4 pH, where Ce and Er switch.

CALORIMETRIC AND STRUCTURAL CHARACTERIZATION OF GAMMA IRRADIATED RARE EARTH RHABDOPHANES

Emma Carlsen Kindall[1], Shinhyo Bang[1], Margaret Reece[2], Xiaofeng Guo[1]

[1] Washington State University, Pullman, WA 99164, USA
[2] Los Alamos National Laboratory, Los Alamos, NM 87545, USA

As one of the primary sources of critical resource rare earth elements (REEs), the orthophosphate minerals monazite (for light REEs) and xenotime (for heavy REEs), along with their hydrated structures rhabdophane and churchite, respectively, are the focus of many ongoing research efforts. Although naturally occurring monazite and xenotime are primarily REE minerals, they are known to contain small amounts of U and Th as well (Long et al., 2010). Unlike many other U- and Th-containing minerals that undergo metamictization, monazite has not been found in substantially amorphous states, suggesting some mechanism of resistance to radiation-induced defects (Boatner, 2002). Consequently, monazite has been studied as a potential nuclear waste form (Schlenz et al., 2013; Leys et al., 2022; Rafiuddin et al., 2022). Because rhabdophanes, which undergo a two-step dehydration and phase transformation to become monazite (Mesbah et al., 2017), are considered metastable under most aqueous conditions and therefore less relevant to nuclear waste storage (Shelyug et al., 2018), little effort has focused on studying their radiation-induced structural changes. However, emerging research indicates that rhabdophanes may control solubility of the REE-phosphate system, bringing greater relevance to understanding their behavior under irradiation (Du Fou de Kerdaniel et al., 2007; Gausse et al., 2016).

To this end, in this work, hydrated orthophosphate samples—$NdPO_4 \bullet nH_2O$, $GdPO_4 \bullet nH_2O$, and $ErPO_4 \bullet nH_2O$—were synthesized and γ-irradiated at 10–100 kGy. The irradiated samples were structurally characterized at the Canadian Light Source (CLS) with synchrotron pair distribution function (PDF) analysis, and the thermodynamics and kinetics of their dehydration process were characterized with thermogravimetric analysis combined with differential scanning calorimetry (TGA-DSC). Initial TGA-DSC results, shown in Figure 1, looking at the rhabdophane dehydrations, suggest that although irradiation-induced defects have no effect on the second dehydration enthalpy, they do affect the temperature at which the sample undergoes the second dehydration. In Figure 1, increased γ irradiation level is seen to lower the temperature of dehydration, suggesting that irradiation-induced defects may be lowering kinetic barriers governing how tightly channel waters are bound. Continued work is needed to determine the role this may play in orthophosphate minerals' long-term resistance to irradiation-induced amorphization and their consequential candidacy as a nuclear waste form.

REFERENCES

Boatner L. A. (2002) Synthesis, structure, and properties of monazite, pretulite, and xenotime. *Reviews in Mineralogy and Geochemistry* **48**(1), 87–121.

Du Fou de Kerdaniel E., Clavier N., Dacheux N., Terra O., and Podor R. (2007) Actinide solubility-controlling phases during the dissolution of phosphate ceramics. *Journal of Nuclear Materials* **362**(2–3), 451–458.

Gausse C., Szenknect S., Qin D. W., Mesbah A., Clavier N., Neumeier S., Bosbach D., and Dacheux N. (2016) Determination of the solubility of rhabdophanes $LnPO_4{\cdot}0.667H_2O$ (Ln = La to Dy). *European Journal of Inorganic Chemistry* **2016**(28), 4615–4630.

Leys J. M., Ji Y., Klinkenberg M., Kowalski P. M., Schlenz H., Neumeier S., Bosbach D., and Deissmann G. (2022) Monazite-type $SMPO_4$ as potential nuclear waste form: Insights into radiation effects from ion-beam irradiation and atomistic simulations. *Materials* **15**(10), 3434.

Long K. R., Van Gosen B. S., Foley N. K., and Cordier D. (2010) The principal rare earth elements deposits of the United States—A summary of domestic deposits and a global perspective: U.S. Geological Survey Scientific Investigations Report 2010–5220.

Mesbah A., Clavier N., Elkaim E., Szenknect S., and Dacheux N. (2017) In pursuit of the rhabdophane crystal structure: From the hydrated monoclinic $LnPO_4 \bullet 0.667H_2O$ to the hexagonal $LnPO_4$ (Ln = Nd, SM, Gd, Eu and Dy). *Journal of Solid State Chemistry* **249**, 221–227.

Rafiuddin M. R., Donato G., McCaugherty S., Mesbah A., and Grosvenor A. P. (2022) Review of rare-earth phosphate materials for nuclear waste sequestration applications. *ACS Omega* 7(44), 39482–39490.

Schlenz H., Heuser J., Neumann A., Schmitz S., and Bosbach, D. (2013) Monazite as a suitable actinide waste form. *Zeitschrift für Kristallographie - Crystalline Materials*, **228**(3), 113–123.

Shelyug A., Mesbah A., Szenknect S., Clavier N., Dacheux N., and Navrotsky A. (2018) Thermodynamics and stability of rhabdophanes, hydrated rare earth phosphates $REPO_4 \bullet nH_2O$. *Frontiers in Chemistry* **6**, 604.

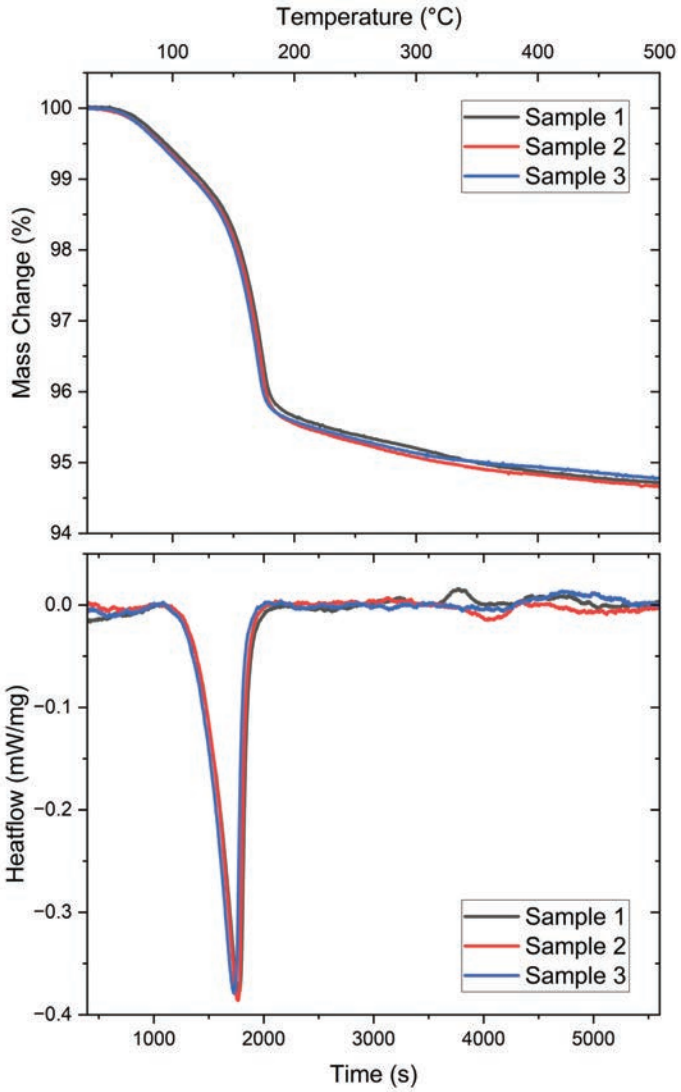

Figure 1. TGA-DSC results for $GdPO_4 \bullet 0.75H_2O$, where samples 1, 2, and 3 were irradiated with 10, 50, and 100 kGy, respectively.

COMPUTATIONAL CHEMISTRY: POTENTIAL APPLICATIONS IN ECONOMIC GEOLOGY

James D. Kubicki[1]

[1] Department of Earth, Environmental and Resource Sciences, The University of Texas at El Paso, El Paso, TX 79968, USA

Modern methods in computational chemistry combined with high-performance computers have the capability of supplementing experimental studies and predicting reaction thermodynamics and kinetics. The flexibility of quantum methods as applied in density functional theory (DFT; Fig. 1) calculations allows one to investigate almost any type of reaction in any environment (e.g., T, P, pH, etc.). Connecting the results of these simulations with experiments allows the researcher to benchmark their accuracy while filling in details that analytical methods may not be able to detect. However, these methods have not been applied extensively in the areas of ore formation and hydrometallurgy. Studies that have been conducted show great promise for improving the efficiency of resource extraction. This talk will cover the fundamentals of molecular modeling methods, discuss example papers where these methods have been applied in economic geology, and explore potential future studies where computational chemistry could be useful, especially related to Li and rare earth elements.

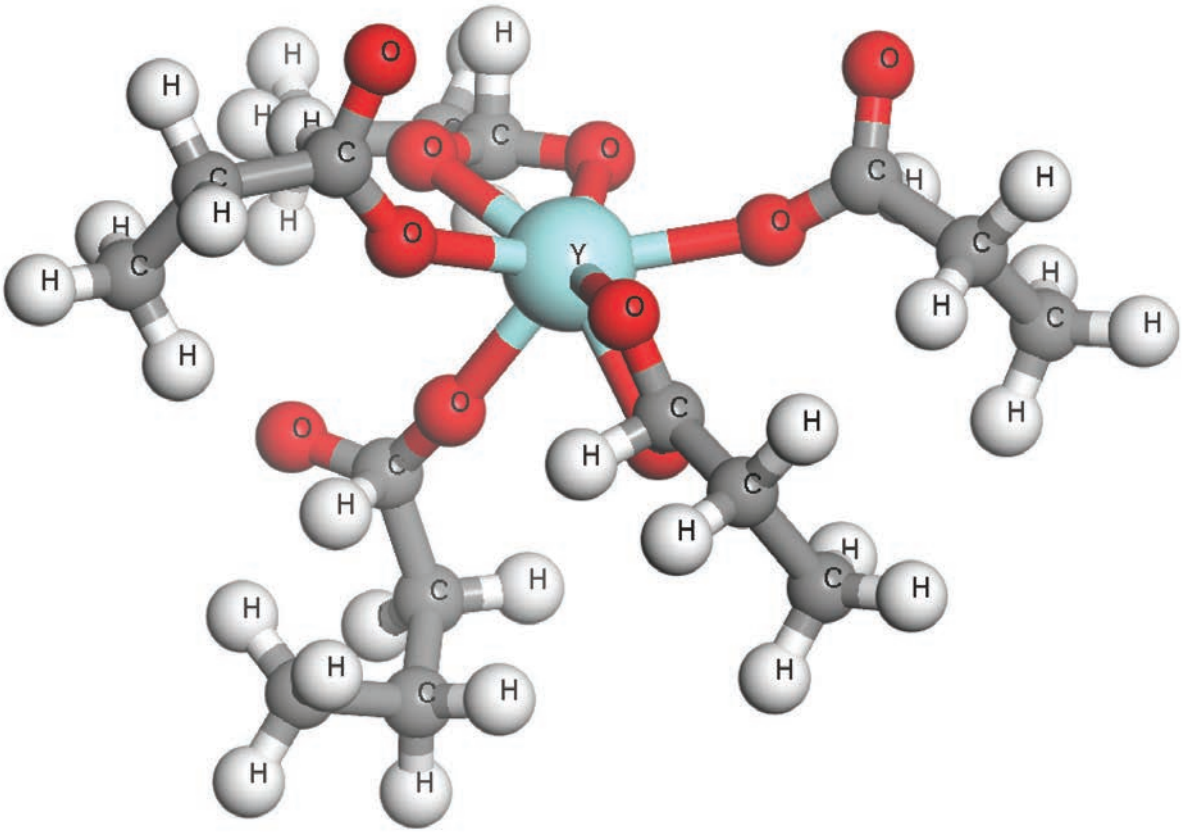

Figure 1. Yttrium bonding in pocket of lanmodulin as modeled with density functional theory (DFT) calculations.

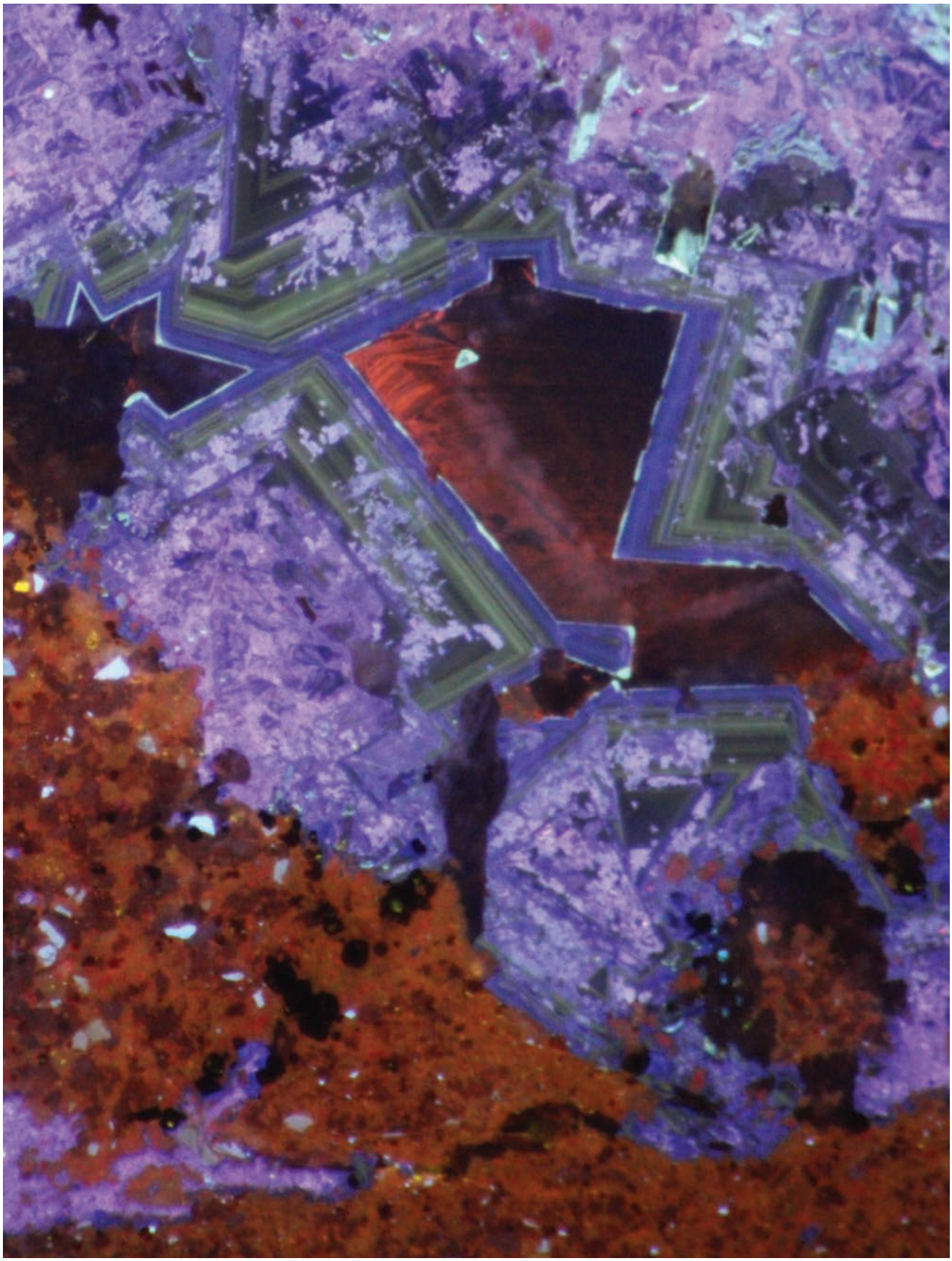

Cathodoluminescence image of Gallinas Mountains fluorite. *Photo by Teagan Skinner and Eric Ruggles*

GEMS AS AN ASSET OF GEOCHEMICAL MODELING: 24 YEARS OF DEVELOPMENT AND USE

Dmitrii A. Kulik[1], G. Dan Miron[1]

[1] Laboratory for Waste Management (LES), Paul Scherrer Institute, 5232 Villigen PSI, Switzerland

The Gibbs energy minimization software (GEMS) is a collection of free geochemical modeling code tools and thermodynamic databases developed at LES PSI since June 2000. During the 24-year development and support "epoch," GEMS was used in >60 projects (PhD, postdoc, hydrothermal and environmental geochemistry, cement industry, waste management). Distributed free of charge since 2003 and open source since 2013, GEMS was downloaded >11,000 times, attracted >1,100 active users worldwide, and was cited in >1,500 publications and >50 reports. Over 20 GEMS training workshops were held at PSI and by collaborating enthusiasts (B. Lothenbach, A.P. Gysi, N. Hurtig, and others). Why do so many scientists and students choose GEMS? This may be because GEMS' algorithms can solve for (partial) chemical equilibria in complex heterogeneous (highly) non-ideal chemical systems (Kulik et al., 2013, 2017) involving many solid, liquid, aqueous, and gaseous mixtures with different activity models up to sublattice solutions and phase separation (Wagner et al., 2012), as well as various (ad)sorption models. GEMS calculates intrinsic redox states (fO_2, pe, Eh) and pH from the bulk chemical composition of the system and can utilize multiple metastability constraints to simulate species metastability and mineral dissolution/precipitation kinetics. The GEM-Selektor code GUI integrates calculations of chemical equilibria with management of thermodynamic and composition datasets. In other words, GEMS facilitates many tasks that are hard to solve using PHREEQC or similar LMA chemical speciation codes. In this presentation, along with some interesting example applications for aqueous-solid solution systems, the state-of-the-art and some lessons learned during 24 years of GEMS development will be summarized. Some future trends, such as the advancement of parameterization tools (Miron et al., 2015), the integration with databases, and the transition from GEMS desktop to web apps (Kulik et al., 2021) and Python APIs, will be discussed.

REFERENCES

Kulik D. A., Wagner T., et al. (2013) GEM-Selektor geochemical modeling package: Revised algorithm and GEMS3K numerical kernel for coupled simulation codes. *Computational Geosciences* **17**, 1–24.

Kulik D. A., Kosakowski G., et al. (2017) The Gibbs energy minimization software for thermodynamic modelling (GEMS TM) project: Codes, databases and relevant applications. *Nagra Work Report* **NAB 17-43**, 123 pp.

Kulik D. A., Winnefeld F., Kulik A., Miron G. D., and Lothenbach B. (2021) CemGEMS—An easy-to-use web application for thermodynamic modeling of cementitious materials. *RILEM Technical Letters* **6**, 36–52 .

Miron G. D., Kulik D. A., Dmytrieva S. V., and Wagner T. (2015) GEMSFITS: Code package for optimization of geochemical model parameters and inverse modeling. *Applied Geochemistry* **55**, 28–45.

Wagner T., Kulik D. A., Hingerl F. F., and Dmytrieva S. V. (2012) GEM-Selektor geochemical modeling package: TSolMod library and data interface for multicomponent phase models. *The Canadian Minerologist* **50**, 1173–1195.

Carbonatite dike with fragments of fenitized mafic host rock, Lemitar Mountains, New Mexico. *Photo by A. Gysi*

DIRECT LITHIUM EXTRACTION FROM GEOTHERMAL BRINES: THE NEW OIL

Hermann Lebit[1], Benjamin Brunner[2], Natalya Kharitonova[1], Eva Deemer[3]

[1] Alma Energy, Houston, TX 77004, USA

[2] Department of Earth, Environmental and Resource Sciences, The University of Texas at El Paso, El Paso, TX 79968, USA

[3] Department of Civil Engineering, The University of Texas at El Paso, El Paso, TX 79968, USA

The energy transition is an inevitable global development driven by geopolitical, environmental, economic, and societal factors. It will fundamentally change how we access energy resources and will rebalance the growing demand in critical minerals (U.S. Department of Energy, 2021).

The global mobility sector consumes about two-thirds of the world's crude oil production, which currently stands at or above 105 million barrels of oil per day (mmbopd; U.S. Energy Information Administration, 2024). Even a minor reduction, for instance by increasing the electric vehicle fleet, would reduce greenhouse gas emissions but would further stress our power grids and increase demand for critical minerals, which are required by clean tech manufacturing. Strategic planning in research and technology development have to address this conundrum (IEA, 2023).

Renewable energy sources already significantly contribute to the domestic electrical grid (13% in the United States in 2021) but are dominated by intermittent resources like wind and solar energy, whereas dispatchable, clean energy resources are neglected. The potential of dispatchable geothermal energy is undisputed, although challenges in subsurface risk assessment, completion technologies, upfront investments, and lengthy permitting processes impact the economic potential of this technology (Lund and Toth, 2020; Faulds et al., 2021; Tester et al., 2021).

Lithium is the key critical mineral in clean technology development, particularly for rechargeable batteries in the mobility sector due to its excellent energy density to weight ratio. Detrimental environmental impacts caused by invasive lithium mineral mining or large evaporation ponds can be avoided by direct lithium extraction (DLE) from brines (Ventura et al., 2020). It is a valuable solution, particularly when deployed in proximity to mature hydrocarbon basins, leveraged by a wealth in subsurface data, existing infrastructure, and qualified human resources (Ji et al., 2018; Hammarstrom et al., 2020). Several DLE technologies are facing significant challenges in terms of fresh water usage, the application of chemical agents, excessive land usage, and reliance on external energy supply. Finally, not every brine chemistry is suitable for the envisaged DLE technology (Zavahir et al., 2021).

Direct lithium extraction based on electrodialysis employs ion-selective membranes in a clean, emission-free process (Ji et al., 2018). The technology is robust and takes advantage of successful membrane applications at multiple desalination plants around the world. Along with battery-grade lithium, the electrodialysis produces green hydrogen, outputs fresh water, and sequesters CO_2 as byproducts. Moreover, ion-selective membrane-based DLE offers the potential for targeted extraction of additional elements that can be used in vertically integrated lithium metal production from brines. When combined with geothermal power generation, the technology uses onsite energy and the produced brine in a clean and environmentally friendly process.

Lithium-rich reservoirs with a favorable geothermal signature have been reported from mature hydrocarbon basins across the United States (Blondes et al., 2016; Daitch, 2018), and their direct lithium extraction offers attractive economics, given the growing lithium demand forecasted for the next decades. The operations are 100% green and self-sustainable when combined with novel low- to medium-enthalpy geothermal power

production technology. It opens a new running room to rejuvenate mature hydrocarbon basins into energy super basins where the DLE technology offers a positive revenue stream by extracting valuable critical minerals from produced water. The combined solution further expands prospective thermo-chemical exploration and production into new territories, such as rift systems (Sanjuan et al., 2022).

REFERENCES

Blondes M. S., Gans K. D., Thordsen J. J., Reidy M. E., Thomas B., Engle M. A., Kharaka Y. K., and Rowan E.L. (2016) U.S. Geological Survey national produced waters geochemical database v2. 3 (PROVISIONAL).

Daitch P. J. (2018) Lithium extraction from oilfield brine [Thesis]: The University of Texas at Austin.

Faulds J. E., Shervais J. W., Wannamaker P. E., Forson C., and Lautze N. (2021) Challenges and opportunities for geothermal exploration and hydrothermal research: Recent advances utilizing geothermal play fairway analysis in the Western USA. In *Symposium on the Application of Geophysics to Engineering and Environmental Problems* 167–168. Society of Exploration Geophysicists and Environment and Engineering Geophysical Society.

Hammarstrom J. M., Dicken C. L., Day W. C., Hofstra A. H., Drenth B. J., Shah A. K., McCafferty A. E., et al. (2020) Focus areas for data acquisition for potential domestic resources of 11 critical minerals in the conterminous United States, Hawaii, and Puerto Rico—Aluminum, cobalt, graphite, lithium, niobium, platinum-group elements, rare earth elements, tantalum, tin, titanium, and tungsten. *No. 2019-1023-B*. U.S. Geological Survey.

IEA (2023), Global EV outlook 2023, IEA, Paris https://www.iea.org/reports/global-ev-outlook-2023, Licence: CC BY 4.0 https://iea.blob.core.windows.net/assets/dacf14d2-eabc-498a-8263-9f97fd5dc327/GEVO2023.pdf

Ji P. Y., Ji Z. Y., Chen Q. B., Liu J., Zhao Y. Y., Wang S. Z., Li F., and Yuan J. S. (2018) Effect of coexisting ions on recovering lithium from high Mg2+/Li+ ratio brines by selective-electrodialysis. *Separation and Purification Technology* **207,** 1–11.

Lund J. W. and Toth A. N. (2020) Direct utilization of geothermal energy 2020 worldwide review. In *Proceedings World Geothermal Congress 2020*, Reykjavik, Iceland.

Sanjuan B., Gourcerol B., Millot R., Rettenmaier D., Jeandel E., and Rombaut A. (2022) Lithium-rich geothermal brines in Europe: An up-date about geochemical characteristics and implications for potential Li resources. *Geothermics* **101,** 102385.

Tester J. W., Beckers K. F., Hawkins A. J., and Lukawski M. Z. (2021) The evolving role of geothermal energy for decarbonizing the United States. *Energy & Environmental Science* **14,** 6211–6241.

U.S. Department of Energy (2021) Battery critical materials supply chain challenges and opportunities. DOE/EE-2535. https://www.energy.gov/sites/default/files/2022-01/Battery%20Critical%20Materials%20Workshop%20Report%20-%20FINAL.pdf

U.S. Energy Information Administration (2024) Short-term energy outlook March 2024. https://www.eia.gov/outlooks/steo/pdf/steo_full.pdf

Ventura S. et al. (2020) Selective recovery of lithium from geothermal brines. California Energy Commission. https://www.energy.ca.gov/sites/default/files/2021-05/CEC-500-2020-020.pdf

Zavahir S., Elmakki T., Gulied M., Ahmad Z., Al-Sulaiti L., Shon H. K., Chen Y., Park H., Batchelor B., and Han D. S. (2021) A review on lithium recovery using electrochemical capturing systems. *Desalination* **500,** 114883.

LARGE LANGUAGE MODEL-BASED STRUCTURED INFORMATION RETRIEVAL AND DATASET CONSTRUCTION: EXAMPLES ON RARE EARTH MINERAL THERMODYNAMIC PROPERTIES

Juejing Liu[1], Haydn Anderson[2], Noah Irving Waxman[2], Deven Biehler[2], Haridhar Pulivarthy[2], Xiaofeng Guo[1]

[1] Department of Chemistry, Washington State University, Pullman, WA 99164, USA

[2] School of Electrical Engineering & Computer Science, Washington State University, Pullman, WA 99164, USA

Predicting the transporting and depositing behaviors of rare earth elements (REE) in various ligand systems requires comprehensive thermodynamic understanding. Establishing an open-source thermochemistry database helps those efforts. However, it is still challenging to effectively integrate existing databases or reviews with the constantly increasing number of scientific publications. Recent developments of large language models (LLMs) and related retrieval-augmented generation (RAG) technique enables a potential solution to automatically retrieve the information of interest from the publications (Dunn et al., 2022; Szymanski et al., 2023; Dagdelen et al., 2024). In our ongoing study, we are developing an information retrieval pipeline to obtain the thermodynamic and solubility properties of rare earth minerals automatically and constantly. This pipeline includes automatic publication searching and downloading along with RAG-based structural information retrieval and dataset update, and will eventually upload retrieved information to our publicly available websites. Among these steps, the major challenge is to retrieve information from publications due to the inconsistency of the document formats. Three strategies are used to tackle these two issues: (1) a few shot learning approach teaching LLMs to recognize the information by few examples, (2) split one complicated task into several simpler and digestible steps, and (3) utilize LLMs capable of analyzing images to extract information from tables. By combining all these approaches, we significantly improve the accuracy when retrieving the structured data from the publications. We deployed this pipeline to constantly monitor the relating publications and incorporate the rare earth mineral thermodynamic and solubility properties into the dataset. The retrieved up-to-date data are publicly available on our website.

REFERENCES

Dagdelen J., Dunn A., Lee S., Walker N., Rosen A. S., Ceder G., Persson K. A., and Jain A. (2024) Structured information extraction from scientific text with large language models. *Nature Communications* **15**(1), 1418. DOI: 10.1038/s41467-024-45563-x.

Dunn A., Dagdelen J., Walker N., Lee S., Rosen A. S., Ceder G., Persson K., and Jain A. (2022) Structured information extraction from complex scientific text with fine-tuned large language models. *arXiv preprint arXiv,* 2212.05238.

Szymanski N. J., Rendy B., Fei Y., Kumar R. E., He T., Milsted D., McDermott M. J., Gallant M., Cubuk E. D., Merchant A., et al. (2023) An autonomous laboratory for the accelerated synthesis of novel materials. *Nature* **624**(7990), 86–91. DOI: 10.1038/s41586-023-06734-w

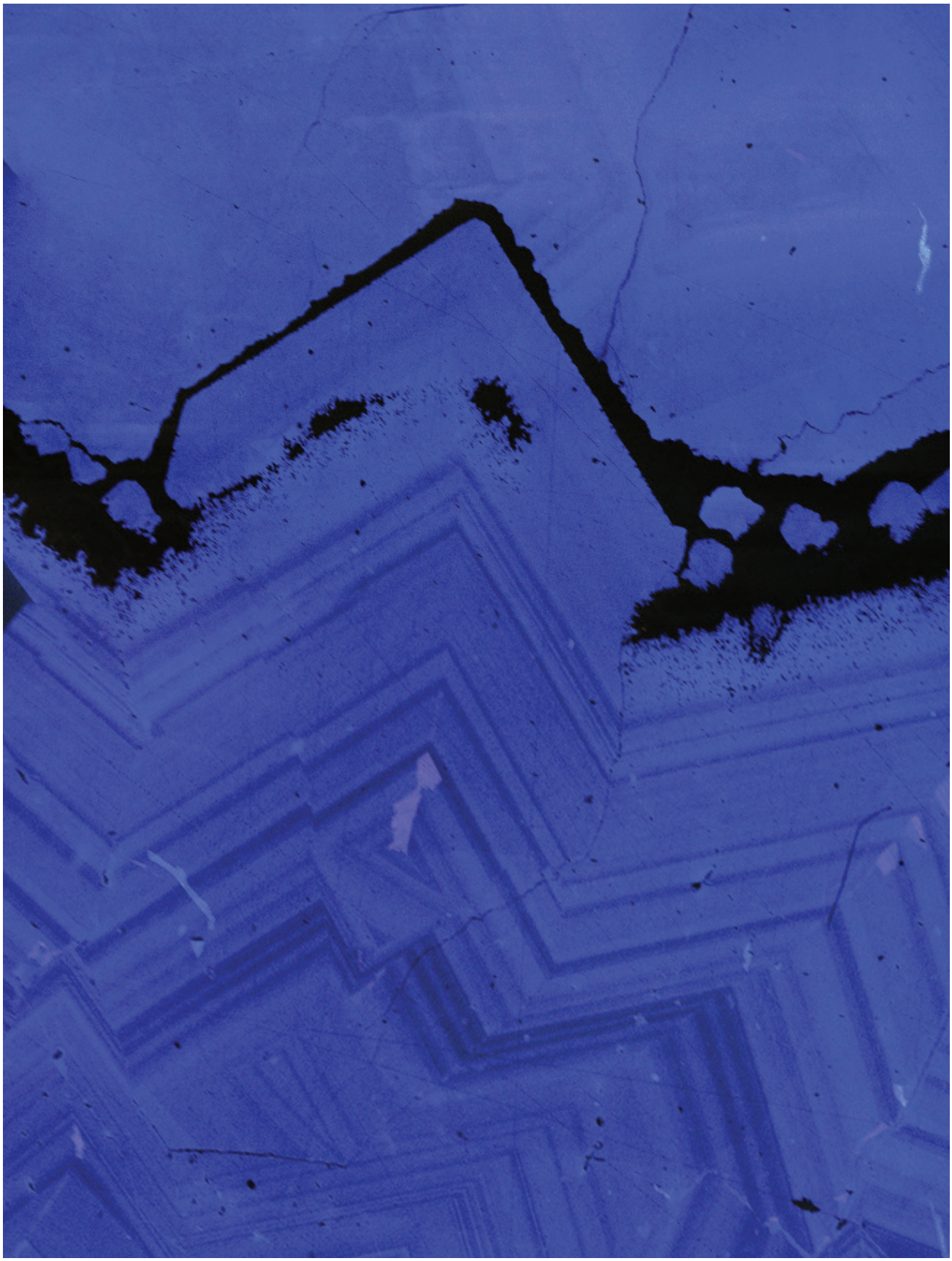

Zoned fluorite from the Surprise Mine, Cookes Peak, New Mexico. *Photo by Cody Schwenk*

CHARACTERIZATION OF THE SPECIATION, SOLUBILITY, AND PARTITIONING OF METALS IN MAGMATIC-HYDROTHERMAL SYSTEMS USING IN SITU X-RAY SPECTROSCOPY

Marion Louvel[1], Jean-Louis Hazemann[2], Denis Testemale[2]

[1] Institut des Sciences de la Terre d'Orleans (ISTO), Orleans, France
[2] Institut Néel, Grenoble, France

The development of thermodynamic models to simulate metal uptake from magmas, their solubility in high P-T fluids, or precipitation upon fluid-rock interactions over a wide range of P-T-X conditions requires a detailed understanding of high-P-T fluids' properties and their capacity to incorporate ligands (Cl, S, and F, but also sulfates or carbonates) and metals.

In this contribution, I wish to present the FAME autoclave developed around 20 years ago at the Neel Institute (Grenoble, France) to study metal concentration and speciation in hydrothermal fluids using X-ray absorption spectroscopy (XAS) at the FAME beamlines at the ESRF synchrotron (Testemale et al., 2005). Over the years, this setup has provided the Earth science community with a novel view on the hydration and complexation of metals in hydrothermal fluids, including a thorough evaluation of the nature and stability of various hydrated, Cl- or S-bearing complexes (review in Brugger et al. [2016]) and evidence for the formation of (HS)S3- complexes in S-bearing fluids (Pokrovski et al., 2022) or complexation of REE with carbonates in alkaline fluids (Louvel et al., 2022). Recent collaboration between the Neel Institute and ISTO (Orleans, France) also led to the update of the autoclave to reach T >800 °C, thus becoming, to the best of our knowledge, the first transparent internally heated pressure vessel (T-IHPV) enabling the *in situ* study of magmatic-hydrothermal processes.

As a first step, we have used the T-IHPV combined with high-energy resolution fluorescence detected HERFD-XAS to investigate the nature of Cu complexes in low-density high-T fluids and assess whether neutral alkali complexes (e.g., $(Na,K)CuCl_2^0$ or $(Na,K)CuCl(HS)^0$) suggested by fluid-melt partitioning experiments (Zajacz et al., 2011) and *ab initio* molecular dynamic (MD) simulations (Mei et al., 2014) could be detected with high-resolution spectroscopy. The high-T experiments (up to 550 °C at 60 MPa) investigated five different compositions: 0.15–0.82m HCl, 0.5m LiCl, 1m KCl–0.15m HCl, and 1m NaCl–0.2m HCl. In low-density fluids (ρ = 0.25–0.45g.cm^{-3}), we find noticeable differences in the XANES spectra of HCl versus (Li/Na/K)Cl solutions that suggest the formation of complexes involving either one or two Cl atoms (Fig. 1). While the formation of $CuCl(H_2O)$ in HCl low-density fluids had been previously suggested through conventional XAS measurements (Fulton et al., 2000; Louvel et al., 2017), these experiments provide the first spectroscopic evidence for the formation of neutral alkali complexes $(Li,Na,K)CuCl_2$.

Further developments include *in situ* XAS and Raman to 900–1000 °C to characterize the fluid-melt partitioning of volatiles (Br, S, Se) and metals (Cu, Zn, Pb) that we hope will provide new insights on the extent of metal scavenging upon magmatic degassing.

REFERENCES

Brugger J., Liu W., Etschmann B., Mei Y., Sherman D. M., and Testemale, D. (2016) A review of the coordination chemistry of hydrothermal systems, or do coordination changes make ore deposits? *Chemical Geology* **447**, 219–253.

Fulton J. L., Hoffmann M. M., and Darab J.G. (2000) An X-ray absorption fine structure study of copper(I) chloride coordination structure in water up to 325C. *Chemical Physics Letter* **330**, 300–308.

Louvel M., Bordage A., Tripoli B., Testemale D., Hazemann J-L., and Mavrogenes J. (2017) Effect of S on the aqueous and gaseous transport of Cu in porphyry and epithermal systems: Constraints from in situ XAS measurements up to 600C and 300bars. *Chemical Geology* **466**, 500–511.

Louvel M., Etschmann B., Guan Q., Testemale D., and Brugger J. (2022) Carbonate complexation enhances hydrothermal transport of rare earth elements in alkaline fluids. *Nature Communications* **13**, 1456.

Mei Y., Liu W., Sherman D. M., and Brugger J. (2014) Metal complexation and ion hydration in low density hydrothermal fluids: Ab initio molecular dynamics simulation of Cu(I) and Au(I) in chloride solutions (25-1000C, 1-5000bar). *Geochimica et Cosmochimica Acta* **131**, 196–212.

Pokrovski G. S., Desmaele E., Laskar C., Bazarkina E. F., Testemale D., Hazemann J-L., Vuilleumier R., Seitsonen A. P., Ferlat G., and Saitta A. M. (2022) Gold speciation in hydrothermal fluids revealed by in situ high energy resolution X-ray absorption spectroscopy. *American Mineralogist* **107**, 369–376.

Testemale D., Argoud R., Geaymond O., and Hazemann J-L. (2005) High pressure/high temperature cell for x-ray absorption and scattering techniques. *Review of Scientific Instruments* **76**, 043905.

Zajacz Z., Seo J. H., Candela P. A., Piccoli P. M., and Tossell J. A. (2011) The solubility of copper in high-temperature magmatic vapors: A quest for the significance of various chloride and sulfide complexes. *Geochimica et Cosmochimica Acta* **75**, 2811–2827.

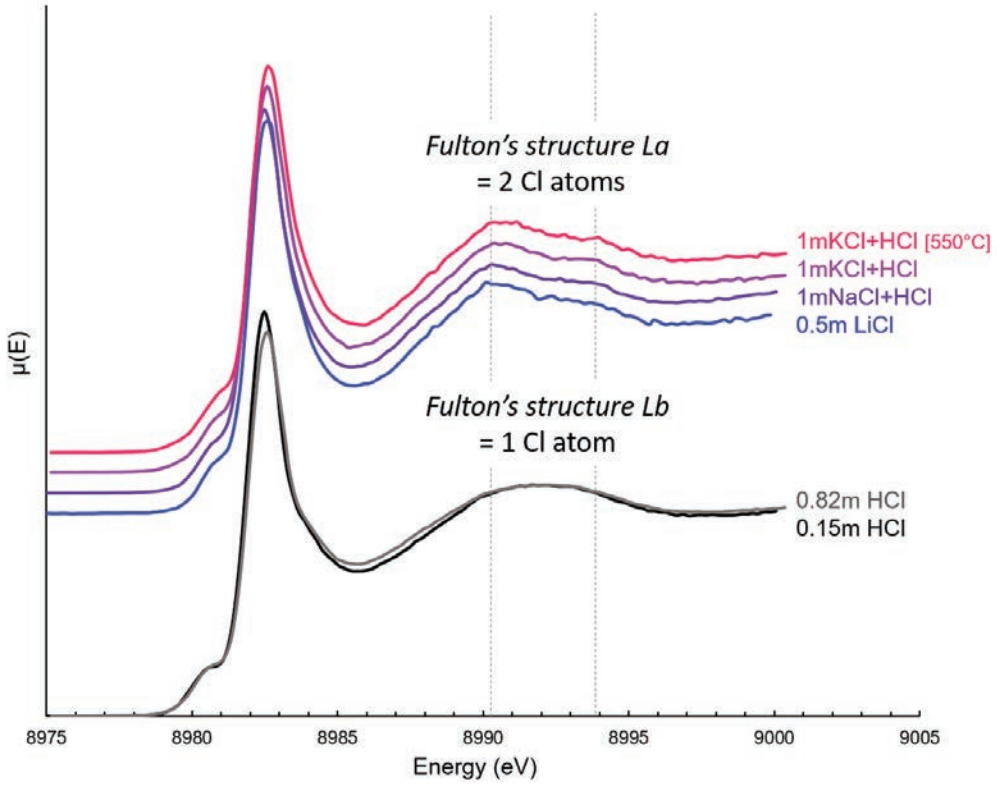

Figure 1. XANES spectra of Cu high-temperature low-density fluids. The arrows underline differences in the spectra that are attributed to the formation of $CuCl(H_2O)$ vs. $(Li,Na,K)CuCl_2$ neutral complexes.

IMPACT OF AMMONIA ON PLATINUM(II) BINDING TO GOETHITE

Fernanda Loza[1], Olwen Stagg[1], Elaine D. Flynn[1], Jeffrey G. Catalano[1]

[1] Department of Earth, Environmental, and Planetary Sciences, Washington University, St. Louis, MO 63130, USA

Platinum group elements (PGEs) are critical materials, with an increasing global demand and low natural abundance in the Earth's crust. Particularly, economic PGE deposits are typically associated with ultramafic rocks, with subsequent weathering resulting in the remobilization of PGEs (Zientek et al., 2017). Complexation with environmental ligands is shown to aid in remobilizing and releasing PGEs in the environment. Ammonia is a common environmental ligand predicted to form aqueous complexes with platinum (Pt) under neutral pH conditions (Colombo et al., 2008). However, data on the geochemical behavior of PGE-ammine complexes is limited, and therefore it is unclear whether such species will be retained by secondary iron (oxyhydr)oxide minerals formed during weathering.

We studied the impact of dissolved ammonia on platinum(II) adsorption to goethite at pH 7. In this study, experiments were conducted using varying concentrations of ammonia and platinum reacted with a suspension of goethite particles. A sodium chloride background salt was used to maintain constant ionic strength; prior work predicts weak to negligible complexation of platinum(II) by chloride at pH 7 (Colombo et al., 2008). After reaction, dissolved platinum concentrations were measured using inductively coupled plasma optical emission spectroscopy (ICP-OES). Goethite-free control reactors were prepared to determine whether platinum precipitated in an experiment because Pt(II) solubility under the experimental conditions is uncertain. Additionally, kinetic experiments were used to investigate the time scale over which equilibrium was reached. Reactors were mixed well and sampled over a 2-week period, with aliquots collected at selected time points.

Initial experiments reveal that Pt(II) binding by goethite varied with ammonia concentration (Fig. 1). Greater platinum binding was observed at elevated ammonia concentrations (e.g., 3–10 mM) compared to lower concentrations (e.g., ≤1 mM; Fig. 1). Simultaneously, the goethite-free reactors showed no precipitation of platinum. Finally, the aliquots collected at selected time points revealed that equilibrium was reached after 5 days, consistent with time scales for trace metal adsorption-desorption (Ledingham et al., 2024).

Overall, this study provides further insight into the fundamental geochemical behavior of platinum in weathering environments, demonstrating that ammonia likely affects platinum mobilization and retention during alteration of ultramafic deposits. Ongoing studies are investigating the oxidation state of platinum associated with goethite because a recent study suggested that feroxyhyte, a different iron oxyhydroxide, oxidizes Pt(II) to Pt(IV) (Li et al., 2023). In addition, we are investigating platinum adsorption to hematite under similar chemical conditions because this phase is also abundant in weathered PGE deposits.

REFERENCES

Colombo C., Oates C. J., Monhemius A. J., and Plant J. A. (2008) Complexation of platinum, palladium and rhodium with inorganic ligands in the environment. *Geochemistry: Exploration, Environment, Analysis* 8, 91–101.

Ledingham G. J., Fang Y., and Catalano J. G. (2024) Irreversible trace metal binding to goethite controlled by the ion size. *Environmental Science & Technology* 58, 2007–2016.

Li Z., Sun X., Li D., Liang Y., Li S., and Peng J. (2023) Platinum enrichment in marine ferromanganese oxides: Constraints from surface adsorption behavior on synthetic feroxyhyte (δ-FeOOH). *Chemical Geology* **615**, 121204.

Zientek M. L., Loferski P. J., Parks H. L., Schulte R. F., and Seal R. R. II (2017) Platinum-group elements, In: Schulz K. J., DeYoung J. H. Jr., Seal R. R. II, and Bradley D. C. (eds.), *Critical Mineral Resources of the United States—Economic and Environmental Geology and Prospects for Future Supply*. U.S. Department of the Interior, U.S. Geological Survey.

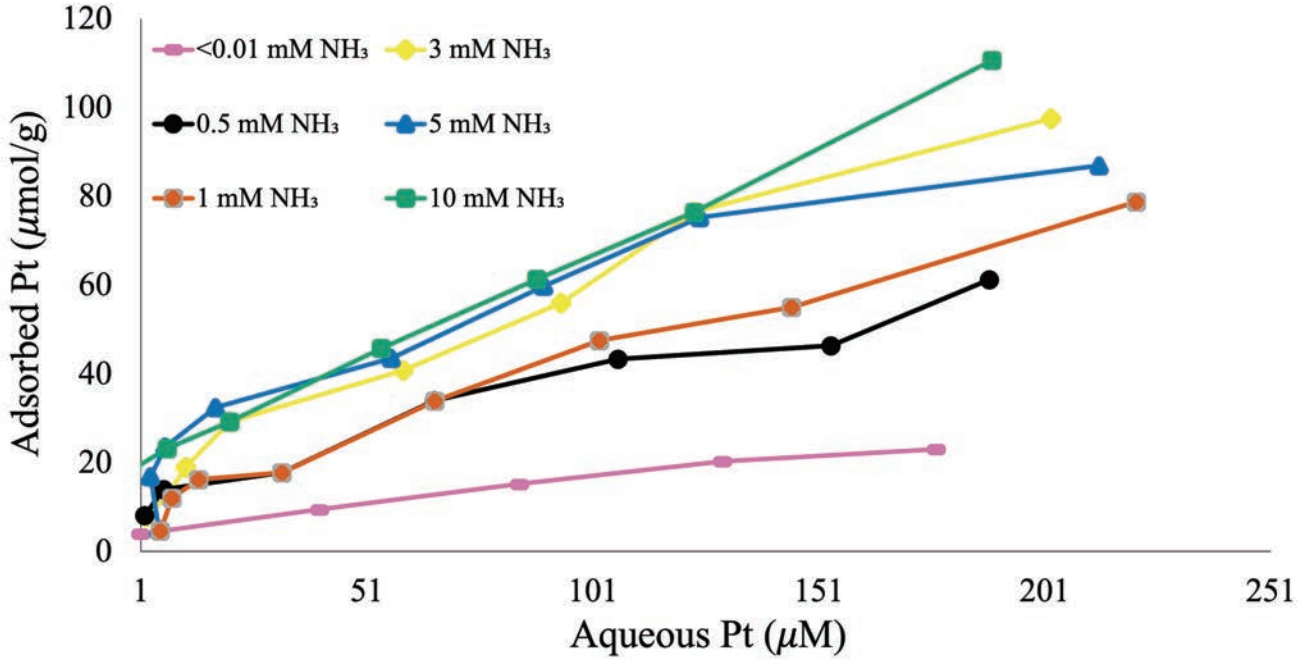

Figure 1. Platinum (Pt) adsorption to goethite in the presence of varying ammonia concentrations at pH 7.

IN SITU RAMAN SPECTROSCOPY OF RARE EARTH ELEMENT SPECIATION IN ACIDIC SULFATE-BEARING AQUEOUS FLUIDS FROM 25 TO 500 °C

Bryan J. Maciag[1], Alexander P. Gysi[1,2], Nicole C. Hurtig[2]

[1] New Mexico Bureau of Geology and Mineral Resources, New Mexico Institute of Mining and Technology, Socorro, NM 87801, USA
[2] Department of Earth and Environmental Science, New Mexico Institute of Mining and Technology, Socorro, NM 87801, USA

Rare earth elements (REE) are essential for the continued development of green and advanced technologies. In natural geologic systems, REE mineral deposits form through an interplay of magmatic and hydrothermal processes (Gysi et al., 2016). Aqueous fluids mobilize, fractionate, or concentrate REE depending on the ligands present in solution (Migdisov et al., 2016). Experimental and modeling studies show that chloride (Cl^-) and sulfate (SO_4^{2-}) mobilize the REE in acidic fluids, whereas complexes such as fluoride (F^-) sequester the REE due to the precipitation of insoluble minerals such as the REE fluorocarbonates (Migdisov et al., 2016). The formation constants of REE sulfate (i.e., $REESO_4^+$ and $REE(SO_4)_2^-$) species are summarized in Migdisov et al. (2016) up to 250 °C, whereas the REE bisulfate ($REEHSO_4^{2+}$) complexes have only recently been identified by Raman spectroscopy in the study by Wan et al. (2021).

In this study, we use a hydrothermal diamond anvil cell (HDAC; Fig. 1a) and capillary quartz cells to determine the speciation of Nd and Yb *in situ* via confocal Raman spectroscopy. The experiments were conducted in acidic (pH <3) aqueous sulfate-bearing solutions [$Nd_2(SO_4)_3$- or $Yb_2(SO_4)_3$-H_2SO_4-H_2O] from 25 to 500 °C and pressures up to 500 MPa in the HDAC cell and at saturated water vapor pressure in the quartz capillary cells. The sulfate and bisulfate Raman vibrational bands at ~980 cm^{-1} and 1050 cm^{-1} are used to determine the stabilities of REE sulfate and bisulfate complexes (Figs. 1b and 1c).

At 25 °C (Fig. 1b), the bisulfate vibrational band in a REE-free solution with 0.09 m Na_2SO_4 is positioned at ~1052 cm^{-1}. For the 0.03 m Nd-bearing solution, this band is broader, and the 0.03 m Yb-bearing solution shows a clearer asymmetry caused by an additional peak at ~1047 cm^{-1}. These changes in the bisulfate peak are interpreted to be from REE bisulfate complexes, which appear more prominent for the heavy REE (i.e., Yb). The sulfate vibrational band in a REE-free solution is positioned at ~981 cm^{-1}. Both REE-bearing solutions have shoulders at ~981 cm^{-1} and ~996 cm^{-1} for Nd- or Yb-bearing solutions, respectively. These shoulders indicate the presence of abundant REE mono-sulfate complexes that are more prominent for the light REE (i.e., Nd).

At 300 °C (Fig. 1c), the bisulfate peak measured in the 0.09 m Na_2SO_4 solution is larger than the sulfate peak, and its position shifts to a slightly higher wavenumber of ~1053.5 cm^{-1}. In the Yb-bearing solution, the measured bisulfate vibrational band is also dominant and is slightly asymmetric, with a tailing appearing on the lower wavenumber's side. Deconvolution of this peak indicates a vibrational band at 1046 cm^{-1} that is interpreted as the presence of a Yb bisulfate complex. At these acidic conditions (initial pH of 1.7), the REE bisulfate is the only REE-S complex at 300 °C due to the absence of sulfate ions. At slightly less

acidic conditions (initial pH of 2.5), sulfate is present at 300 °C and both REE sulfate and REE bisulfate are present in the solution.

In conclusion, our study agrees with the observations of Wan et al. (2021), which indicate the presence of REE bisulfate complexes in hydrothermal sulfate-bearing aqueous fluids. In strongly acidic sulfate-bearing solutions, the abundance of the REE bisulfate complexes increases from 25 to 300 °C (Fig. 1), with the predominance of REE sulfate versus bisulfate complexes depending on the solution pH. Future studies need to assess the stability of the REE bisulfate complex to more accurately model REE transport in acidic sulfate-rich systems. The REE bisulfate species could account for significant fractionation between light and heavy REE, which was not previously recognized based on the stability of REE sulfate complexes.

REFERENCES

Gysi A. P., Williams-Jones A. E., and Collins P. (2016) Lithogeochemical vectors for hydrothermal processes in the Strange Lake peralkaline granitic REE-Zr-Nb deposit. *Economic Geology* **111**, 1241–1276.

Migdisov A., Williams-Jones A. E., Brugger J., and Caporuscio F. A. (2016) Hydrothermal transport, deposition, and fractionation of the REE: Experimental data and thermodynamic calculations. *Chemical Geology* **439**, 13–42.

Wan Y., Wang X., Chou I.-M., and Li X. (2021) Role of sulfate in the transport and enrichment of REE in hydrothermal systems. *Earth and Planetary Science Letters* **569**, 117068.

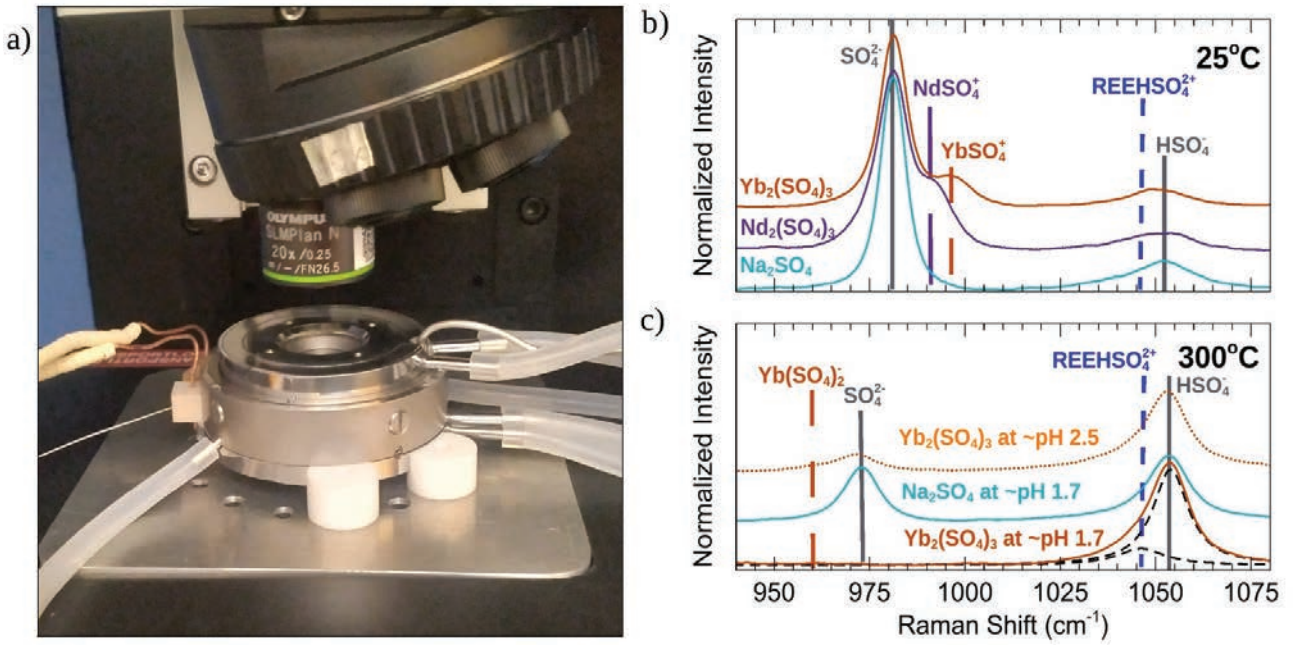

Figure 1. a) Hydrothermal diamond anvil cell equipped with a gas membrane, 1 mm culet diamonds, and a gasket heater mounted on a confocal Raman microscope. b) Normalized Raman spectra of the sulfate and bisulfate band for pH ~1.7 solutions containing 0.03 m $Nd_2(SO_4)_3$, 0.03 m $Yb_2(SO_4)_3$, and 0.09 m Na_2SO_4 at 25 °C. c) Normalized Raman spectra of the sulfate and bisulfate band at 300 °C. Asymmetry of the SO_4^{2-} and HSO_4^- peaks indicates the presence of REE sulfate complexation. Dashed curves are subpeak deconvolutions of the pH 1.7 0.03 m $Yb_2(SO_4)_3$ spectra at 300 °C, highlighting the presence of $YbHSO_4^{2+}$.

TRANSPORT AND DEPOSITION OF ND IN CARBONATE-BEARING HYDROTHERMAL SYSTEMS

A. Migdisov[1], M. Reece[1], H. Xu[1], A. Gysi[2,3]

[1] Earth and Environmental Sciences Division, Los Alamos National Laboratory, Los Alamos, NM 87545, USA
[2] Department of Earth and Environmental Science, New Mexico Institute of Mining and Technology, Socorro, NM 87801, USA
[3] New Mexico Bureau of Geology and Mineral Resources, New Mexico Institute of Mining and Technology, Socorro, NM 87801, USA

Carbonate-rich solutions often serve as the main vehicle for the transport and concentration of rare earth elements (REE; e.g., Gysi et al. [2016]), and this has been observed in many natural systems (e.g., Lipin and McKay [2018]). However, surprisingly little is currently known about the fundamental chemical controls of these processes. A qualitative and quantitative understanding of these processes requires the assembly of two major parts of the puzzle: (1) understanding the speciation of REE in high-temperature carbonate-bearing aqueous solutions (mobilization) and (2) characterizing the high-temperature stability of the main REE-bearing minerals (immobilization). In this study, we attempt to address and quantify both of these effects for a system containing neodymium (Nd), which is a light REE.

Solubility experiments were performed in Teflon-lined Ti autoclaves at temperatures of 100–250 °C at saturated water vapor pressure, and in cold seal vessels at 400–600 °C at 1 kbar. The first stage involved determining the solubility of synthetic monazite ($NdPO_4$) in Na_3PO_4-buffered carbonate-bearing solutions to determine the stoichiometry and stability of the predominant Nd-carbonate complexes. The following stage involved determining the solubility of fluorobastnaesite ($NdCO_3F$) in NaF-buffered (2.5×10^{-3} and 5×10^{-2} mol kg^{-1}) carbonate-bearing solutions. This stage focused on quantifying the stability of fluorobastnaesite-(Nd), and interpretation of the solubilities obtained at this stage was based on the data from the Nd-monazite experiments. The experiments employed the phase separation technique in which the reference solid phase is separated from experimental solutions in a holder and the interaction between the phase and the solution is artificially slowed down using either a porous membrane (in the case of 100–250 °C experiments) or a crumpled but not sealed end of a 1 mm gold tube, which served as a sample holder in cold-seal experiments. The experimental design thus employed two operational volumes: a large external volume containing the experimental solution and a small micro-volume containing the solid phase. Slowing down the re-equilibration between these two volumes allows for avoiding effects associated with heating and quenching of the autoclaves: if the time required to saturate the solution through the porous membrane is 4–5 days, and heating/quenching manipulations are limited to less than 1–2 hours, the effects associated with changing temperature can be ignored. This approach also ensures that all Nd found in the external volume (quenched in the solutions or precipitated on the walls) is due to the dissolution of the reference phase at experimental conditions and is not altered by any other sources. After quenching and opening, the holders were removed, concentrated sulfuric acid was added, and potential precipitates were dissolved at 200 °C. Experiments were performed with $NaHCO_3$ and Na_2CO_3 solutions with concentrations ranging from 0.01 to 1 mol kg^{-1}.

Experimental data suggest that the Nd-bearing carbonate complex predominant at experimental conditions is $NdCO_3OH^o$. The thermodynamic stability of this species was determined, and the parameters for the Helgeson-Kirkham-Flowers (HKF) model were derived. These parameters, along with the data collected for the solubility of bastnaesite, were used to derive the solubility products, and, in turn, the values of the Gibbs energy of formation (ΔG^o_T) for

this phase. The data suggest that carbonate complexes can be extremely efficient in transporting Nd under hydrothermal conditions. For example, the solubility of bastnaesite at 450 °C can be as high as 2000 ppm in solutions containing a moderate 0.1 mol kg^{-1} mCO_3^{tot}, and 100 ppm of F^-.

REFERENCES

Gysi A. P., Williams-Jones A. E., and Collins P. (2016) Lithogeochemical vectors for hydrothermal processes in the Strange Lake peralkaline granitic REE-Zr-Nb deposit. *Economic Geology* **111**, 1241-1276.

Kestin J., Sengers J. V., Kamgar-Parsi B., and Sengers J. M. H. L. (1984) Thermophysical properties of fluid H_2O. *Journal of Physical and Chemical Reference Data* **13**, 175–183.

Konings R. J. M., Beneš O., Kovács A., Manara D., Sedmidubský D., Gorokhov L., Iorish V. S., Yungman V., Shenyavskaya E., and Osina E. (2014) The thermodynamic properties of the f-elements and their compounds. Part 2. The lanthanide and actinide oxides. *Journal of Physical and Chemical Reference Data* **43**, 013101.

Lipin B. R. and McKay G. A. (eds.) (2018) *Geochemistry and mineralogy of rare earth elements* **21**. Walter de Gruyter GmbH & Co KG.

BEYOND GEMS: INTEGRATION OF THERMODYNAMIC DATASETS, ACTIVITY MODELS, AND PARAMETER OPTIMIZATION

G. Dan Miron[1], Dmitrii A. Kulik[1]

[1] Laboratory for Waste Management (LES), Paul Scherrer Institute, 5232 Villigen PSI, Switzerland

The quality of any geochemical model cannot be better than the quality of input thermodynamic data. The model applicability also depends on the selection of relevant chemical species with reliable standard-state data, as well as on *T,P* ranges covered (Miron et al., 2017; Lothenbach et al., 2019). The task of retrieving good thermodynamic data from critically reviewed literature and improving the internal consistency of a thermodynamic dataset (TDS) is far from trivial and must be supported by dedicated computational parameter fitting and data management tools, some of which have been developed at LES PSI already for 10 years. When enough experimental data are available, a consistent TDS extension is possible via the multiparameter optimization by inverse modelling of experimental systems using, e.g., the GEMSFITS code (Miron et al., 2015). In many practically important cases, there are gaps in experimental data, and some relevant species are missing. The "gap" errors can be minimized using LFER correlations or isocoulombic reactions (Miron et al., 2020). Finally, thermodynamic datasets need to be maintained, efficiently corrected to *T,P* of interest, and delivered to GEMS, PHREEQC, or other chemical equilibria modelling codes. This tedious labor can be reduced by currently developed dedicated online and local property-graph databases (ThermoHub) and computational codes such as ThermoFun (Miron et al., 2023). Our "ecosystem" of databases and tools, called ThermoEcos (in progress), will include databases of parameters of mixing activity models, predefined compositions, and experimental data, integrated with code libraries performing geochemical modelling (xGEMS, Reaktoro), web apps, or parameter optimization calculations (ThermoFit). When available, ThermoEcos will support a totally new level of education, research, and collaboration in geochemical modelling. Some achievements will be shown on a few application examples.

REFERENCES

Lothenbach B., Kulik D. A., Matschei T., Balonis M., Baquerizo L., Dilnesa B., Miron G. D., and Myers R. J. (2019) Cemdata18: A chemical thermodynamic database for hydrated Portland cements and alkali-activated materials. *Cement and Concrete Research* **115**, 472–506.

Miron G. D., Kulik D. A., Dmytrieva S. V., and Wagner T. (2015) GEMSFITS: Code package for optimization of geochemical model parameters and inverse modeling. *Applied Geochemistry* **55**, 28–45.

Miron G. D., Wagner T., Kulik D. A., and Lothenbach B. (2017) An internally consistent thermodynamic dataset for aqueous species in the system Ca-Mg-Na-K-Al-Si-O-H-C-Cl to 800 °C and 5 kbar. *American Journal of Science* **317**, 754–805.

Miron G. D., Kulik D. A., and Thoenen T. (2020) Generating isocoulombic reactions as a tool for systematic evaluation of temperature trends of thermodynamic properties: Application to aquocomplexes of lanthanides and actinides. *Geochimica et Cosmochimica Acta* **286**, 119–142.

Miron G. D., Leal A. M. M., Dmytrieva S. V., and Kulik D. A. (2023) ThermoFun: A C++/Python library for computing standard thermodynamic properties of substances and reactions across wide ranges of temperatures and pressures. *Journal of Open Source Software* **8**, 4624.

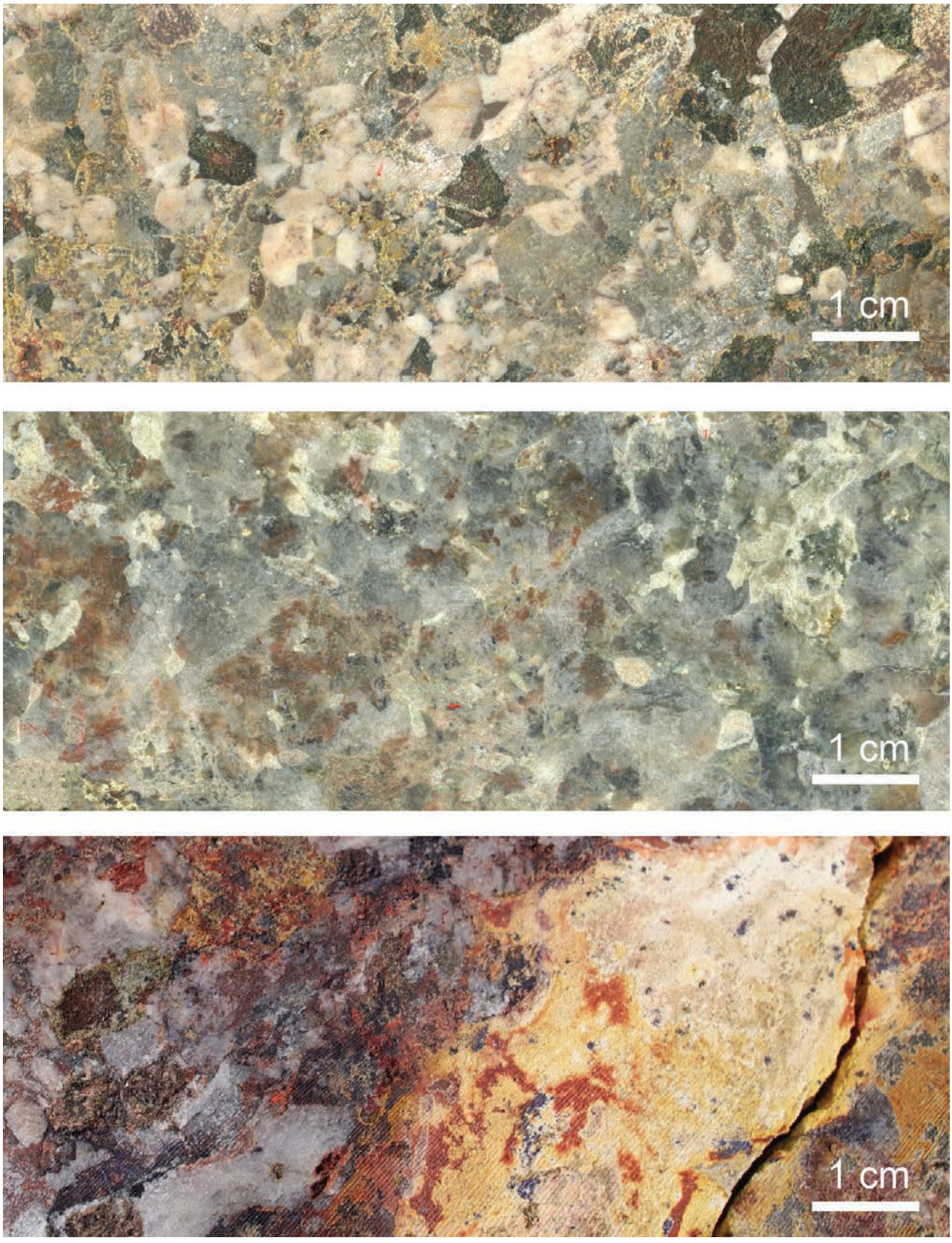

Rock scans of mineralized pegmatites overprinted by hydrothermal alteration from the Strange Lake REE-Zr-Nb deposit, Quebec, Canada.
Photo by A. Gysi

HYDROTHERMAL SOLUBILITY EXPERIMENTS AND DETERMINATION OF THE STABILITY OF LA^{3+} AQUA ION AND LA HYDROXYL COMPLEXES IN ACIDIC TO MILDLY ACIDIC AQUEOUS SOLUTIONS TO 250°C

Kevin Padilla[1,2], Alexander P. Gysi[1,2]

[1] Department of Earth and Environmental Science, New Mexico Institute of Mining and Technology, Socorro, NM 87801, USA
[2] New Mexico Bureau of Geology and Mineral Resources, New Mexico Institute of Mining and Technology, Socorro, NM 87801, USA

The mobility of the rare earth elements (REE) in natural hydrothermal systems can be modeled if reliable thermodynamic data are available. The aqueous REE chloride and sulfate complexes are predicted to be stable in acidic to mildly acidic hydrothermal fluids (Migdisov et al., 2016), whereas hydroxyl complexes are expected to become important at higher pH (Perry and Gysi, 2018). However, data on the thermodynamic stability of hydroxyl complexes are still largely based on the Helgeson-Kirkham-Flowers equation of state parameters and extrapolations using data from Haas et al. (1995).

Batch-type hydrothermal solubility experiments (Figs. 1a and 1b) were conducted to evaluate the controls of pH and temperature on lanthanum (La) hydroxyl speciation. Synthetic La hydroxide powders were equilibrated for up to 14 days in perchloric acid-based aqueous solutions with starting pH values of 2–5 at 150–250 °C. The total dissolved La concentrations are measured in the quenched experimental solutions using inductively coupled plasma optical emission spectroscopy (ICP-OES). The pH is calculated at the experimental conditions using the GEMS code package (**https://gems.web.psi.ch/**) and the MINES thermodynamic database (Gysi et al., 2023). The thermodynamic properties for La hydroxyl complexes are optimized using GEMSFITS (Miron et al., 2015).

The La hydroxide solubility is retrograde with temperature and displays a strong pH dependence (Fig. 1c). With increased pH from acidic to mildly acidic, the measured log(*m*La) values decrease from -2.4 to -5.4 at 150 °C, -2.4 to -5.8 at 200 °C, and -2.4 to -7.2 at 250 °C. The equilibrium pH values of the experimental solutions were initially calculated using the thermodynamic properties for La hydroxyl complexes from Haas et al. (1995). These calculations resulted in problematic slopes in a log(*m*La) versus pH diagram, which are inconsistent with the expected trends based on the stoichiometry of La speciation: $La^{3+} + nOH^- = La(OH)_n^{3-n}$. In contrast, optimization of the thermodynamic properties of La^{3+}, $LaOH^{2+}$, and $La(OH)_2^+$ aqueous species results in more consistent trends; the calculated pH values range from 4.6 to 5.6 at 150 °C, 4.1 to 5.2 at 200 °C and 3.4 to 5.0 at 250 °C.

The experimental data indicate inaccurate predictions of the stability of the La^{3+} ion and La hydroxyl complexes in acidic solutions, particularly above 200–250 °C. The experimentally derived standard partial molal Gibbs energy values for La^{3+}, $LaOH^{2+}$, $La(OH)_2^+$ differ by ~1 to 20 kJ/mol in comparison those derived from Haas et al. (1995). Furthermore, the calculated equilibrium pH values differ by 0.5 to 1 units in comparison to predictions. The optimized thermodynamic properties for La aqueous species have important implications for modeling the solubility of REE minerals (e.g., monazite) and the mobility of REE in nature. These experiments are aimed at building an internally consistent dataset that is integrated in the MINES thermodynamic database (Gysi et al., 2023).

This work is supported by the U.S. Department of Energy under Award DE-SC0021106.

REFERENCES

Gysi A. P., Hurtig, N. C., Pan, R., Miron, G. D., and Kulik, D. A. (2023) MINES thermodynamic database, New Mexico Bureau of Geology and Mineral Resources, version 23, https://doi.org/10.58799/mines-tdb.

Haas J. R., Shock E. L., and Sassani D. C. (1995) Rare earth elements in hydrothermal systems: Estimates of standard partial molal thermodynamic properties of aqueous complexes of the rare earth elements at high pressures and temperatures. *Geochimica et Cosmochimica Acta* **59**, 4329–4350.

Migdisov A. A., Williams-Jones A. E., Brugger J., and Caporuscio F. A. (2016) Hydrothermal transport, deposition, and fractionation of the REE: Experimental data and thermodynamic calculations. *Chemical Geology* **439**, 13–42.

Miron G. D., Kulik D. A., Dmytrieva S. V., and Wagner T. (2015) GEMSFITS: Code package for optimization of geochemical model parameters and inverse modeling. *Applied Geochemistry* **55**, 28–45.

Perry E. P. and Gysi A. P. (2018) Rare earth elements in mineral deposits: Speciation in hydrothermal fluids and partitioning in calcite. *Geofluids* **2018**, 1–19.

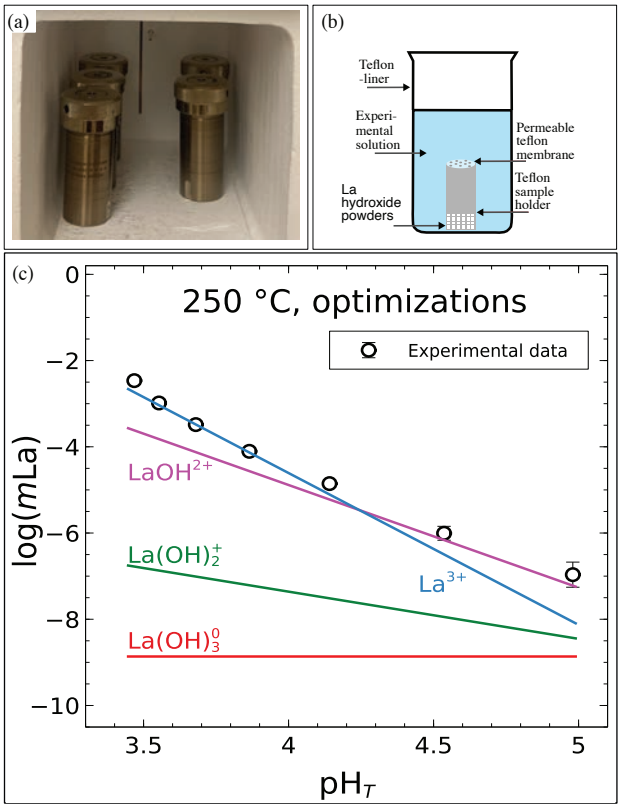

Figure 1. (a) Experimental setup for the La hydroxide solubility experiments showing a photograph of batch-type reactors placed in the furnace, and (b) a schematic of the inside of the reactors. (c) Experimental results showing the logarithm of total dissolved La concentrations [log(*m*La)] measured in the quenched experimental solutions as a function of calculated equilibrium pH based on the optimized thermodynamic properties for La aqueous species derived in this study at 250 °C.

APATITE RARE EARTH ELEMENTS CHEMISTRY AND FLUID EVOLUTION IN THE LEMITAR MOUNTAINS CARBONATITE, NEW MEXICO

Eric Ruggles[1], Nicole C. Hurtig[1], Alexander P. Gysi[1,2], Virginia T. McLemore[2], Jay Thompson[3]

[1] Department of Earth and Environmental Science, New Mexico Institute of Mining and Technology, Socorro, NM 87801, USA
[2] New Mexico Bureau of Geology and Mineral Resources, New Mexico Institute of Mining and Technology, Socorro, NM 87801, USA
[3] USGS-LTRACE Laboratory, Geology, Geophysics, and Geochemistry Science Center, Denver, CO 80225, USA

The 515 Ma Lemitar Mountains carbonatite (Fig. 1A) is a rare earth element (REE) mineral deposit in New Mexico composed of over one hundred carbonatite dikes intruded into Proterozoic igneous rocks (McLemore, 1987; Haft et al., 2022). The carbonatite displays grades of up to 1.1% total REE and exhibits variable degrees of hydrothermal autometasomatism and overprinting of the surrounding host rocks via fenitization and veining (McLemore, 1987; Perry, 2019; Haft et al., 2022). Here we use a combination of petrography, optical cold-cathode cathodoluminescence, and scanning electron microscopy to constrain mineral paragenesis of the carbonatites and crosscutting hydrothermal veins (Fig. 1). LA-ICP-MS was used to determine REE concentrations in apatite. Fluid inclusions were studied in thick sections using optical microscopy, microthermometry, and confocal Raman spectroscopy to determine their salinity, homogenization temperature, and chemical composition.

Magmatic minerals in carbonatite dikes comprise calcite, dolomite, phlogopite, magnetite, apatite, baddeleyite, and pyrochlore. Three hydrothermal vein types were distinguished in this study (Figs. 1A and 1B): type I veins (albite-quartz), which represent the earliest hydrothermal veins; type II veins (quartz-chlorite ± calcite), which crosscut type I veins and are associated with REE-bearing minerals, including parisite, zircon, and monazite; and type III veins, which comprise calcite, fluorite-calcite, and barite ± hematite (± parisite) veins. Alteration associated to type I veins includes silicification and sodic fenitization. Alteration styles associated to types II veins include silicification, chloritization, potassic fenitization, and hematization. Alteration associated to type III veins is characterized by silicification and/or Ca-F metasomatism.

Three different generations of apatite were distinguished based on textures and REE chemistry. Apatite 1 is present as rounded xenocrysts in the carbonatite matrix and shows a dull yellow fluorescence. Apatite 2 is commonly associated with hydrothermally altered carbonatites and occurs as euhedral crystals with dull to bright yellow fluorescence. Apatite 3 occurs in the fenitized mafic rocks adjacent to the carbonatite dikes and is characterized by 100–500 µm long euhedral crystals with a distinct yellow to blue fluorescence. Apatite 1 contains on average ~0.2 wt% REE, apatite 2 contains up to 3.2 wt% REE, and apatite 3 contains on average ~0.4 wt% REE. Average chondrite-normalized REE profiles of the three apatite generations display distinct light versus heavy REE variations (Fig. 1C). Apatite 2 is enriched in light REE and apatite 3 displays a flat REE profile with heavy REE enrichment.

Fluid inclusions (FI) hosted in apatite are complex, multi-phase, solid dominated inclusions. Quartz-hosted inclusions from type I veins are characterized by liquid-vapor inclusions with up to 40 vol% vapor. Calcite- and quartz-hosted FI in type II and calcite-, fluorite-, and quartz-hosted FI in type III veins are liquid dominated with up to 15 vol% vapor, with some of them containing a halite daughter crystal coexisting with vapor dominated inclusions. Microthermometry in inclusions from type III veins indicates homogenization temperatures of ~180 °C, with salinities ranging from ~2–15 wt% NaCl equivalent. The presence of H_2 and CH_4 gaseous species and SO_4^{2-}, CO_3^{2-}, and dissolved CO_2 species was measured in quartz from type I veins.

Type III veins containing fluorite-hosted inclusions from the fenitized country rock are observed with H_2 and CH_4 gas, whereas fluorite crosscutting the carbonatites is observed containing SO_4^{2-}.

In conclusion, three different vein generations are distinguished, with types II and III containing REE minerals. Apatite 1 displays a clear magmatic REE signature, whereas apatites 2 and 3 display an enrichment in light and heavy REE, respectively. Fluid inclusions indicate decreasing temperature from type I to type III veins, with reducing gases (i.e., H_2 and CH_4) present in the fenitized zone and an oxidizing sulfate-bearing fluid in the carbonatite, with SO_4^{2-} representing an important ligand for REE transport in this system.

REFERENCES

Haft E. B., McLemore V. T., Ramo O. T., and Kaare-Rasmussen J. (2022) Geology of the Cambrian Lemitar carbonatites, Socorro County, New Mexico: Revisited. In *New Mexico Geological Society Fall Field Conference Guidebook–72 Socorro Region III*, 365–373. New Mexico Geological Society.

McLemore V. T. (1987) Geology and regional implications of carbonatites in the Lemitar Mountains, central New Mexico. *The Journal of Geology* **95**, 255–270.

Perry E. P. (2019) Rare Earth Element Signatures in Hydrothermal Calcite: Insights from Numerical Modeling, Experimental Geochemistry, and Mineral Deposits in New Mexico. Ph.D. Dissertation, Colorado School of Mines.

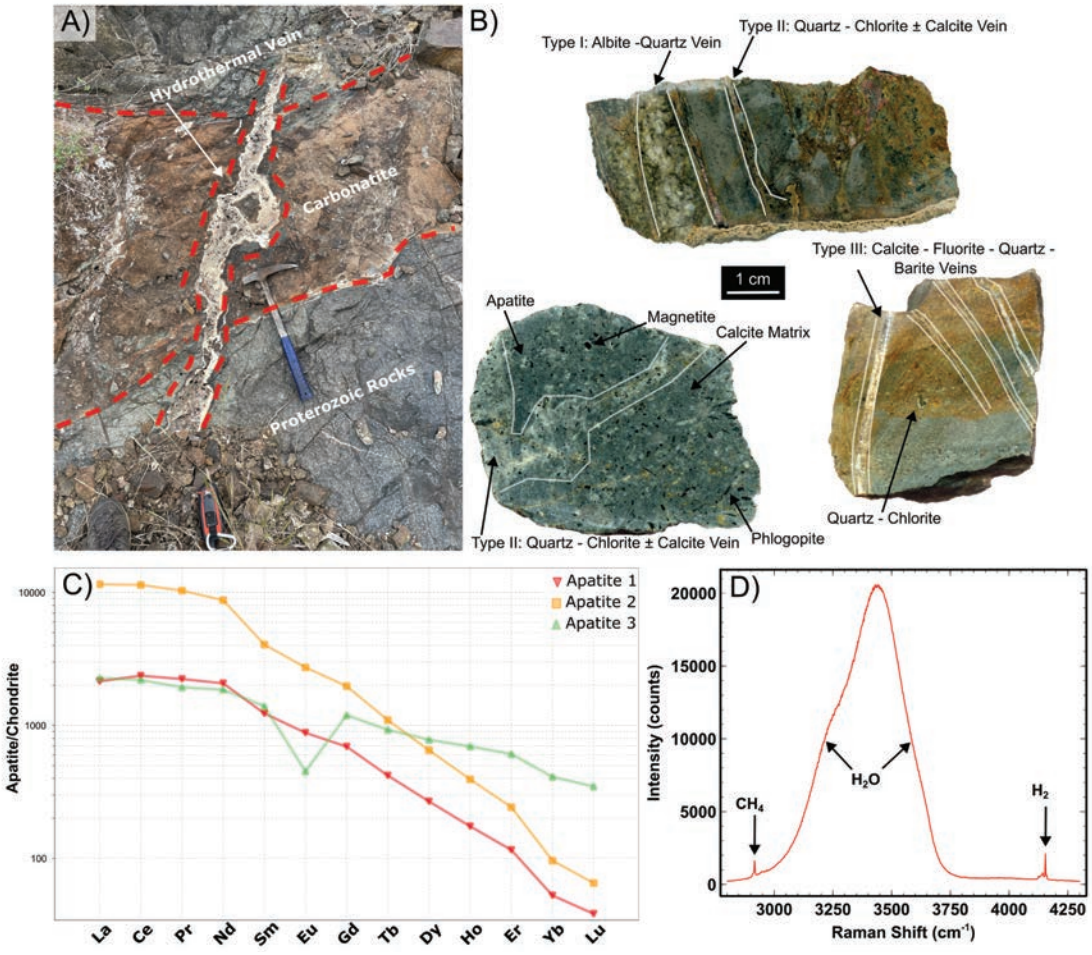

Figure 1. A) Primary carbonatite crosscutting Proterozoic host rocks and hydrothermal calcite vein crosscutting the carbonatite dike. B) Carbonatite hand samples displaying varying levels of overprint by type I, II, and III veins. C) Chondrite-normalized REE diagram displaying the three generations of apatite. D) Raman spectra of quartz-hosted FI in type I vein displaying the presence of liquid H_2O and CH_4 and H_2 gases.

UNDERSTANDING WHAT'S BELOW: USING THE OPEN-SOURCE TOOLBOX HYDROTHERMALFOAM TO SIMULATE SUBMARINE HYDROTHERMAL SYSTEMS

Lars Rüpke[1], Zhikui Guo[1,2], Jasper Engelmann[1]

[1] GEOMAR Helmholtz Centre for Ocean Research Kiel, Germany

[2] Key Laboratory of Submarine Geosciences, MNR, Second Institute of Oceanography, China

Hydrothermal discharge at so-called black smokers along the global mid-ocean ridge system continues to amaze and fascinate the interdisciplinary marine sciences community. Seawater penetrates into the newly formed seafloor along cracks and fractures to reach and react at high temperatures with partially molten rock to form a metal-rich hydrothermal fluid that rises buoyantly toward a vent site at the seafloor. These systems efficiently mine heat from the young ocean crust, sustain unique ecosystems in the otherwise bleak environment of the deep seafloor, and mobilize metals from the crust to form economically interesting ore deposits. Much has been learned about these systems and their role in the Earth system from marine surveys of mid-ocean ridge segments and direct observations of vent sites at the seafloor. Yet the deep chemical and physical processes that control hydrothermalism remain inaccessible to direct sampling and observations.

Here, numerical models can help because they can be used to relate seafloor observations to processes and to elucidate the physical connections between interdisciplinary datasets. At least two major challenges remain: resolving the multiphase nature of hydrothermal fluid flow and incorporating chemistry into these models. In this presentation, we will present our open-source toolbox, HydrothermalFoam. It is based on the computational fluid dynamics package OpenFOAM (Guo et al., 2020) and serves as a basis for modeling approaches and workflows addressing the first challenge. This toolbox works with our new implementation, xthermal, of the Driesner and Heinrich (2007) equation of state for the H_2O-NaCl system. The xthermal API allows for exploring and visualizing representative PTX paths for the phase state and computing fluid properties over the full pressure, temperature, and salinity ranges relevant for magmatic-hydrothermal systems (available for C++, Python, Matlab, and Julia). Furthermore, we demonstrate how so-called geomodels can be built, which integrate diverse geological and geophysical datasets into geometric representations of the subsurface. Such geomodels can serve as a basis for formulating and testing hydrothermal flow scenarios by performing HydrothermalFoam simulations with realistic geometries and boundary conditions.

The application of these tools and workflows will be shown for the TAG hydrothermal field (Guo et al., 2023). The TAG hydrothermal mound at 26°N on the Mid-Atlantic Ridge is located on the hanging wall of a detachment fault and has formed through distinct phases of high-temperature fluid discharge lasting tens to hundreds of years throughout at least the last 50,000 years. Yet the mechanisms that control the episodic behavior, keep the fluid pathways intact, and sustain the observed high heat fluxes of possibly up to 1800 MW remain poorly understood. Using the aforementioned workflows, we will show various plausible and implausible flow solutions for the TAG hydrothermal system.

REFERENCES

Driesner T. and Heinrich C. A. (2007) The system H_2O-NaCl. Part I: Correlation formulae for phase relations in temperature-pressure-composition space from 0 to 1000 degrees C, 0 to 5000 bar, and 0 to 1 X-NaCl. *Geochimica Et Cosmochimica Acta* **71**(20), 4880–4901.

Guo Z., Rüpke L., and Tao C. (2020) HydrothermalFoam v1.0: A 3-D hydro-thermo-transport model for natural submarine hydrothermal systems. *Geoscientific Model Development*.

Guo Z., Rüpke L., Petersen S., German C. R., Ildefonse B., Hasenclever J., Bialas J., and Tao C. (2023) Detachment-parallel recharge can explain high discharge fluxes at the TAG hydrothermal field. *Earth and Planetary Science Letters* **617**, 118245.

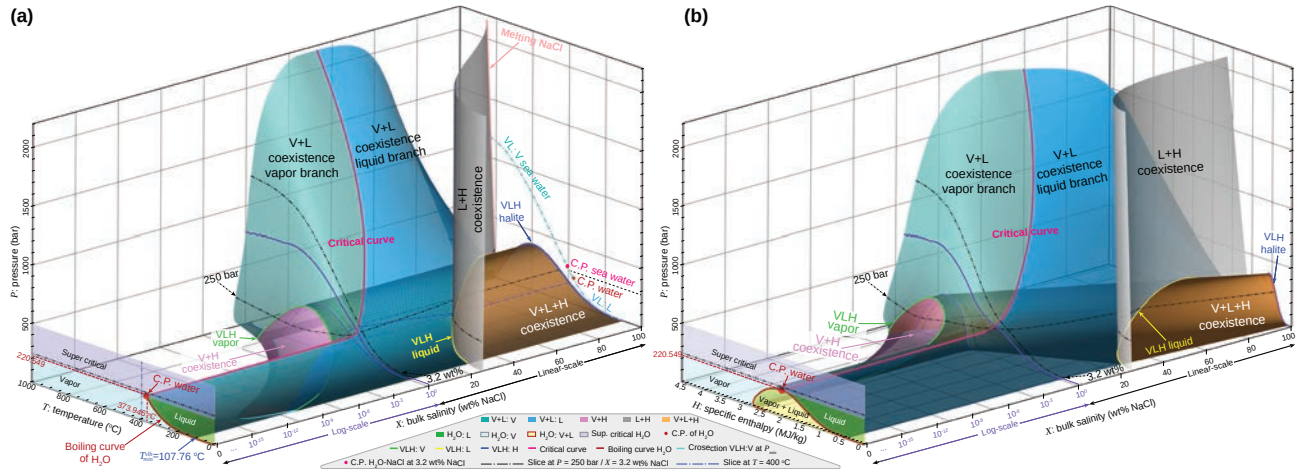

Figure 1. Phase diagram of saltwater in (a) TPX space and (b) HPX space. The x-axis is presented as a hybrid log-scale to better show details of phase relations in low-salinity regions. The log- and linear-scale segments of the x-axis are split by 1 wt% NaCl (purple solid line) and marked by purple and black color, respectively.

TOWARD THE DEVELOPMENT OF NEW THERMODYNAMIC MODELS FOR HYDROTHERMAL FLUIDS USING MOLECULAR DYNAMICS SIMULATIONS

Maximilian Schulze[1], Sandro Jahn[1]

[1] Institute of Geology and Mineralogy, University of Cologne, Köln, Germany

On Earth, aqueous fluids occur under a variety of different conditions, from the Earth's surface to the upper mantle. They are key agents in many geological and geochemical processes, including deep metamorphic or metasomatic reactions, ore formation processes, and chemical weathering. They are also important technologically; for example, in the geothermal energy sector or for many other industrial processes using water and steam. Despite the great relevance of such fluids, there are still major gaps in our knowledge of their thermodynamic and kinetic behavior, especially at supercritical conditions. One reason is the lack of thermodynamic data because experimental measurements of such properties are challenging considering the high temperatures and/or pressures, the chemical complexity, and the continuous change of properties with the environmental conditions. The other problem is the limited applicability of existing theoretical models for a thermodynamic description of fluids, such as the Pitzer (Pitzer, 1995) or Helgeson-Kirkham-Flowers (Johnson et al., 1992) models. For instance, none of these models is suitable to describe correctly the properties of "superhot" geothermal fluids at near supercritical or supercritical temperatures and low densities.

Molecular-scale numerical simulations offer an alternative and complementary approach to new experimental and theoretical efforts to advance our knowledge and description of thermodynamic properties of aqueous fluids. Within the approximations of the interatomic potential used to describe the chemical interactions between ions and molecules, such simulations are predictive in terms of molecular structure as well as physicochemical properties of the studied fluids. This computational approach has been used by us (and by other research groups) (1) to develop molecular structure models for hydrothermal fluids under a wide range of conditions; (2) to compute species stability constants, partial molar volumes, and other important thermodynamic properties (Stefanski et al., 2020; Schulze et al., 2024); and (3) to help the interpretation of *in situ* experimental data using methods of theoretical spectroscopy (Loges et al., 2024).

After giving a short overview of our recent research activities in the field of hydrothermal fluids, this presentation will focus on simulation results that yield the density (ρ) dependence of alkali halide solute properties in aqueous fluids at near critical temperatures. First, the possible extrapolation of the experimentally observed linear relation between the $\log(K)$, with K being the dissociation constant of NaCl, and $\log(\rho)$ to lower and higher densities is critically assessed (Fig. 1). While this linear relation holds at high density, there are significant deviations below the critical density of water. Second, we derive the so-called Krichevskii parameter, which describes the change of pressure upon addition or removal of solutes at constant volume. This parameter turns out to smoothly vary with fluid density, even across the critical point. Furthermore, it largely determines the change of sign of the partial molar volume, which for electrolyte solutes change from negative at low density to positive at high density. The molecular origin of this behavior is rationalized in terms of a cavity analysis. Finally, implications of the simulation results on the development of new density-based thermodynamic models are discussed.

REFERENCES

Johnson J. W., Oelkers E. H., and Helgeson H. C. (1992) SUPCRT92: A software package for calculating the standard molal thermodynamic properties of minerals, gases, aqueous species, and reactions from 1 to 5000 bar and 0 to 1000°C. *Computers & Geosciences* **18**, 899–947.

Loges A., Manni M., Louvel M., Wilke M., Jahn S., Welter E., Borchert M., Qiao S., Klemme S., Keller B. G., and John, T. (2024) Complexation of Zr and Hf in fluoride-rich hydrothermal aqueous fluids and its significance for high field strength element fractionation. *Geochimica et Cosmochimica Acta* **366**, 167–181.

Pitzer K. S. (1995) *Thermodynamics*. McGraw-Hill series in advanced chemistry.

Schulze M., Driesner T., and Jahn S. (2024) Assessing the validity and limits of linear density models for predicting dissociation-association equilibria in supercritical waters. *Geochimica et Cosmochimica Acta* submitted.

Stefanski J. and Jahn S. (2020) Yttrium speciation in subduction-zone fluids from ab initio molecular dynamics simulations. *Solid Earth* **11**, 767–789.

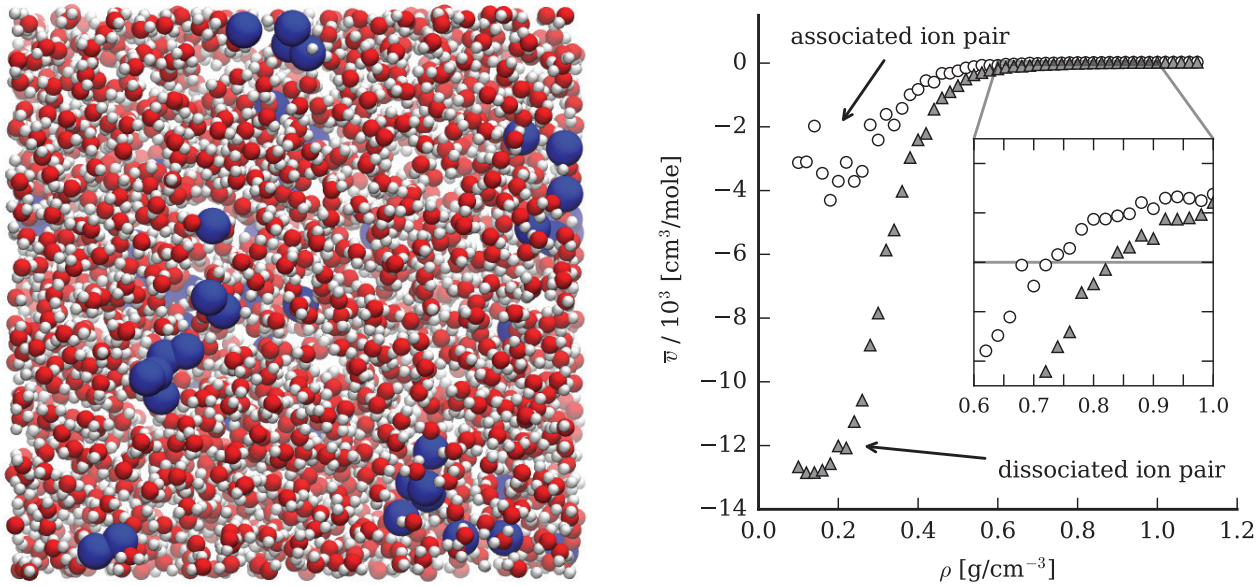

Figure 1. The availability of cavities (blue spheres in the left figure) within the structure of supercritical water (H–white, O–red) determines the sign of the partial molar volume $\bar{v}$ of the NaCl solute, which strongly depends on fluid density ρ (right figure).

RAMAN SPECTROSCOPIC INVESTIGATION OF DY COMPLEXATION IN CL-BEARING HYDROTHERMAL SOLUTIONS

Sarah E. Smith-Schmitz[1], Nicole C. Hurtig[2], Alexander P. Gysi[1,2]

[1] New Mexico Bureau of Geology and Mineral Resources, New Mexico Institute of Mining and Technology, Socorro, NM 87801, USA
[2] Department of Earth and Environmental Science, New Mexico Institute of Mining and Technology, Socorro, NM 87801, USA

The rare earth elements (REE) are considered critical elements and are used to build components of many modern technologies, including communication, optical, and sustainable energy. Hydrothermal aqueous fluids can play a key role in the formation of REE mineral deposits (Gysi et al., 2016). The REE complexation by ligands, such as sulfate (SO_4^{2-}), chloride (Cl^-), carbonate (CO_3^{2-}), and hydroxyl (OH^-), is of particular interest for understanding the transport and fractionation mechanisms of REE in geologic fluids. Raman spectroscopy provides a method for *in situ* characterization of aqueous REE speciation at the molecular level, including hydration and complexation chemistry (Rudolf and Irmer, 2015). However, Raman spectroscopic studies of REE in chloride-bearing solutions have largely been limited to ambient temperature.

In this study, *in situ* confocal Raman spectroscopic experiments were conducted to determine the speciation of Dy in chloride-bearing aqueous solutions from 25 to 300 °C. The experimental solutions measured contain 0.14 to 1.8 mol/kg dissolved $DyCl_3$ and HCl with starting pH values of 2, 4, or 5 at ambient temperature. These solutions were sealed in fused quartz capillary cells and used in a capillary cell heating stage designed and built at New Mexico Tech (Fig. 1). Raman spectra were collected at ambient temperature and every 50 °C from 100 to 300 °C using a 532 nm Nd-YAG excitation laser. Raman spectra were also collected for ultra-pure water and background solutions with 1.0 to 1.7 mol/kg NaCl.

Comparison of the spectra for Dy chloride solutions with the spectra for background solutions from each temperature step allows us to isolate Raman bands specific to the Dy-bearing solutions at ~370 cm^{-1} and ~240 cm^{-1}. The Raman band at ~370 cm^{-1} is attributed to the ν_1 Dy-O stretching mode of the hydrated Dy^{3+}(aq) ion, representative of the form $[Dy(H_2O)_8]^{3+}$(aq), in agreement with Rudolf and Irmer (2020). The Raman band at ~240 cm^{-1} is attributed to the Dy chloride species represented by Dy-Cl stretching mode of Dy-chloro complexes of the form $[DyCl_n(H_2O)_{8-n}]^{3-n}$(aq).

The Dy-O band was observed to decrease systematically with an increase in temperature for all of the $DyCl_3$ solutions. The Dy-O band becomes indistinguishable from the background above 100 °C for 0.14 *m*$DyCl_3$, 200 °C for 0.3 *m*$DyCl_3$, 250 °C for 0.6 *m*$DyCl_3$, and 300 °C for 1.8 *m*$DyCl_3$. The Dy-Cl band could not be quantified at temperatures below 150 °C due to interference from the low-frequency water acoustic modes (Fig. 1). However, from 150 to 300 °C, the Dy-Cl band increases systematically in all of the $DyCl_3$ solutions, indicating a systematic increase in the stability of Dy chloride complexes.

The experimental results are consistent with geochemical modeling of Dy speciation using the MINES thermodynamic database (Gysi et al., 2023) implemented in the GEM-Selektor code package (Kulik et al., 2013). At 25 °C and pH of 2–5, Dy^{3+} is predicted to be the dominant species for solutions with up to 0.6 *m*$DyCl_3$, whereas at temperatures above 100 °C for 0.6 *m*$DyCl_3$ to 200 °C for 0.14 *m*$DyCl_3$ and pH of 1.9–3.6, the Dy chloride complexes (i.e., $DyCl^{2+}$ and $DyCl_2^+$) predominate. These findings form the basic framework that will support the extension of Raman spectroscopic research on the complexation of REE to supercritical conditions.

This work is supported by the U.S. Department of Energy under Award DE-SC0022269.

REFERENCES

Gysi A. P., Williams-Jones A. E., and Collins P. (2016) Lithogeochemical vectors for hydrothermal processes in the Strange Lake peralkaline granitic REE-Zr-Nb deposit. *Economic Geology* **111**, 1241–1276.

Gysi A. P., Hurtig N. C., Pan R., Miron G. D., and Kulik D. A. (2023) MINES thermodynamic database, New Mexico Bureau of Geology and Mineral Resources, version 23. https://doi.org/10.58799/mines-tdb

Kulik D. A., Wagner T., Dmytrieva S. V., Kosakowski G., Hingerl F. F., Chudnenko K. V., and Berner U. (2013) GEM-Selektor geochemical modeling package: revised algorithm and GEMS3K numerical kernel for coupled simulation codes. *Computational Geosciences* **17**, 1–24.

Rudolph W. W. and Irmer G. (2015) Hydration and ion pair formation in common aqueous La (III) salt solutions–A Raman scattering and DFT study. *Dalton Transactions* **44**, 295–305.

Rudolph W. W. and Irmer G. (2020) On the hydration of the rare earth ions in aqueous solution. *Journal of Solution Chemistry* **49**, 316–331.

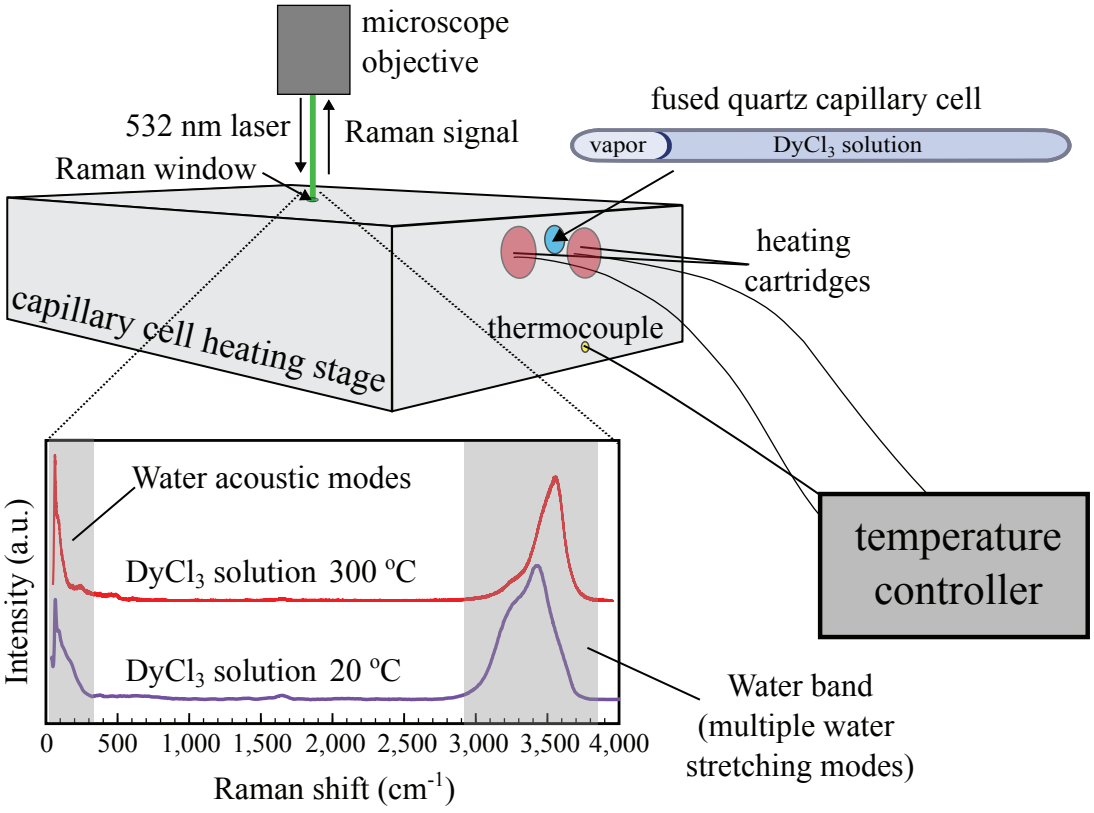

Figure 1. Schematic diagram showing experimental setup for Raman spectroscopic experiments in this study.

MACHINE LEARNING TO CONSTRAIN GEOLOGIC CONTROLS ON CRITICAL MINERAL OCCURRENCE AT WYODAK MINE, POWDER RIVER BASIN, WYOMING

Sophia Stuart[1,2], Bulbul Ahmmed[2], Peter L. Watson[3], Dan O'Malley[2], Brent M. Goehring[2], John P. Kaszuba[1,4], Davin Bagdonas[4]

[1] Department of Geology and Geophysics, University of Wyoming, Laramie, WY 82701, USA
[2] Earth and Environmental Sciences Division, Los Alamos National Laboratory, Los Alamos, NM 87545, USA
[3] Analytics, Intelligence, and Technology Division, Los Alamos National Laboratory, Los Alamos, NM 87545, USA
[4] School of Energy Resources, University of Wyoming, Laramie, WY 82701, USA

In this study, we used unsupervised machine learning (ML) to make predictions about the occurrence and distribution of critical minerals (CM) at Wyodak Mine in the Powder River Basin (PRB), Wyoming. The PRB is the most prolific coal field in the United States, generating over 300 million tons annually since the early 2000s (Luppens et al., 2015). Currently, the PRB and other U.S. coal basins are being evaluated as a prospective domestic source for rare earth elements and CM, with the goal to couple existing infrastructure with a new extractive industry. Our ability to predict where economic CM resources might exist within PRB sedimentary strata requires a better understanding of the geologic processes controlling transport and deposition of CM throughout the basin. We applied non-negative matrix factorization with *k*-means clustering (NMF*k*; Alexandrov and Vesselinov, 2014; Alexandrov et al., 2022) to discover hidden signatures within our geologic data. The NMF*k* model was trained on thousands of geochemical data points from historical and new wells drilled within or near Wyodak Mine. Signatures identified in this data were used to locate hotspots of anomalous CM occurrence. We then created a 3D geological model of the study area (de la Varga et al., 2019; Korzani et al., 2020) using 56 core stratigraphy logs (Haacke and Scott, 2013). To infer geologic controls on CM deposition in the western PRB, we compared the ML-identified CM hotspots to the geology at depth. Correlating the CM hotspots to sedimentary units in the geological model also allowed for increased spatial coverage. This project explores the utility of unsupervised ML for unconventional CM resource evaluation at the mine scale. Our findings have implications for future work at the basin scale and provide insights to potential sources of CM to the PRB, which is presently unknown.

REFERENCES

Alexandrov B. S. and Vesselinov V. V. (2014) Blind source separation for groundwater level analysis based on non-negative matrix factorization. *Water Resources Research* **50,** 7332–7347.

Alexandrov B. S., Vesselinov V. V., Stanev V., Sybrandt J., and O'Malley D. (2022) NMFk: Nonnegative matrix factorization + k-means clustering and physics constraints [Software]. Available from https://github.com/SmartTensors/NMFk.jl

de la Varga M., Schaaf A., Vassallo M., and Caumon G. (2019) GemPy 1.0: Open-source stochastic geological modeling and inversion. *Journal of Open Source Software* **4,** 1566.

Haacke J. E. and Scott D. C. (2013) Drill hole data for coal beds in the Powder River Basin, Montana and Wyoming. *U.S. Geological Survey, Data Series* **713**.

Korzani M. G., de la Varga M., Reuber G., and Caumon G. (2020) GemPy (Version 2.2.5) [Software]. Available from **https://github.com/cgre-aachen/gempy**

Luppens J. A., Scott D. C., Haacke J. E., Osmponson L. M., and Pierce P. E. (2015) Coal geology and assessment of coal resources and reserves in the Powder River Basin, Wyoming and Montana. *U.S. Geological Survey Professional Paper* **1809**.

HYDROTHERMAL RARE EARTH ELEMENTS PARTITIONING INTO FLUORITE: A FLUID INCLUSION STUDY FROM THE GALLINAS MOUNTAINS REE-BEARING FLUORITE DEPOSIT IN NEW MEXICO

Aadish Velmani[1,2], Alexander Gysi[1,2], Nicole Hurtig[2]

[1] New Mexico Bureau of Geology and Mineral Resources, New Mexico Institute of Mining and Technology, Socorro, NM 87801, USA
[2] Department of Earth and Environmental Science, New Mexico Institute of Mining and Technology, Socorro, NM 87801, USA

Rare earth elements (REE) are important in modern society due to their numerous uses in manufacturing components for green and high-tech energy industries. Studying the mechanisms of REE mineralization in geologic systems is vital for understanding where and how these mineral deposits form. Previous studies have shown that hydrothermal fluids play a key role in the mobilization and enrichment of REE in mineral deposits (Williams-Jones et al., 2000; Gysi et al., 2016; Vasyukova and Williams-Jones, 2018). Fluorite is ideal for studying the behavior of REE because it is compatible in its structure and because it is a ubiquitous vein mineral found together with the REE fluorocarbonate bastnäsite. However, the controls on hydrothermal fluid-mineral REE partitioning in these deposits are not yet fully understood.

In this study, we present petrographic observations of fluorite veins and fluid inclusions (Fig. 1) from the Gallinas Mountains REE-bearing fluorite veins/breccia deposit in New Mexico (Williams-Jones et al., 2000; McLemore, 2010). The Gallinas Mountains deposit notably contains hydrothermal fluorite and bastnäsite associated with ~30 Ma alkaline igneous rocks intruded into Permian sedimentary rock formations (McLemore, 2010). Optical microscopy and cathodoluminescence (CL) are used to distinguish different fluorite generations and fluid inclusion types (Fig. 1a). Scanning electron microscopy (SEM) is used to identify REE minerals and zonation in fluorite and to acquire elemental compositions of different vein minerals.

Fluorite samples collected in this study include sandstone- and trachyte-hosted veins/breccias classified into (i) bastnäsite-quartz-fluorite veins, (ii) barite-calcite crosscut by barren calcite-fluorite veins, (iii) barite-calcite veins crosscut by mineralized bastnäsite-(calcite)-fluorite veins, (iv) barite-fluorite and bastnäsite-fluorite breccia and vein infills containing base metal sulfides, and (v) bastnäsite-(calcite)-fluorite breccia. Three different fluorite generations are distinguished based on CL with distinct fluid inclusion types. Fluorite 1 is euhedral and zoned with bright blue to purple CL colors, and commonly occurs in bastnäsite-(calcite)-fluorite veins as brecciated fluorite clasts and cubes with bastnäsite rimming or replacement textures in a calcite matrix (Fig. 1b). Fluorite 1 is also present in bastnäsite-quartz-fluorite and barite-fluorite veins/breccias, with the latter crosscutting finer-grained fluorite ± bastnäsite infills (Fig. 1a). The latter is classified as fluorite 2, with a green to dark blue/purple CL color. Fluorite 3 displays a bright green to lavender luminescence and forms euhedral cubes with complex growth zoning. Another very fine-grained fluorite is distinguished in the matrix of some veins and breccias in the vicinity of the sandstone, and possibly as replacements of quartz clasts as observed also by Williams-Jones et al. (2000).

Several types of fluorite-hosted fluid inclusions (FI) were identified including vapor-rich (V) inclusions, liquid (L)+V inclusions, and L+V+solid inclusions. The L+V inclusions (Fig. 1c) can be classified into high-temperature inclusions with high vapor proportions

between ~30 and 40 vol% and low-temperature inclusions with smaller vapor proportions ranging between ~5 and 15 vol%. The next step in this study is to relate the FI petrography to the different fluorite generations, and to conduct microthermometry heating/freezing experiments to determine their salinities and homogenization temperatures.

In conclusion, fluorite can be classified into different vein types depending on the presence or absence of barite, bastnäsite, calcite, and quartz. Three main different fluorite generations were distinguished, but more CL work is needed to identify some of the more complex fluorite intergrowth relationships. The FI petrography indicates a potential to link between the fluorite generations and the different FI types based on their varying V/L ratios. The latter are indicative of fluid homogenization temperatures, with inclusions with larger V/L ratios reflecting a higher fluid entrapment temperature.

REFERENCES

Gysi A. P., Williams-Jones A. E., and Collins P. (2016) Lithogeochemical vectors for hydrothermal processes in the Strange Lake peralkaline granitic REE-Zr-Nb deposit. *Economic Geology* **111**, 1241–1276.

McLemore V. T. (2010) Geology and mineral deposits of the Gallinas Mountains, Lincoln and Torrance counties, New Mexico: Preliminary report. *New Mexico Bureau of Geology and Mineral Resources, Open-File Report* **OF-532**, 92 p.

Vasyukova O. V. and Williams-Jones A. E. (2018) Direct measurement of metal concentrations in fluid inclusions, a tale of hydrothermal alteration and REE ore formation from Strange Lake, Canada. *Chemical Geology* **483**, 385–396.

Williams-Jones A. E., Samson I. M., and Olivo G. R. (2000) The genesis of hydrothermal fluorite-REE deposits in the Gallinas Mountains, New Mexico. *Economic Geology* **95**, 327–341.

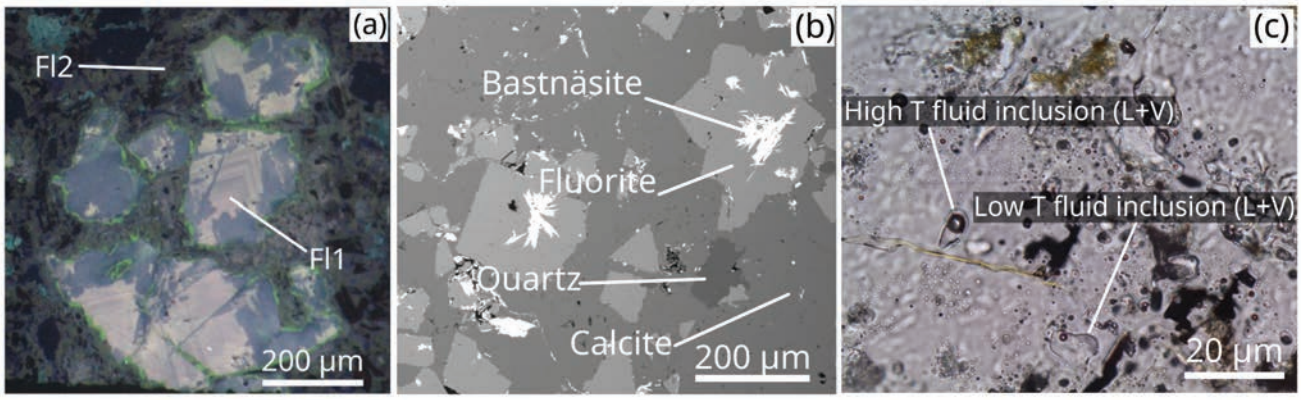

Figure 1. (a) Cathodoluminescence thin section photomicrograph showing crystal zoning and different fluorite generations in a bastnäsite-quartz-fluorite vein. (b) Backscattered electron SEM image of fluorite and bastnäsite intergrowths hosted within a calcite matrix in a bastnäsite-(calcite)-fluorite breccia vein. (c) Fluorite-hosted L+V fluid inclusion assemblages found in a fluorite-barite vein, showing a V/L ratio of ~40 vol% in high-temperature inclusions and a V/L ratio of ~5–10% in low-temperature inclusions.

ISOTOPE DILUTION METHODS IN SMALL EXPERIMENTAL CHARGES AT HIGH TEMPERATURES IN COLD-SEAL PRESSURE VESSELS AND APPLICATIONS

Laura E. Waters[1], Debarati Banerjee[1], Nicole C. Hurtig[1], Alexander P. Gysi[1,2], Daniel Harlov[3,4,5], Chen Zhu[6], Artas Migdisov[7]

[1] Department of Earth and Environmental Science, New Mexico Institute of Mining and Technology, Socorro, NM 87801, USA
[2] New Mexico Bureau of Geology and Mineral Resources, New Mexico Institute of Mining and Technology, Socorro, NM 87801, USA
[3] Division of Chemistry and Physics of Earth Materials, Deutsches GeoForschungsZentrum GFZ, Telegrafenberg, 14473 Potsdam, Germany
[4] Faculty of Earth Resources, China University of Geosciences, Wuhan 430074, China
[5] Department of Geology, University of Johannesburg, South Africa
[6] Department of Earth and Atmospheric Sciences, Indiana University, Bloomington, IN 47408, USA
[7] Earth and Environmental Sciences Division, Los Alamos National Laboratory, Los Alamos, NM 87545, USA

A well-known problem that occurs in high-temperature (>300 °C) mineral solubility experiments is precipitation of the mineral phase from solution during quench (e.g., Pourtier et al. [2010]). Precipitation can occur on capsule walls and the crystalline starting materials, which prevents determination of mineral solubility via analyses of the reacted experimental solutions and through change in mass of the starting crystal. We present two isotope dilution methods for determining the high-temperature (500–700 °C) solubility of $NdPO_4$ and $DyPO_4$ in non-saline and saline aqueous fluids, despite pervasive mineral precipitation upon quench. The two methods are designed for small-volume experiments conducted in cold-seal pressure vessels that test mineral solubility by combining synthetic $NdPO_4$ and $DyPO_4$ with aqueous fluids in gold capsules.

For experiments using $NdPO_4$, we add fluids (50–90 mg) that contain 0.25 ppm Nd, enriched in ^{145}Nd ($^{145}Nd/^{144}Nd$ =87) to our capsules, along with $NdPO_4$ crystals (~7–15 mg), which have a natural abundance of ^{145}Nd ($^{145}Nd/^{144}Nd$ =0.34). At run conditions, the $NdPO_4$ crystals dissolve, reducing the $^{145}Nd/^{144}Nd$ ratio in the solution, toward natural abundances. During quench, $NdPO_4$ precipitates but no isotopic fractionation occurs. Thus, the isotopic ratio of $^{145}Nd/^{144}Nd$ in the fluid measured using multi-collector inductively coupled plasma mass spectrometry (MC-ICP-MS) provides a record of the total mass of $NdPO_4$ dissolved at temperature and can be used to calculate the solubility of $NdPO_4$ via the equation for binary mixing. Solubility of $NdPO_4$ in replicate experiments at 500 °C ranges from 28.2–59 ppm at 500 °C, which suggests this method has an experimental reproducibility of ± 30 ppm (50% uncertainty). For experiments using $DyPO_4$, we add fluids (50–90 mg) that contain ~100 ppm Dy, enriched in ^{162}Dy ($^{162}Dy/^{161}Dy$ =97) to our capsules, along with $DyPO_4$ crystals (10–15 mg), which have a natural abundance of ^{162}Dy ($^{162}Dy/^{161}Dy$ =1.3). Solubility of $DyPO_4$ in replicate experiments at 500 °C ranges from 47.8–48.2 ppm at 500 °C, which suggests this method has an experimental reproducibility of ± 0.4 ppm (1% uncertainty). $^{162}Dy/^{161}Dy$ dilution method has an experimental error of ± 0.4 ppm, which corresponds to 1%. The difference in experimental error between the $^{145}Nd/^{144}Nd$ and $^{162}Dy/^{161}Dy$ dilution methods arises from the concentration of the spike in the experimental fluids. We suggest the $^{145}Nd/^{144}Nd$ isotope dilution method can be improved by modestly increasing the concentration of the Nd spike in the starting experimental solutions. Finally, we suggest that an additional application of the

isotope dilution method presented here is to determine the solubility of a binary or multicomponent monazite crystal. We outline a method for using the $^{145}Nd/^{144}Nd$ dilution method to determine the $NdPO_4$ and $LaPO_4$ solubilities from a binary mixture of $(La,Nd)PO_4$, using a recently published solution model for $La_{1-x}Nd_xPO_4$ monazite-type solid solutions (Schlenz et al., 2019).

REFERENCES

Pourtier E., Devidal J.-L., and Gibert F. (2010) Solubility measurements of synthetic neodymium monazite as a function of temperature at 2 kbars, and aqueous neodymium speciation in equilibrium with monazite. *Geochimica et Cosmochimica Acta* **74**, 1872–1891.

Schlenz H., Dellen J., Kegler P., Gatzen C., Schreinemachers C., Shelyug A., Klinkenberg M., Navrotsky A., and Bosbach D. (2019) Structural and thermodynamic mixing properties of $La_{1-x}Nd_xPO_4$ monazite-type solid solutions. *Journal of Solid State Chemistry* **270**, 470–478.

LANTHANIDE ADSORPTION IN MUSCOVITE AND PHLOGOPITE MICAS: IMPLICATIONS FOR RARE EARTH ELEMENTS SEPARATIONS

Yu Wen[1], Krishna K. Verma[1], Michael D. Lacount[2], Shawn M. Kathmann[2], Tanya Prozorov[1]

[1] Chemical and Biological Sciences Division, Ames National Laboratory, Ames, IA 50011, USA
[2] Physical Sciences Division, Pacific Northwest National Laboratory, Richland, WA 99354, USA

Rare earth elements (REEs) are vital to the economic growth and national security of the United States (U.S. Department of Energy, 2024). There is an urgent need to learn about the localized environment of REEs in diverse underutilized sources, thereby enabling enhanced recovery and separation approaches optimized across a broad variety of REEs. Ion-adsorption clay minerals preferentially adsorb heavy REEs (HREEs) released through the weathering and dissolution of granites and igneous rocks by rainwater (Hoshino et al., 2016). Seemingly, the most soluble and lightest elements (LREEs) pass through clays, while the least soluble and heaviest remain adsorbed, resulting in the formation of heavy REE-enriched minerals with concentrations ranging from 50–1500 ppm (Hoshino et al., 2016).

Ion-adsorption clays and micas are structurally and chemically similar; however, lanthanide adsorption in micas is different from a well-documented trend of ion-adsorption clays to adsorb preferentially HREEs. Furthermore, micas were shown to adsorb on average higher amounts of REE cations than the ion-adsorption clays, such as kaolinite and halloysite, under the same experimental conditions. Our results are also indicative of the co-localization of lanthanides and impurities found in natural muscovite (Ames National Laboratory, 2024). Inspired by this REE adsorption behavior, we are set to unravel the structural and chemical parameters and understand how various impurity ions can be used as tuning agents to achieve highly localized level control over REE adsorption and separation in layered minerals (Zou et al., 2021). The basic understanding of the chemical environment of REEs in clays and micas remains elusive. Probing the REE-specific spatio-chemical environment of micas and clays will further aid in understanding this result and improve our understanding of the REE adsorption mechanisms.

Previous reports on ion exchange in micas using high-resolution scanning transmission electron microscopy indicated significant electron beam damage to the specimen (Kogure and Okunishi, 2010; Fuller et al., 2015). While the e-beam damage to the specimen cannot be avoided altogether, in our work we employ lower operating voltages and use low beam currents in combination with infrequent monitoring to obtain structural and chemical parameters of muscovite micas exposed to aqueous Nd- and Yb-containing solutions. To this end, we operate scanning transmission electron microscopes at 120 kV and 200 kV. We monitor d-spacing of muscovite as a single indicator of the damage dealt by the electron beam to the specimen throughout the process of high-resolution imaging and elemental mapping, as shown in Figure 1. Using this approach, we have determined the threshold dose to the specimen, as well as the suitable working dose rates with low to moderate electron beam damage. Our results are complemented by atom probe tomography, X-ray photoelectron spectroscopy, and computational modeling.

By determining the speciation, spatio-chemical environment, polarity, and quantum mechanical interactions of rare earths in micas, we are learning the key differences affecting REE adsorption, including structural, electrostatic, and hydration effects; coordination of the rare earth cations; and cation mobility in this natural layered mineral compared to ion-adsorption clays analogs. This knowledge will aid in designing novel geo-inspired materials for effective separations of REEs from diverse feedstocks.

This work was supported by the U.S. Department of Energy, Office of Science, Basic Energy Sciences, Chemical Sciences, Geosciences, and Biosciences Division, Separation Science Program. The research was performed at Ames National Laboratory, which is operated by Iowa State University under contract No. DE-AC0207CH11358. STEM imaging and analytical spectroscopy analysis was performed using instruments in the Sensitive Instrument Facility at the Ames Laboratory.

REFERENCES

Ames National Laboratory. (2024) Geo-inspired separation of rare-earth elements. **https://www.ameslab.gov/cbs/geo-inspired-separation-of-rare-earth-elements**

Fuller, A. J., Shaw S., Ward M. B., Haigh S. J., Mosselmans J. F. W., Peacock C. L., Stackhouse S., Dent A. J., Trivedi D., and Burke I. T. (2015) Caesium incorporation and retention in illite interlayers. *Applied Clay Sciences* **108**, 128–134.

Hoshino M., Sanematsu K., and Watanabe Y. (2016) REE mineralogy and resources. *Handbook on the Physics and Chemistry of Rare Earths* **49**, 129–291.

Kogure T. and E. Okunishi. (2010) Cs-corrected HAADF–STEM imaging of silicate minerals. *Journal of Electron Microscopy* **59**(4), 263–271.

U.S. Department of Energy. (2024) What are critical materials and critical minerals? https://www.energy.gov/cmm/what-are-critical-materials-and-critical-minerals.

Zou Y. C., Mogg L., Clark N., Bacaksiz C., Milovanovic S., Sreepal V., Hao G. P., Wang Y. C., Hopkinson D. G., Gorbachev R., and Shaw S. (2021) Ion exchange in atomically thin clays and micas. *Nature Materials* **20**, 1677–1682.

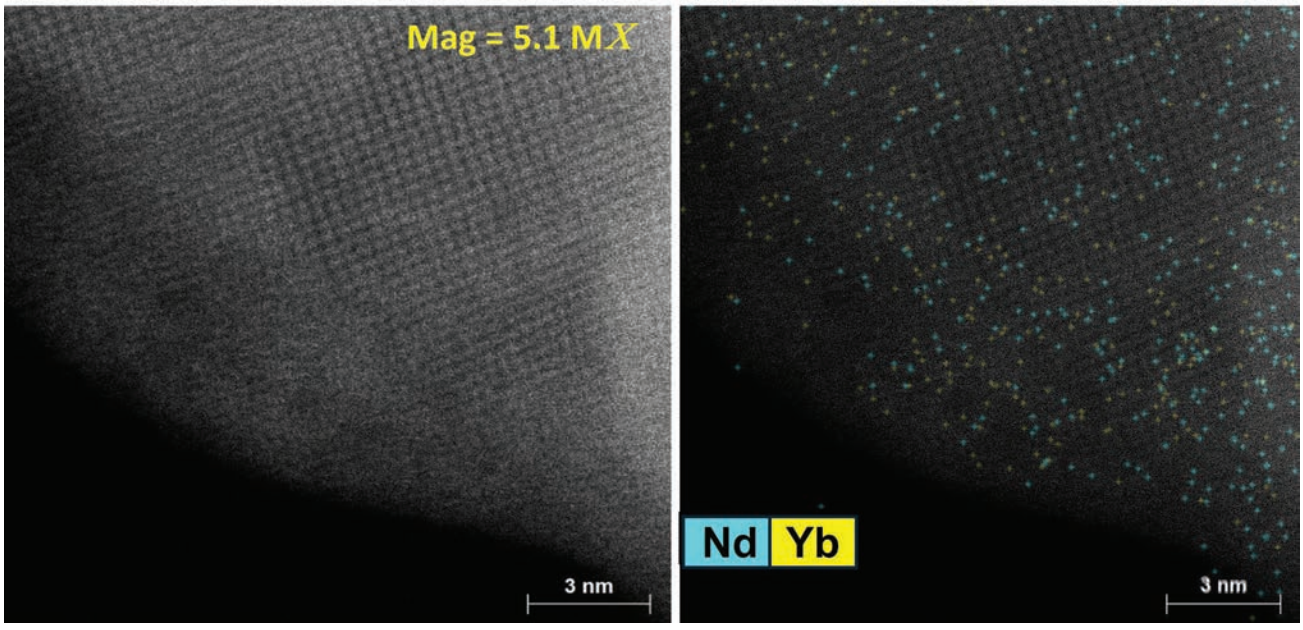

Figure 1. Low-dose imaging and elemental mapping of a muscovite mica crystal exposed to Nd- and Yb-containing aqueous solutions, respectively. Left: High-angle annular dark field scanning transmission electron micrograph (HAADF-STEM) of muscovite mica acquired at 5.1 M*X* magnification. Right: Distribution of Nd and Yb ions in muscovite mica probed with high-resolution energy dispersive spectroscopy (STEM-EDS).

MINERAL-SPECIFIC INHIBITION OF PALLADIUM ADSORPTION TO IRON (OXYHYDR)OXIDES BY CHLORIDE

Emily G. Wright[1], Olwen Stagg[1], Elaine D. Flynn[1], Jeffrey G. Catalano[1]

[1] Department of Earth, Environmental, and Planetary Sciences, Washington University, St. Louis, MO 63130, USA

Studies of weathering zones developed above ultramafic rock, which are potential new resources for platinum-group elements (PGEs), have observed substantial differences in the mineral hosts and distribution of palladium (Pd) compared to primary ore deposits (e.g., Fuchs and Rose [1974], Locmelis et al. [2010], Suárez et al. [2010], Junge et al. [2019]). The partial loss of Pd in these weathering zones under oxidizing, acidic conditions has been attributed to mobilization of Pd by aqueous chloride complexation (Fuchs and Rose, 1974). While prior work has shown that some Pd is retained and associated with iron (oxyhydr)oxides during weathering (e.g., Locmelis et al. [2010], Suárez et al. [2010], Junge et al. [2019]), the fundamental processes that control the distribution and mobility of Pd during weathering are poorly constrained. Adsorption processes may explain Pd retention, but the effect of chloride on this mechanism is currently unclear.

We studied the impact of chloride complexation on Pd(II) adsorption to hematite, goethite, and 2-line ferrihydrite at pH 4. Macroscopic binding experiments were used to investigate adsorption in the presence of multiple chloride concentrations. Speciation modeling, zeta potential measurements, and extended X-ray absorption fine structure (EXAFS) spectroscopy were used to elucidate the effect of chloride on Pd binding mechanisms.

Greater aqueous chloride complexation suppresses Pd(II) adsorption to hematite. However, when this effect is corrected for using speciation modeling, there are still differences in adsorption observed, suggesting an additional mechanism is required. We observed a negligible effect on surface charge due to chloride adsorption, indicating that electrostatic activity corrections are unlikely to contribute to adsorption differences. Our EXAFS measurements of adsorbed Pd on hematite are consistent with a mixture of Pd-hydroxy and -chloro surface complexes, with Pd-Cl ternary surface complexation increasing with increasing aqueous chloride.

Pd(II) adsorption behavior to ferrihydrite is similar to hematite at the same total chloride concentration, and the EXAFS spectra suggest surface speciation on ferrihydrite and hematite is the same. However, compared to the other iron (oxyhydr)oxides studied, Pd displays a substantially greater affinity for goethite (Fig. 1). The bimodal adsorption behavior displayed by goethite also suggests the presence of multiple Pd surface species with differing binding affinities. Similar to hematite and ferrihydrite, the EXAFS spectra of goethite samples are consistent with a mixture of Pd-hydroxy and -chloro surface complexes. However, for goethite, we additionally observe the presence of a second shell feature. This feature is consistent with either iron, suggesting incorporation into surface vacancies, or Pd, indicating the formation of polymeric Pd hydrolysis products.

Our results demonstrate that Pd is readily mobilized as a chloride complex in acidic weathering zones, with increasing chloride suppressing retention by all iron (oxyhydr)oxides studied. The differences in adsorption behavior observed are likely linked to changes in Pd surface speciation. The substantially greater affinity of Pd for goethite compared to the two other minerals studied indicates that goethite likely plays a key role in Pd retention during weathering. Our results suggest that larger-scale controls on iron (oxyhydr)oxide mineralogy, such as climate and weathering zone pH, will likely affect Pd mobility, with Pd being preferentially retained under conditions that favor goethite formation.

REFERENCES

Fuchs W. A. and Rose A. W. (1974) The geochemical behavior of platinum and palladium in the weathering cycle in the Stillwater Complex, Montana. *Economic Geology* **69**, 332–346.

Junge M., Oberthür T., Kraemer D., Melcher F., Piña R., Derrey I. T., Manyeruke T., and Strauss H. (2019) Distribution of platinum-group elements in pristine and near-surface oxidized Platreef ore and the variation along strike, northern Bushveld Complex, South Africa. *Mineralium Deposita* **54**, 885–912.

Locmelis M., Melcher F., and Oberthür T. (2010) Platinum-group element distribution in the oxidized Main Sulfide Zone, Great Dyke, Zimbabwe. *Mineralium Deposita* **45**, 93–109.

Suárez S., Prichard H. M., Velasco F., Fisher P. C., and McDonald I. (2010) Alteration of platinum-group minerals and dispersion of platinum-group elements during progressive weathering of the Aguablanca Ni-Cu deposit, SW Spain. *Mineralium Deposita* **45**, 331–350.

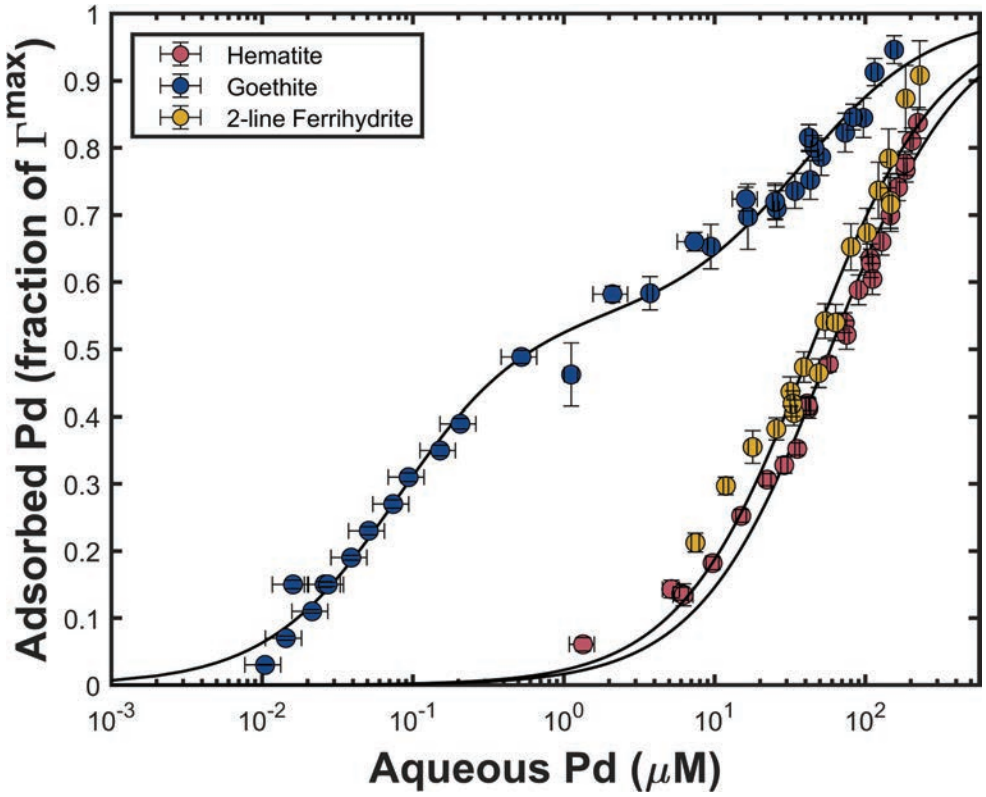

Figure 1. Palladium (Pd) adsorption to goethite, 2-line ferrihydrite, and hematite at pH 4 (normalized to the calculated maximum binding capacity) compared to the final measured dissolved Pd in the presence of approximately 10 mM total chloride. Single Langmuir isotherms are shown for hematite and ferrihydrite; a double Langmuir isotherm is shown for goethite.

PREPARATION OF DIVALENT EU MATERIALS FOR THERMODYNAMIC STUDY UNDER HYDROTHERMAL CONDITIONS

Natalie Yaw[1], Yecenia Cortez[1], Artas Migdisov[2], Xiaofeng Guo[1]

[1] Department of Chemistry, Washington State University, Pullman, WA 99164, USA

[2] Earth and Environmental Sciences Division, Los Alamos National Laboratory, Los Alamos, NM 87545, USA

Europium (Eu) is a rare earth element (REE) valuable for its high-tech applications, often involving its luminescent properties. Like all REE, Eu is scattered diffusely throughout the Earth's crust and often found in deposits mixed with elements of similar chemistry, making its extraction costly and time consuming. While most REE are dominated by the +3-oxidation state, Eu also has access to +2-chemistry due to the relatively stable $4f^7$ electron configuration of Eu(II). This unique chemistry gives rise to geochemical consequences, namely the "europium anomaly," where Eu is present in much lower concentrations than expected in REE deposits. This anomalous behavior is a powerful tool for studying geodynamic histories and the formation of REE minerals (Nakada et al., 2017; Triantafyllou et al., 2022). In order to understand and exploit this fractionation of Eu from REE deposits, fundamental thermodynamic properties of Eu(II) must be studied to feed into predictive models. Herein, we report the synthesis and thermodynamic characterization of several Eu(II) materials that are geochemically relevant (Fig. 1). Synthesized with solid-state and sol-gel techniques, the materials have been isolated in large quantities and are stable in air. Their material properties have been characterized by X-ray diffraction and X-ray absorption spectroscopy to validate crystalline and oxidation state purity. The enthalpy of formation and thermal stability will be evaluated using high-temperature oxide melt solution calorimetry and TGA-DSC, respectively. With this project progressing, we will also determine the aqueous speciation by *in situ* high P-T XAFS and thermodynamic constants of Eu(II) species by solubility study. The combined results can help to model the transport and formation of Eu(II) mineral phases under hydrothermal conditions. To date, little if any work exists in the literature on the fundamental thermodynamic properties of Eu(II) (Bau, 1991; Liu et al., 2017); thus, this work will enrich our wholistic understanding of Eu behavior.

REFERENCES

Bau M. (1991) Rare-earth element mobility during hydrothermal and metamorphic fluid-rock interaction and the significance of the oxidation state of europium. *Chemical Geology* **93**, 219–230.

Liu W., Etschmann B., Migdisov A., Boukhalfa H., Testemale D., Müller H., Hazemann J.-L., and Brugger J. (2017) Revisiting the hydrothermal geochemistry of europium(II/III) in light of new in-situ XAS spectroscopy results. *Chemical Geology* **459**, 61–74.

Nakada R., Shibuya T., Suzuki K., and Takahashi Y. (2017) Europium anomaly variation under low-temperature water-rock interaction: A new thermometer. *Geochemistry International* **55**, 822–832.

Triantafyllou A., Ducea M. N., Jepson G., Hernández-Montenegro J. D., Bisch A., and Ganne J. (2022) Europium anomalies in detrital zircons record major transitions in Earth geodynamics at 2.5 Ga and 0.9 Ga. *Geology* **51**, 141–145.

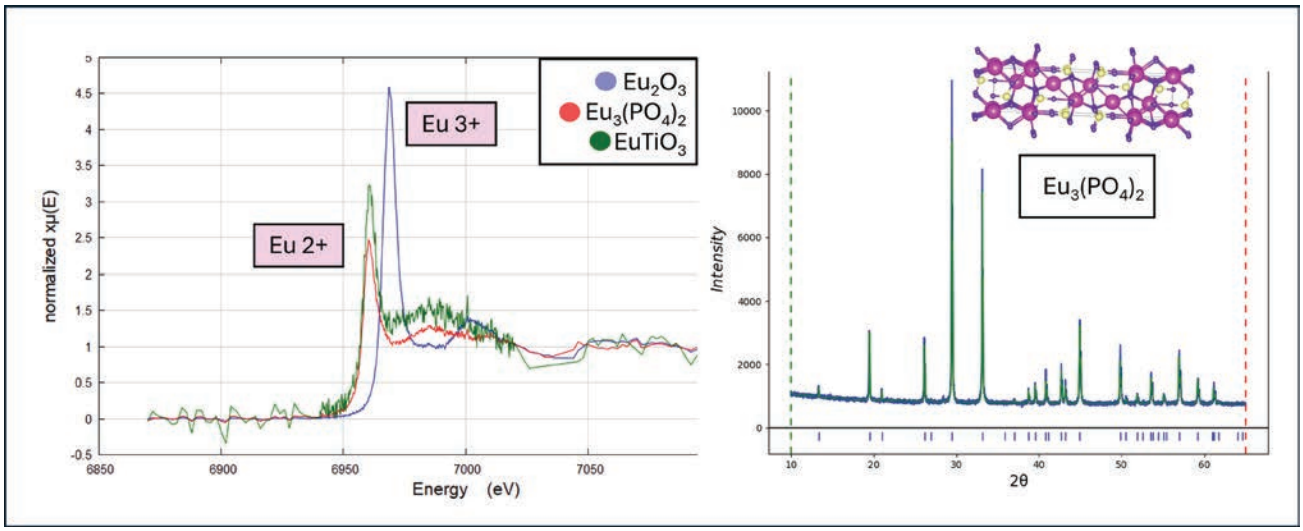

Figure 1. (left) XAS data of two Eu(II) compounds that have already been synthesized, demonstrating nearly complete Eu(II) occupancy; (right) XRD pattern of Eu(II) compound, demonstrating phase purity. These are just two examples of Eu(II) materials that are being advanced for thermodynamic study.

PORE-SCALE MODELING AND EXPERIMENTAL APPLICATIONS FOR REACTIVE TRANSPORT AND FLOW BEHAVIOR ALONG MINERAL-FLUID INTERFACES

Hongkyu Yoon[1]

[1] Geoscience Research and Applications, Sandia National Laboratories, Albuquerque, NM 87123, USA

Reactive transport and chemical reactions are governed by pore morphology, mineralogy, and interfacial characteristics in porous media. These coupled processes with hydrodynamics in flowing systems are critical to various subsurface applications such as geologic carbon storage, enhanced geothermal, and environmental fate and transport. Over the past two decades, our understanding of pore-scale reactive transport processes has been dramatically improved using both experimental and numerical methods (e.g., Yoon et al. [2015]). For example, mixing-controlled (bio)geochemical reactions in porous media and the feedback of reaction products (e.g., precipitants, dissolved species, biofilms) on reaction processes have been studied in a fluidic system where experimental conditions are relatively well controlled. Microfluidics is an especially robust device to account for pore-scale systems, which can identify mineral-fluid interfaces with optical and confocal microscopy accurately (Fig. 1). The experimental works with computational simulations have been studied to provide fundamental mechanistic explanation of how (bio)geochemical processes and pore-scale interfacial reactions interact and alter hydrodynamics and reaction processes under different geochemical compositions and pore configurations. In this presentation, we will highlight how a pore-scale experimental approach can be utilized to validate pore-scale reactive transport modeling, with examples from the literature, and improve our understanding of (bio)geochemical reactions for calcium carbonate precipitation and dissolution processes. In addition, recent applications of laboratory devices that can be relatively easily built using 3D printing and natural minerals/rocks will be presented for pore-scale flow and transport processes, which are governed by coupled reaction processes at the mineral-fluid interface.

Sandia National Laboratories is managed and operated by NTESS under DOE NNSA contract DE-NA0003525.

REFERENCES

Yoon H., Kang Q., and Valocchi A. J. (2015) Lattice Boltzmann-based approaches for pore-scale reactive transport. *Reviews in Mineralogy and Geochemistry,* **80**(1), 393–431.

Yoon H., Chojnicki K. N., Martinez M. J. (2019) Pore-scale analysis of calcium carbonate precipitation and dissolution kinetics in a microfluidic device. *Environmental Science & Technology* **53**(24), 14233–14242.

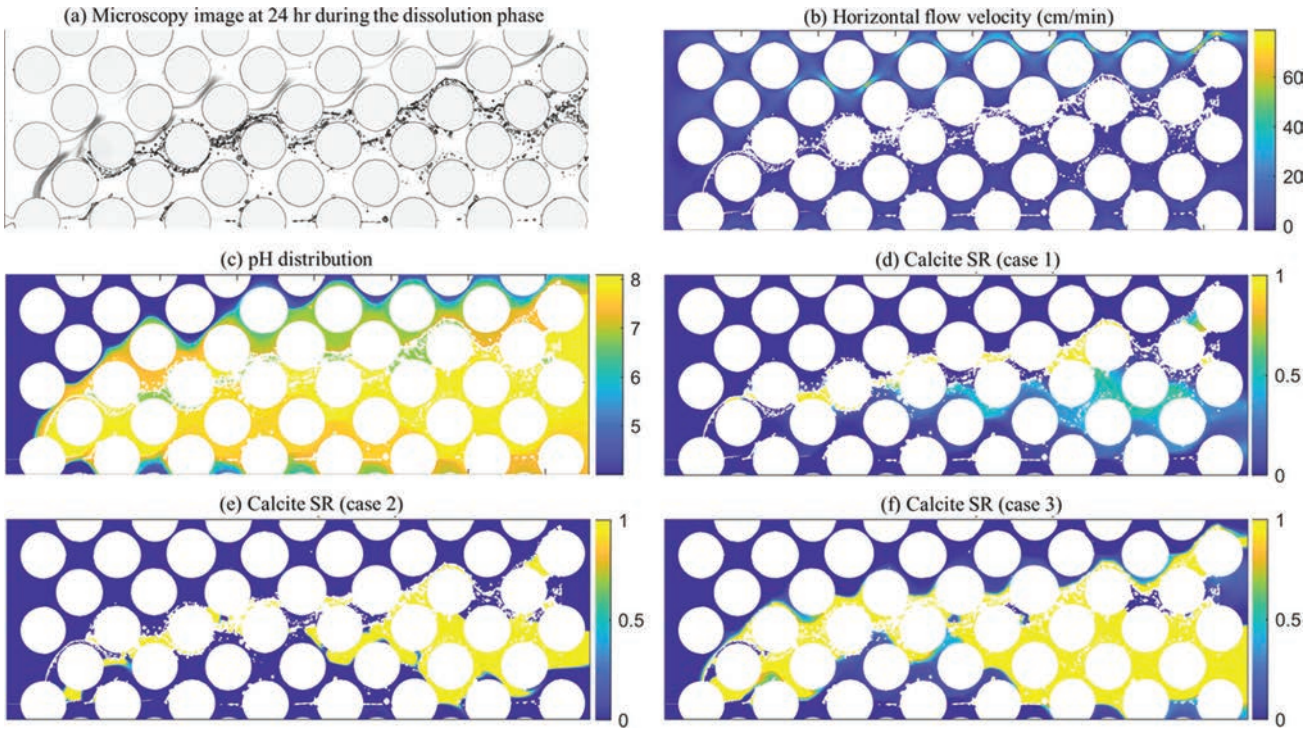

Figure 1. (a) Experimental image of precipitate distribution at 24 h during the dissolution phase and (b–f) simulation results of the distribution of pH, flow velocity field, and supersaturation ratio (SR) with respect to calcite. (Copied from Yoon et al. [2019].)

THE STRUCTURE OF YB(III) SULFATE COMPLEXES IN AQUEOUS SOLUTIONS AT ELEVATED PRESSURE AND TEMPERATURE

Xiaodong Zhao[1], Xiaofeng Guo[2], Xin Zhang[1]

[1] Physical & Computational Science Directorate, Pacific Northwest National Laboratory, Richland, WA 99354, USA
[2] Department of Chemistry, Washington State University, Pullman, WA 99164, USA

Hydrothermal fluids are critical in the formation of economic ore deposits, as is evident in places like the Gallinas Mountains in New Mexico, the Snowbird Deposit in Montana, the Pea Ridge in Missouri, and Bayan Obo in Inner Mongolia (Castor and Hedrick, 2006). These fluids, enriched in ligands like Cl^-, SO_4^{2-}, and F^-, facilitate the transport and deposition of rare earth elements (REEs) by forming stable complexes with REE^{3+} ions. Among these, sulfate ions (SO_4^{2-}) have traditionally been viewed as a primary transporter for REEs, and understanding the behavior of REE sulfate complexes under extreme conditions is essential for expanding the REE complex structural database and for developing molecular dynamics simulations and *ab initio* models to elucidate the sulfate ligand's role in REE transportation.

In exploring these dynamics, X-ray absorption spectroscopy (XAS) has been key in understanding the molecular structures, such as coordination number and geometry. Previous *in situ* XAS experiments with $REECl_3$ solutions (REE = La, Nd, Gd, Yb) as a function of temperature (25–500 °C, P to 2 kbar) revealed that light REE-chlorides have greater stability over the temperature, which is contrary to simulation results (Mayanovic et al., 2007, 2009a, 2009b). Despite these insights, research on the speciation and structures of REE solutions under elevated P–T conditions is very limited so far, especially for REE sulfate solutions. This study utilizes a hydrothermal diamond anvil cell (HDAC) to attain the necessary P–T conditions. However, HDAC coupled with XAFS faces two main obstacles: low signal efficiency due to limited sample thickness and Bragg glitches caused by the diamond anvil's orientation. Hence, a high concentration (0.05 M) of $Yb_2(SO_4)_3$ was used to enhance data quality. To mitigate Bragg glitches, the cell was rotated ± 4 degrees relative to the synchrotron beam, displacing Bragg peaks in energy space and allowing for clearer data collection by using glitch-free regions from multiple scans. Traditionally, the Yb-sulfate complex system can be determined by the following three reaction equations:

$$Yb^{3+} + SO_4^{2-} \rightleftharpoons YbSO_4^+ \quad (1)$$

$$Yb^{3+} + 2SO_4^{2-} \rightleftharpoons Yb(SO_4)_2^- \quad (2)$$

$$YbSO_4^+ + SO_4^{2-} \rightleftharpoons Yb(SO_4)_2^- \quad (3)$$

Although previous research indicated a $REESO_4^+$ to $REE(SO_4)_2^-$ transition and that $REE(SO_4)_2^-$ (e.g., REE = Nd^{3+}) will become the dominant species with increasing temperature, especially above 150 °C (Migdisov et al., 2016; Wan et al., 2021), the preliminary EXAFS analysis from our study showed a reduced Yb^{3+}-SO_4^{2-} interaction. As shown in Table.1, the average number of sulfur atoms in the second coordination shell decreased by ~0.8 from ~2.5 to ~1.7; at the same time, the oxygen number in first coordination shell also decreased by ~0.7, indicating a partial amount of Yb-SO_4^{2-} bonding disintegrated. However, the high-temperature EXAFS is difficult to achieve high quality *ab initio*, and molecular dynamic (MD) is planned to be conducted to provide contemporary data for the EXAFS data interpretation and for sanity check.

Table.1 Curvefit parameters for Yb L-III edge EXAFS.

Temperature	Path	CN	R/Å	σ^2/ Å^2
100 °C	Yb-O	8.5	2.35(1)	0.010(3)
100 °C	Yb-S	2.5	3.68(16)	0.017(31)
200 °C	Yb-O	7.8	2.34(2)	0.017(3)
200 °C	Yb-S	1.7	3.64(1)	0.006(20)

REFERENCES

Castor S. B. and Hedrick J. B. (2006) Rare earth elements. *Industrial Minerals and Rocks* **7**, 769–792.

Mayanovic R. A., Anderson A. J., Bassett W. A., and Chou I.-M. (2007) On the formation and structure of rare-earth element complexes in aqueous solutions under hydrothermal conditions with new data on gadolinium aqua and chloro complexes. *Chemical Geology* **239**, 266–283.

Mayanovic R. A., Anderson A. J., Bassett W. A., and Chou I.-M. (2009a) Steric hindrance and the enhanced stability of light rare-earth elements in hydrothermal fluids. *American Mineralogist* **94**, 1487–1490.

Mayanovic R. A., Anderson A. J., Bassett W. A., and Chou I. M. (2009b) The structure and stability of aqueous rare-earth elements in hydrothermal fluids: New results on neodymium (III) aqua and chloroaqua complexes in aqueous solutions to 500 C and 520 MPa. *Chemical Geology* **259**, 30–38.

Migdisov A., Williams-Jones A., Brugger J., and Caporuscio F. A. (2016) Hydrothermal transport, deposition, and fractionation of the REE: Experimental data and thermodynamic calculations. *Chemical Geology* **439**, 13–42.

Wan Y., Wang X., Chou I.-M., and Li X. (2021) Role of sulfate in the transport and enrichment of REE in hydrothermal systems. *Earth and Planetary Science Letters* **569**, 117068.

New Mexico Bureau of Geology and Mineral Resources
A research and service division of New Mexico Tech
geoinfo.nmt.edu
801 Leroy Place
Socorro, NM 87801-4796
(575) 835-5490

NEW MEXICO TECH
SCIENCE · ENGINEERING · RESEARCH · UNIVERSITY